DYNAMIC PROPERTIES OF CONCRETE AND FIBER REINFORCED CONCRETE AT ROOM AND ELEVATED TEMPERATURES

by

Anna Marie Weidner

A thesis submitted to the faculty of
The University of Utah
in partial fulfillment of the requirements for the degree of

Master of Science

Department of Civil and Environmental Engineering

The University of Utah

May 2013

Copyright © Anna Marie Weidner 2013

All Rights Reserved

The University of Utah Graduate School

STATEMENT OF THESIS APPROVAL

The thesis of **Anna Marie Weidner**

has been approved by the following supervisory committee members:

Chris P. Pantelides	, Chair	**12/10/2012** Date Approved
Luis F. Ibarra	, Member	**12/10/2012** Date Approved
Amanda C. Bordelon	, Member	**12/10/2012** Date Approved

and by **Chris P. Pantelides**, Chair of the Department of **Civil and Environmental Engineering**

and by Donna M. White, Interim Dean of The Graduate School.

ABSTRACT

A drop hammer facility, which allows steel weights to be dropped from a height of 16 ft, was built at The University of Utah Structures Laboratory. The drop hammer facility was used to perform a series of dynamic tests on concrete cylinders with and without fiber reinforcement from heights of 16 ft and 8 ft. In July 2011 strain gauges, load cells and high speed cameras were used to collect data from dynamic splitting tension (tension) and compression tests performed on cylinders at room temperature. Additional cylinders were heated to 400 ^{o}F before they were tested in April 2012.

After testing, various methods were considered to determine the strain rate of the concrete. The dynamic impact factor (DIF), a ratio of peak dynamic load to quasi-static strength was also determined. Concrete has been known to have higher capacities when loaded dynamically. Thus, it is of interest to determine a factor that can be applied during design to account for this increase in strength. Models that have been produced to determine the DIF based on the strain rate were reviewed and compared with the test results.

As predicted by these models, the DIF results for both the compression and tension tests increased as the strain rate increased. The tension results were comparable with the model, whereas, the compression model was much more conservative than the results. When compared to the tension model, compression specimens require much higher strain rates to produce similar DIFs. For tension specimens, DIFs were recorded as

high as 4.1 at a strain rate of 1.2 in./in./sec. For compression specimens, the highest DIF was 3.2 at a strain rate of 12.1 in./in./sec.

For compression tests at room temperature, fiber reinforce concrete (FRC) specimens did not perform as well as normal weight concrete (NWC) specimens when tested dynamically. For compression and tension tests on NWC, heated specimens had lower DIFs than room temperature specimens at higher strain rates. However, when tested at lower strain rates, there was no significant decrease. FRC specimens tested in tension at elevated temperatures exhibited a decrease in DIF when compared to room temperature.

TABLE OF CONTENTS

LIST OF TABLES

NOMENCLATURE

ASTM	American Society for Testing and Materials
CF	Compression, Fiber Reinforced Concrete, Static
CF0-400-4	Compression, Fiber Reinforced Concrete, Static, 400°F, 4 in. diameter cylinder
CF0-400-6	Compression, Fiber Reinforced Concrete, Static, 400°F, 6 in. diameter cylinder
CF0-R-6	Compression, Fiber Reinforced Concrete, Static, Room Temperature, 6 in. diameter cylinder
CF8	Compression, Fiber Reinforced Concrete, 8 ft Drop Height
CF8-400-4	Compression, Fiber Reinforced Concrete, 8 ft Drop Height, 400°F, 4 in. diameter cylinder
CF16	Compression, Fiber Reinforced Concrete, 16 ft Drop Height
CF16-400-4	Compression, Fiber Reinforced Concrete, 16 ft Drop Height, 400°F, 4 in. diameter cylinder
CN	Compression, Normal Weight Concrete, Static
CN0-400-4	Compression, Normal Weight Concrete, Static, 400°F, 4 in. diameter cylinder
CN0-R-4	Compression, Normal Weight Concrete, Static, Room Temperature, 4 in. diameter cylinder

CN8	Compression, Normal Weight Concrete, 8 ft Drop Height
CN8-0-4	Compression, Normal Weight Concrete, 8 ft Drop Height, Room Temperature, 4 in. diameter cylinder
CN8-400-4	Compression, Normal Weight Concrete, 8 ft Drop Height, 400 °F, 4 in. diameter cylinder
CN16	Compression, Normal Weight Concrete, 16 ft Drop Height
CN16-0-4	Compression, Normal Weight Concrete, 16 ft Drop Height, Room Temperature, 4 in. diameter cylinder
CN16-400-4	Compression, Normal Weight Concrete, 16 ft Drop Height, 400 °F, 4 in. diameter cylinder
CN16-cooled-4	Compression, Normal Weight Concrete, 16 ft Drop Height, Cooled for roughly 18 hours, 4 in. diameter cylinder
DIF	Dynamic Increase Factor
FRC	Fiber Reinforce Concrete
INL	Idaho National Laboratory
NWC	Normal Weight Concrete
TF	Tension, Fiber Reinforced Concrete, Static
TF0-400-4	Tension, Fiber Reinforced Concrete, Static, 400 °F, 4 in. diameter cylinder
TF0-R-6	Tension, Fiber Reinforced Concrete, Static, Room Temperature, 6 in. diameter cylinder
TF8	Tension, Fiber Reinforced Concrete, 8 ft Drop Height

TF8-400-4	Tension, Fiber Reinforced Concrete, 8 ft Drop Height, 400 °F, 4 in. diameter cylinder
TF16	Tension, Fiber Reinforced Concrete, 16 ft Drop Height
TF16-400-4	Tension, Fiber Reinforced Concrete, 16 ft Drop Height, 400 °F, 4 in. diameter cylinder
TN	Tension, Normal Weight Concrete, Static
TN0-400-4	Tension, Normal Weight Concrete, Static, 400 °F, 4 in. diameter cylinder
TN0-R-4	Tension, Normal Weight Concrete, Static, Room Temperature, 4 in. diameter cylinder
TN8	Tension, Normal Weight Concrete, 8 ft Drop Height
TN8-0-4	Tension, Normal Weight Concrete, 8 ft Drop Height, Room Temperature, 4 in. diameter cylinder
TN8-400-4	Tension, Normal Weight Concrete, 8 ft Drop Height, 400 °F, 4 in. diameter cylinder
TN16	Tension, Normal Weight Concrete, 16 ft Drop Height
TN16-0-4	Tension, Normal Weight Concrete, 16 ft Drop Height, Room Temperature, 4 in. diameter cylinder
TN16-400-4	Tension, Normal Weight Concrete, 16 ft Drop Height, 400 °F, 4 in. diameter cylinder

ACKNOWLEDGMENTS

I would like acknowledge the assistance of Timothy Garfield, former University of Utah graduate student, for his work on the drop hammer facility and his involvement in the project and initial tests. I would also like to thank Mark Bryant, University of Utah Structures Laboratory Technician, for his assistance in building and operating the drop hammer facility. A special acknowledgment is given for William Richins, Thomas Larson and Jeb Blakeley from Idaho National Laboratories (INL). I thank them, and any additional INL staff, for their involvement in making this research possible and for their knowledge and extensive assistance during testing.

I would especially like to thank my advisor, Dr. Chris Pantelides, for giving me this great research opportunity, and for his continual dedication and guidance throughout my project. I would also like to thank my committee members, Dr. Luis Ibarra and Dr. Amanda Bordelon, for the time and interest that they showed in this project.

Lastly, and most of all, I would like to thank my good friends and amazing family. They have been extremely patient and supportive throughout my entire schooling.

1. INTRODUCTION

Concrete, when loaded dynamically, has been reported to have a higher strength than when loaded quasi-statically (statically). A variety of tests have been performed on different specimen types to determine dynamic increase factors (DIFs) for concrete. The DIF is a ratio of the dynamic to quasi-static (static) strength and is often reported as a function of the strain rate. Here, the DIF is taken as the ratio of the maximum dynamic to average static load. Several methods were developed to calculate the dynamic strain rate, the results of which were analyzed to determine which method was most accurate.

The DIF is of importance for defensive design purposes. The first phase of this project involved analyzing the performance of 4 ft x 4 ft concrete panels under blast loading (Garfield, 2011). The results of these tests provided information about how different reinforcement types influence the performance of a structural member. To determine how the concrete material was influenced by dynamic loading at high strain rates, concrete cylinders were cast at the same time as the panels. The cylinders were 4 in. diameter by 8 in. high, and 6 in. diameter by 12 in. high. These cylinders were tested dynamically by dropping steel plates from elevated heights, using what is referred to as the drop hammer facility.

One form of reinforcement considered in the blast tests was fiber reinforced concrete (FRC), which is composed of macrosynthetic polypropylene fibers. One percent by volume of the FRC specimens consisted of 2 in. long Propex Concrete

Systems Enduro 600 fibers. In July 2011, both FRC and normal weight concrete (NWC) cylinders were tested under different rates of dynamic impact by releasing a drop hammer weight from heights of 8 ft and 16 ft.

When concrete is loaded dynamically in defense related facilities or nuclear power plants it is likely that it is also at an elevated temperature. In April 2012 additional tests were performed to determine how temperature, up to 400 ^{o}F, affects the response of different concrete types under dynamic loading. These tests were of special interest in the case of fiber reinforced concrete, since the fibers used had a melting point of 328 ^{o}F. It is also possible that heated concrete can be loaded dynamically after it has had time to cool. A small number of tests were performed on cylinders that were allowed to cool down for approximately 18 hours after being heated to 400 ^{o}F.

Tests were performed to determine both dynamic splitting tension (tension) and compression properties at high strain rates for all specimen types. The dynamic test was designed and analyzed to follow standard static test procedures as close as possible so that a comparison between the two could be made. For this purpose, all types of dynamic tests were also preformed statically.

For dynamic tests, various combinations of drop heights and weights were used to test various specimen types. To compare the results of different specimen types, the impact energy was determined for each drop height and weight combination. This impact energy was taken as the kinetic energy of the drop hammer when the hammer first impacts the specimen.

It was the objective of this research to determine the DIF of NWC and FRC at room and elevated temperature using various impact energies. Comparisons were made to

determine how different specimen types performed dynamically. It was also desired to know the relationship between DIFs and strain rates. Previous dynamic impact research has been performed on various types of specimens, of which, models have been produced relating DIFs to strain rates. These models were reviewed and compared with the results obtained for the various specimen types considered in this research.

2. LITERATURE REVIEW

Various methods have been considered by many researchers in an effort to determine the dynamic properties of concrete. Reviews have been conducted on past research regarding the effects of elevated temperature on concrete with and without fiber reinforcement. Various research projects related to dynamic and drop hammer tests were reviewed. Finally, proposed models for determining the effect of strain rate on the dynamic behavior of concrete were reviewed.

2.1. Effects of Temperature on Normal Weight and Fiber Reinforced Concrete

Polypropylene fibers are added to concrete mixtures to improve the mechanical properties of concrete. When concrete is subjected to elevated temperature the improved properties from the fibers can be adversely affected. To determine how elevated temperatures affect the properties of high strength concrete with fibers Lam et al. (2012) conducted a series of compressive tests.

The high strength concrete mixture for these tests used fibers that were 0.709 in. long with a fiber density of 0.125 lb/ft^3. Three specimen sizes were considered: 4 in. cubes that had a 28 day compressive strength of 14.55 ksi, 6 in. diameter by 12 in. high cylinders that had a 28 day compressive strength of 12.18 ksi and 3 in. diameter by 6 in. high cylinders. The temperatures considered for the tests were 212 ^oF, 392 ^oF, 572 ^oF,

752 °F, 932 °F and 1292 °F. The specimens were heated and tested in an electrical oven that incorporated a hydraulic testing machine so that the cylinders were held at the desired temperature throughout the test.

Past research has shown that high strength concrete that is exposed to elevated temperatures is more susceptible to explosive spalling. This is one of the major disadvantages of using high strength concrete. Lam et al. (2012) note that the use of polypropylene fibers can reduce spalling of concrete at elevated temperatures, but it may also reduce the compressive strength. To better define the effects of heating high strength concrete with polypropylene fibers the compressive strength was measured and compared at a variety of temperatures. When heated to 212 °F the concrete only reached 70% of the compressive strength at room temperature. Increasing the temperature to 392 °F resulted in a slight increase to 75% of the room temperature compressive strength. This compressive strength was steady until 752 °F, at which point the compressive strength began to decrease significantly. At 932 °F only 50% of the room temperature compressive strength was achieved. Increasing the temperature further to 1292 °F had only a slight reduction in compressive strength. To determine why a change in compressive strength occurs, a scanning electron microscope was used to study the cement paste at the various test temperatures. After being heated to 212 °F voids were noticed in the cement. This was attributed to the evaporation of free water, which causes a significant reduction in compressive strength.

At 338 °F the polypropylene fibers reached their melting point and were no longer visible. This did not reduce the strength of the concrete. In fact, at this temperature there was a slight increase in compressive strength. Lam et al. (2012) believed that the increase

was from the "stiffening of the cement gel, the increase in surface forces between gel particles, and/or the removal of absorbed moisture."

At 935 °F the electron microscope showed that the water from the cement paste had evaporated. The loss of water in the cement paste reduces the bonding strength of the cement, resulting in microcracks and further voids in the concrete. This loss of bond water resulted in a significant decrease in compressive strength.

In addition to the compressive strength, the strain rates and stress-strain relationships were considered to better understand the effects of temperature. It was found that the strain rate increased significantly with increasing temperature. An even more substantial increase in strain was noted at 572 °F, which was believed to be a result of cracks forming in the cement paste began. From the stress strain graphs, it was found that as the temperature increased the stress reduced more gradually after peak load. This stress reduction behavior became most significant for temperatures above 932 °F. This means that the concrete became less brittle as the temperature increased.

To further understand the effects of temperature on concrete with polypropylene fibers, Behnood and Ghandehari (2009) performed both compressive and tensile tests on concrete with and without fibers. Also of importance in these tests were the effects that temperature had on normal versus high strength concrete. The specimens were heated in an oven and held at the desired temperature for 3 hours. The temperatures tested were 212 °F, 392 °F, 572 °F and 1112 °F. In variation to Lam et al. (2012), after the specimens were heated they were cooled to room temperature before being tested.

To test how temperature affects concrete without fiber reinforcement, concrete mixtures were cast from Type 1 ordinary Portland cement with water-to-cement ratios of

0.4 and 0.3. Two additional mixes were cast using silica fume in place of 6% and 10% of the cement. At room temperature, the 10% silica fume concrete had the highest compressive strength; whereas, the 0.4 water-to-cement-ratio concrete had the lowest compressive strength.

When heated to 212 °F, all mixes decreased in strength. The 10% silica concrete was affected the most by the temperature increase. When the temperature increased to 392 °F a slight increase in strength was seen for each concrete type. This was similar to what Lam et al. (2012) concluded, for which the same reasoning (the increased bond of the gel particles as a result of the evaporation of water) was given as an explanation for the increase.

Increasing the test temperature to 572 °F resulted in a significant reduction in compressive strength, with the 10% silica fume concrete, once again, being the most affected. Behnood and Ghandehari (2009) explained that the 10% silica fume concrete has a compact composition. When the water content in the concrete and bonding material begins to evaporate the compact composition does not allow for the release of water vapors. This allows for an increase in pressure, which results in inner cracking and thus a reduction in strength.

When the test temperature was increased to 1112 °F all concrete types had a large reduction in compressive strength, similar to what was reported by Lam et al. (2012). Behnood and Ghandehari (2009) provide further explanation as to why, stating that between 842 °F and 932 °F the calcium hydroxide (slaked lime) in the cement begins to decompose. Also, as water evaporates the cement paste contracts while the aggregate

expands resulting in a loss of bond. Once the temperature reached 1112 °F all the specimens had similar compressive strength.

The pattern of results for the tensile tests was very similar to the compressive tests. It is known that the tensile strength is more affected by the formation of cracks than the compressive strength. This was evident by the fact that the tensile strength decreased more quickly with an increase in temperature than the compressive strength.

To summarize Behnood and Ghandehari (2009), the increase of temperature had a greater effect on high strength concrete (10% silica fume). An initial reduction of both compressive and tensile strength occurs at 212 °F. In both cases, the strength then increases slightly until the temperature reaches 392 °F, at which point significant reduction occurs.

Behnood and Ghandehari (2009) proceeded with additional tests to determine how temperature affects concrete with polypropylene fibers; concrete mixtures with a water-to-cement ratio of 0.3 and fiber densities of $0.063\ \mathrm{lb/ft^3}$, $0.125\ \mathrm{lb/ft^3}$, and $0.187\ \mathrm{lb/ft^3}$ were tested. Control specimens with no fibers and 10% silica fume were used for comparisons.

At room temperature the addition of the fibers had no effect on the compressive strength. Increasing the test temperature to 212°F had the same effect as this did for the concrete without fibers. It was noted that the concrete with $0.125\ \mathrm{lb/ft^3}$ fiber density had the least reduction in strength. A small increase in compressive strength, as was seen in previous nonfiber reinforced concrete tests, occurred when the test temperature was increased to 392 °F. The concrete with $0.125\ \mathrm{lb/ft^3}$ fiber density once again had the greatest increase; the concrete without reinforcement had the lowest increase. As Lam et

al. (2012) had concluded, the melting of the fibers creates voids which allow for the dispersion of water vapors, thus increasing the strength. However, it is noted that the concrete with the highest density of fibers ($0.187\ lb/ft^3$) did not have the highest increase in strength.

Consistent with previously discussed tests, increasing the test temperature to 572 °F had a significant reduction in compressive strength. This reduction, as for high strength concrete, was attributed to the compact composition of fiber reinforced concrete. However, fiber reinforced concrete did perform better than plain high strength concrete because of the voids created from the melted fibers. Further increase in temperature to 1112 °F results in further reduction in compressive strength for the same reasons as discussed for nonfiber reinforced concrete.

Fibers, which help to mitigate crack growth, have been proven to be more effective in tension than in compression. Behnood and Ghandehari (2009) found that at room temperature the fiber reinforced concrete had a higher tensile strength than the non-fiber reinforced control specimens. Heating the specimens to 212 °F resulted in a decrease in tensile strength. The nonfiber reinforced control specimen was more negatively affected by the increase in temperature than the fiber reinforced specimens. This is due to the fact that fibers maintain their mechanical properties at this temperature.

The fiber reinforce concrete tested in tension is the only test type that had a decrease in compressive strength when the test temperature increased from 212 °F to 392 °F. The polypropylene fibers, which are a large contributor to the tensile strength, reach their melting point between 338 °F and 347 °F, attributing to the loss of tensile strength.

When the temperature increased further, the tensile strength reduced similarly to the compressive strength for the same reasons. However, the relative reduction was higher for tensile strength than compressive, meaning that temperature had a greater effect on fiber reinforced concrete in tension. At a test temperature of 1112 °F there was no additional strength for the fiber reinforced concrete compared to the nonfiber reinforced control specimen.

In summary, for both the compression and tension test Behnood and Ghandehari (2009) observed that $0.125\ lb/ft^3$ fiber density achieved the best results at every temperature tested. This is the optimum fiber density that is generally recommended and used in concrete mixtures. From these tests, it is shown that this density still produces the best results at elevated temperatures.

Both nonfiber reinforced and fiber reinforced concrete were most affected by temperatures exceeding 572 °F. For compression tests, the addition of polypropylene fibers in the concrete mixture increased the compressive strength at elevated temperatures. For tension, the fibers did not have as great an effect as for compression. The additional strength due to fibers started reducing from the beginning of heating until 1112 °F when it contributed no additional tensile strength.

Behnood and Ghandehari (2009) emphasized that data could vary depending on concrete moisture content and aggregate type, testing methods, the rate of heating specimen and maximum temperatures. Many variables are involved in the testing of concrete at elevated temperatures and must be considered when making conclusions.

2.2. Dynamic and Drop Hammers Testing

1.2.1 Split-Hopkinson pressure bar. To determine the effects of dynamic loading on concrete, Ross et al. (1995) performed impact tests in compression and tension. The tests used split-Hopkinson pressure bars that were capable of a strain rate between 10 in./in./sec and 10^4 in./in./sec. The specimens were made of plain concrete and were 2 in. diameter by 2 in. long bars.

The split-Hopkinson pressure bar test uses an incident steel bar and a transmitter steel bar. The specimen is placed in between the two bars so its height is parallel with the bars. A striker bar is then propelled, impacting the incident bar. Part of the impulse from the impact on the specimen is reflected back into the incident bar and some is transferred into the transmitter bar. A strain gauge on the incident bar records the amount of impulse that was reflected by the specimen. This impulse is proportional to the strain of the specimen. A strain gauge is also placed on the transmitter bar, which measures the amount of impulse that is transmitted through the specimen. This transmitted impulse is proportional to the stress in the specimen.

The test procedure for the direct tension test was similar to that for the compression tests. The only difference is that a tensile stress impulse is placed on the specimen by the transmittal bar. Ross et al. (1995) explain that a compressive pulse is delivered by the striker bar and travels through an outer tube to the free end. At the free end, the pulse is reflected placing a tensile force on the specimen. The strain and stress are determined similar to the compression tests, but here the transmittal strain gauge is proportional to the strain and the incident bar is proportional to the stress.

From these tests, Ross et al. (2005) found that an increase in dynamic to static strength, known as the dynamic increase factor (DIF), occurred at strain rates of 5 in./in./sec for tension and 60 in./in./sec for compression. It was noted that the tension specimens were more sensitive to the increase in strain rate than the compression. This means that the DIF increases more quickly for the tension test than the compression test.

1.2.2 Drop hammer tests on beams. Banthia et al. (1986) performed several different series of drop hammer tests. One of the original drop hammer tests performed by Banthia et al. (1986) used a 760 pound force (lbf) weight that could be dropped up to 8 ft. Simply supported beams with dimensions of 60 x 4 x 5 in. were used as specimens. Specimen types included: normal weight concrete, high strength concrete with superplasticizer cement, fiber reinforced concrete with 2 in. long steel fibers (1.5% by volume), and fiber reinforced concrete with 1.5 in. long polypropylene fibers (0.5% by volume). The compressive strength of normal weight and high strength concrete were 6000 psi and 11900 psi, respectively.

Strain gauges were placed on the striking end of the hammer as well as on the anvils that supported the beam. These strain gauges were used to measure the impact load on the beam. Three accelerometers were placed along the length of the beam. The measured acceleration was integrated to find the velocity, which in turn was integrated to determine the displacement of the beam.

Banthia (1986) concluded that the load measured from the strain gauges is not the actual bending load on the beam; part of the load measured is an inertial force. The inertial force from the hammer was computed using data from the accelerometers and

was subtracted from the measured load from the strain gauges. The new reduced load was considered as the dynamic impact force.

After applying this method, the results showed that for each concrete type, the dynamic load increased with increasing stress rate. The fibers were found to increase the performance of concrete both statically and dynamically, with the steel fibers performing better than polypropylene fibers. Similar to other dynamic tests, it was found that the high strength concrete did not have as large of an increase in strength when loaded dynamically.

In later tests, Banthia (1986) began expressing the loading conditions in terms of energy. Given the mass of the drop hammer, the drop height and gravity, the potential energy of the system could be reported. This allows for better comparisons among various impact tests.

Millard et al. (2010) performed drop hammer tests on smaller concrete beams. Two similar series of drop hammer tests on ultra high performance fiber reinforced concrete (UHPRFC) were performed. Concrete mixtures used over three times the normal amount of cement, none-coarse aggregate, silica sand and silica fume. Short steel fibers with a length of 0.5 in. were used in dosages of 1.5%, 2%, and 6% by volume. A hybrid mixture was also used with 3% of short steel fibers and 3% of long steel fibers (1 in. long).

The first series of tests used beam specimens that were 11 x 0.75 x 0.75 in. The beams were simply supported on steel rollers that rested on load cells. The load cells were on top of a concrete slab that was placed in a sand bed used to reduce signal interference during testing. A transmission bar with a thin layer of fiberboard was

centered on the beam, thus reducing the vibration of the impact load. A 66 lbf, 6.6 ft long, 2 in. diameter cylindrical hammer with a hemispherical end was dropped onto the transmission bar from varying heights.

To determine the strain rate of the beam, the load cell data was used. A plot of the load versus time showed that the load rate was not constant, but increased with time until cracking occurred in the beam. At this point the loading rate began to decrease until the peak load was reached. To calculate the strain rate, the peak loading rate was determined and the engineering theory of bending was applied. A modulus of elasticity of 51×10^6 psi was used for the concrete, which had a compressive strength between 22000 and 29000 psi.

The second series of tests performed by Millard et al. (2010) used beam specimens that were 14 x 4 x 2 in. These beams were also simply supported on steel rollers that rested on load cells. The load cells were placed on a steel plate that was supported by a 0.4 in thick fiberboard. A 50 lbf hammer was dropped from 6.5 ft for each test.

To vary the loading rate, two to six layers of 0.4 in. fiberboard were placed on the beam where the hammer would fall. For this series of tests a laser Doppler anemometer (LDA) was used to measure the speed of the dropping hammer. The acceleration could then be calculated and used along with the weight of the hammer to determine the impact force.

A high speed camera was also used to measure the deflection of the beam, and thus the strain rate could be calculated. The velocity of the falling drop hammer was measured using the high speed camera and LDA to determine the accuracy of the

equipment. Once the laser data was filtered, it was found that the results were in accordance with each other.

To compare the two methods used to determine the strain rate in the two test series, the method used in the first series of tests was also used in the second, with the only exception being that the loading rate was determined using the LDA. Both methods were found to produce similar results. However, it was noted that the engineering theory of bending applied in the first series of tests no longer applies when cracking begins.

To summarize the results of their tests, Millard et al. (2010) stated that each test had similar crack patterns and failure modes. In all cases it was the pull-out strength of the fibers that caused failure, even at high strain rates. It was also concluded that specimens without fibers had higher DIFs when tested in tension.

Millard et al. (2010) explain that for standard static tests microcracks follow the path of least strength. This takes time and standard static testing procedures take this into account when considering the time, or rate, of loading. Fibers are used to resist the loss of strength due to microcracks. When dynamically loaded, these microcracks develop differently, crossing stronger paths. For this reason, fibers do not add as much strength to concrete when tested at higher strain rates as they do when strain rates associated with static tests are used.

The hybrid fiber mixture with the 3% long and 3% short steel fibers by volume had the lowest DIF, which was less than 1.0. Millard et al. (2010) stated that this was a result of different mixing or testing methods, and that that results were not significant. Millard et al. (2010) state that there are conflicting results from various tests about whether higher fiber content reduces the DIF.

Most beams were found to have significant DIFs for strain rates between 0.1 and 10 in./in./sec. Despite the significant DIFs between 0.1 and 1 in./in./sec, Millard et al. (2010) recommended that DIFs should not be applied for tension specimens with strain rates less than 1 in./in./sec. Shear tests were also performed in these series of tests, and it was determined that DIFs do not apply to concrete in shear.

1.2.3 Drop hammer tests on concrete cylinders. Drop hammer tests have been performed using a variety of different specimen sizes and procedures. The effect of specimen size on the DIF was considered when comparing past research with the present research. Watstein (1953) performed dynamic compression tests on concrete cylinders 3 in. in diameter and 6 in. high with two concrete types having static compressive strengths of 2700 psi and 6800 psi.

Two types of dynamic tests were performed. First, a hydraulic machine capable of loading up to 60000 lbf was used to test the cylinders at a strain rate of 0.003 in./in./sec. Second, a drop hammer facility with a 140 lbf, flat surface weight dropped from 5.5 ft was used. The cylinders were capped with steel plates and placed on top of a 3200 lbf anvil. The anvil was supported on compression springs capable of deflecting up to 0.5 in. before being stopped by shock absorbers and rubber buffers.

The rate of loading was controlled by placing a buffer on top of the test cylinder. The strain rates ranged from 0.5 to 10 in./in./sec. Dynamometers were used to measure the load from the drop hammer. Strain gages placed on the cylinder were also used to collect data during testing.

Each concrete type had one specimen tested using the hydraulic machine and two using the drop hammer facility. The DIFs for the weak concrete (2700 psi compressive

strength) were 1.19, 1.57, and 1.84 at strain rates of 0.00364, 0.531 and 10.1 in./in./sec, respectively. For the strong concrete (6800 psi compressive strength), the DIFs were 1.13, 1.53 and 1.85 at strain rates of 0.00296, 2.86 and 6.69 in./in./sec, respectively.

For these same tests, the stress-strain relationship, and thus the modulus of elasticity, was determined. It was found that the ratio between the dynamic and static modulus was 1.02, 1.07 and 1.10 for the weak concrete and 1.06, 1.16 and 1.24 for the strong concrete. This shows how the modulus of elasticity increases with increasing strain rates. It can also be concluded that the higher strength concrete was more affected by the increase in strain rate.

After testing, both the dynamic and static specimens showed the same conic failure mechanisms and had similar amounts of damage.

2.3. Dynamic Increase Factor Models

Models have been proposed to determine DIFs based on strain rates. The Comité Euro-International du Béton (CEB) Model Code (1993) developed a bilinear relationship between strain rates and DIFs for both compression and tension. Since that development, these models have been reviewed and modified as discussed by Malvar and Crawford (1998).

The static strain rate is a fundamental value for these models. According to American Society for Testing and Materials (ASTM) standards (2010), the static test loading rate should be between 20 and 50 psi/sec for compression tests. Considering the concrete strength to be between 3000 and 10000 psi, the corresponding time to failure is between 60 and 500 sec. With a recommended peak strain at failure of 0.002 in./in., the test strain rate would be between $4\ x\ 10^{-6}$ and $33\ x\ 10^{-6}$ in./in./sec. Therefore, as

Malvar and Crawford (1998) concluded, the CEB model's static strain rate ($\dot{\varepsilon}_s$) of $30\ x\ 10^{-6}$ in./in./sec for compression is appropriate. At this strain rate, the DIF is considered to be 1.0.

The model shows that a significant change in DIF occurs when the dynamic strain rate exceeds 30 in./in./sec. At this higher strain rate, the DIF factor increases more rapidly as the dynamic strain rate ($\dot{\varepsilon}$) increases. The CEB model for compression is given in Eqns. (1.1) through (1.4), where (f_{cs}) is the static compressive strength in psi. This model is valid for dynamic strain rates between $30\ x\ 10^{-6}$ and 300 in./in./sec.

$$\text{DIF} = \left(\frac{\dot{\varepsilon}}{\dot{\varepsilon}_s}\right)^{1.026*} \quad \text{for } 30 \text{ x } 10^{-6}\ \text{in./in./sec} \leq \dot{\varepsilon} \leq 30\ \text{in./in./sec} \tag{1.1}$$

$$\text{DIF} = \left(\frac{\dot{\varepsilon}}{\dot{\varepsilon}_s}\right)^{1/3} \quad \text{for } \dot{\varepsilon} > 30\ \text{in./in./sec} \tag{1.2}$$

$$= \frac{1}{5 + 9 * \frac{f_{cs}}{1450\ \text{psi}}} \tag{1.3}$$

$$= 10^{6.156* \ -2} \tag{1.4}$$

When research first began on DIFs, compressive strength was of primary interest. For this reason, not much data was available for tension tests. However, Malvar and Crawford (1998) noted that, when subjected to blasts, concrete walls often failed in tension, thus demonstrating the importance of DIF for tension. A CEB model for tension was created similar to the CEB model for compression.

The CEB model for tension considers the static strain rate to be $3\ x\ 10^{-6}$ in./in./sec. The dynamic strain of 30 in./in./sec is still considered to be the point where the DIF begins to increase more rapidly. The tension model is similar to the compression, but with DIFs that are slightly larger. The CEB tension model is given in Eqns. (1.5) through (1.8) and is valid for dynamic strain rates ranging from $3 \text{ x } 10^{-6}$ to 300 in./in./sec.

$$\text{DIF} = \left(\frac{\dot{\varepsilon}}{\dot{\varepsilon}_s}\right)^{1.016*} \quad \text{for } 30 \text{ x } 10^{-6} \text{ in./in./sec} \leq \dot{\varepsilon} \leq 30 \text{ in./in./sec} \tag{1.5}$$

$$\text{DIF} = \left(\frac{\dot{\varepsilon}}{\dot{\varepsilon}_s}\right)^{1/3} \quad \text{for } \dot{\varepsilon} > 30 \text{ in./in./sec} \tag{1.6}$$

$$= \frac{1}{10 + 6 * \frac{f_{cs}}{1450 \text{ psi}}} \tag{1.7}$$

$$= 10^{7.11* \ -2.33} \tag{1.8}$$

Malvar and Ross (1998) performed dynamic tensile tests so that an appropriate model could be developed and used to determine the DIF for tension. Malvar and Ross (1998) summarized and considered various tensile dynamic tests performed previously by others when developing their model. Mellinger and Birkimer (1966) tested normal weight concrete cylinders that were 10.25 in. long and 2 in. in diameter. They were loaded dynamically on their ends in such a way that "the compression wave from the impact traveled along the specimen and was reflected at the end of the specimen as a tension wave" (Mellinger and Birkimer, 1996). For these tests, DIFs of 6.5 and 8.1 at strain rates of 20 in./in./sec and 23 in./in./sec, respectively, were recorded.

Birkimer (1968) performed additional tests with cylinders that were 35 in. long and 2 in. in diameter. The resulting DIF varied from 2.5 to 6 for strain rates between 2 and 23 in./in./sec, respectively. It can be noted that the change in specimen size resulted in a decrease of DIF from 8.1 for the 10.25 in. long cylinder to 6 for the 35 in. long cylinder at a strain rate of 23 in./in./sec.

Explosion testing was performed on concrete walls by McVay (1988). The DIF reported for these tests were 7.1 for a strain rate of 38 in./in./sec and 6.7 for a strain rate of 157 in./in./sec.

Tests by Ross et al. (1995) for direst tension were performed using split-Hopkinson pressure bars that were between 1.75 to 2 in. high and 2 to 3 in. in diameter. For splitting tension, Brazilian tests were performed using specimens that were 1.75 to 2 in. high and 0.75 to 2 in. in diameter. These specimens were tested at strain rates between 10^{-7} and 20 in./in./sec., with the highest DIF equal to 6.47. Additional split-Hopkinson pressure bar tests were performed by John et al. (1992) with specimens that were 0.25 to 0.5 in. high with 0.5, 1 and 2 in. diameters. The strain rates for these specimens were between $5 \, x \, 10^{-7}$ and 70 in./in./sec, with the highest DIF equal to 4.8.

From the summary of tests given by Malvar and Ross (1998), it can be seen that different specimens gave different DIFs for similar strain rates. Even with this being the case, Malvar and Ross (1998) note that all data above the strain rate of 1 in./in./sec follow the same trend.

Additional tests were also performed at lower strain rates by Cowell (1966), Takeda (1971) and Kormeling et al. (1980). In these tests it was noted that even at low

strain rates a DIF is still applicable. It was also reported by Cowell (1966) and Kormeling (1980) that the DIF is higher for concrete with lower strengths.

Malvar and Crawford (1998) reviewed how Malvar and Ross (1998) applied the available data for dynamically loaded tensile tests and began developing a DIF model for tension. Ross recommended a peak strain at failure of $1.18\ x\ 10^{-4}$ based on ACI 318 (2008) standards. Considering ASTM standard (2004, 2010) loading values of 100 to 200 psi/min and tensile strengths between 300 and 700 psi, the time to failure would be 90 to 420 seconds. This time to failure and peak strain correspond to a static strain rate between $0.28\ x\ 10^{-6}$ in./in./sec and $1.3\ x\ 10^{-6}$ in./in./sec. The CEB's model, which considered the static strain rate to be $3\ x\ 10^{-6}$, does not coincide with the calculated range of static strain rates. For this reason, Ross developed a new model using a static strain rate of $1\ x\ 10^{-6}$.

Originally, Ross considered his model to be applicable from $1\ x\ 10^{-8}$ to 300 in./in./sec. However, if you consider the loading rate of 100 to 200 psi/min and the tensile strengths between 300 psi and 700 psi, a more appropriate origin would be between $1.14\ x\ 10^{-6}$ in./in./sec and $3.49\ x\ 10^{-6}$ in./in./sec. Therefore, Ross modified his model to begin at $3\ x\ 10^{-6}$ in./in./sec, which corresponds to the CEB model.

To better represent different concrete strengths, as is done in the CEB model, and to achieve a bilinear model, Ross applied his parameters to the CEB model to formulate the modified CEB model. Ross also considered experimental data from various dynamic tests and determined that a change in slope occurred around 1 in./in./sec. For the modified CEB model a static strain rate of $1\ x\ 10^{-6}$ in./in./sec and a slightly lower

dynamic strain rate range of $1\ x\ 10^{-6}$ to 160 in./in./sec were used along with Eqns. (1.9) through (1.12).

$$\text{DIF} = \left(\frac{\dot{\varepsilon}}{\dot{\varepsilon}_s}\right) \quad \text{for } \dot{\varepsilon} \leq 1 \text{ in./in./sec} \tag{1.9}$$

$$\text{DIF} = \left(\frac{\dot{\varepsilon}}{\dot{\varepsilon}_s}\right)^{1/3} \quad \text{for } \dot{\varepsilon} > 1 \text{ in./in./sec} \tag{1.10}$$

$$= \frac{1}{1 + 8 * \frac{f_{cs}}{1450 \text{ psi}}} \tag{1.11}$$

$$= 10^{6* \varepsilon - 2} \tag{1.12}$$

When compared with data from dynamic tests, the modified CEB model fits the available data for tensile tests more closely than the original CEB model and Ross' scaled model.

3. EQUIPMENT AND DATA COLLECTION

A drop hammer facility at the University of Utah was built as part of this project and used to perform dynamic tests on concrete cylinders at high strain rates. High speed cameras, strain gauges and a load cell system were used to collect data during dynamic tests. Static tests were also performed using a Satec™ series Instron® machine. During one series of tests, cylinders were heated using a Despatch oven.

3.1. Drop Hammer Facility

To begin constructing the drop hammer facility a new foundation was cast to ensure that the dynamic force from the drop weight would have minimal effects on the surrounding facilities. The existing floor slab was replaced with a 7 x 9 x 4 ft deep concrete foundation. Gravel, 3 in. deep, was used as a base, and large pieces of steel were added as reinforcement. Twelve cubic feet of concrete was then cast and allowed to cure for 28 days to complete the foundation.

The base of the drop hammer structure is a 3 x 5 ft, 2 in. thick steel plate, as shown in Figure 3.1. Welded to the base plate are three, 23 ft tall legs made from 6 x 6 x 0.25 in. thick hollow steel square tubes. The main section of the drop hammer is a 0.25 in. thick, 16 in. diameter pipe, through which the drop weight falls. The legs and tube are connected by welded and bolted plates along the length of the drop hammer. The pipe is slotted in the front to help prevent the drop weight from binding in the tube. One foot increment markings, measured from the impact target where the cylinder is placed, are

shown on the side of the slotted pipe. To complete the facility, a protective cage was built around the base of the drop hammer to reduce the spread of concrete as the specimens break. The finished drop hammer is shown in Figure 3.2.

The drop weight used to deliver the dynamic load is composed of 14 in. diameter steel plates with a thickness of either 0.5 or 1 in. These plates have a central whole diameter of 1.25 in. and were added to a 1 in. thick base plate with a 1 in. diameter rod welded through its center.

Once the desired drop weight was reached, a square tube was placed on the base plate rod. The square tube had a checker board pattern placed on it to calculate the velocity of the drop hammer as it fell using high speed camera recordings. An additional thin plate was then placed on top of the square tube. To finalize the drop hammer, the plates and square tube were tightened together using a fastening gig which was bolted onto the base plate rod. This configuration, shown in Figure 3.3, was designed to distribute the weight along the length of the drop hammer, thus preventing it from oscillating as it fell. The drop hammer was connected to an electric cable hoist using a quick release hook as shown in Figure 3.4.

3.2. High Speed Cameras

During the July 2011 tests, two high speed cameras were used to record failure of the specimens. A Phantom v12 camera with a signal to noise ratio of 7968, an exposure of 99 microseconds and a resolution of 400 by 504 pixels was placed directly in front of the specimen and recorded the tests at a rate of 8000 frames per second (FPS). A second camera, a Phantom v7.3 with a signal to noise ratio of 7966, an exposure of 123

microseconds and a resolution of 640 by 480 pixels, was placed toward the side of the specimen, recording at a rate of 7005 FPS.

To achieve high quality videos, shop lights were required during tests. A touch pad was used to signal the cameras to begin recording. The touch pad was triggered as the hammer was being released. To demonstrate the data recorded, consecutive image shots of the video (time-lapse) are shown in Figure 3.5 for tension and Figure 3.6 for compression.

3.3. Strain Gauges

For the July 2011 tests, 120 ohm strain gauges were placed on each specimen. Vishay Precision Group strain gauges were used. Most specimens had two strain gauges: the first was a model 10CBE, 1 in. gauge (referred to as Strain Gauge 0) and the second a model 20CBW, 2 in. gauge (referred to as Strain Gauge 1). For the splitting tension tests, two strain gauges were placed on the top face of the cylinder and the drop weight was released onto the side of the cylinder, as shown in Figure 3.7. This configuration was typical for most tests; however, some splitting tension specimens had gauges on their sides instead of the top face (Figure 3.8) due to a limitation of appropriate strain gauge configuration. For the compression tests, two strain gauges were placed on opposite vertical sides and the drop weight was released onto the top face of the cylinder as shown in Figure 3.9. There were a number of instances where one of the strain gauges failed and no output was recorded.

3.4. Load Cells

To measure the dynamic load on the concrete cylinders, a load cell system composed of load sensors, steel plates, and mounting hardware, was built. For the load cell sensors to record accurate data, they need to be loaded concentrically to reduce the possibility of induced bending moments. This is best achieved by using multiple sensors placed between two flat plates that prevent the sensor from bending.

Five force sensors were placed between two, 12 x 8 x 1 in. thick steel plates. The load sensors and plates were held together using HEX HD 7/8-14 UNF-2Bx1-3/4 LG beryllium copper mounting studs. These studs are elastic, which allows for the applied force to transfer to the force sensor. A pilot bushing is used between the mounting stud and sensor to ensure that they are centered together. Two antifriction washers, placed above and below each sensor, protect the surface of the sensor when the mounting stud is being tightened. A schematic of the load cell system assembly is shown in Figure 3.10; the layout of the load cell is given in Figure 3.11. The final load cell system used in July 2011 is shown in Figure 3.12.

PCB Piezotronic Inc., model 206C ICP® Dynamic Force Sensors (Figure 3.13), which can record up to 80000 pounds of force, were used in the load cell system. A constant current between 2 and 20 mA was supplied to the sensor from the data acquisition system. When a load was applied, the sensor measured the high impedance of the supplied current and converted it to a low impedance voltage signal that was recorded. The sensors had a target pre-load of 16000 pounds, which is required to ensure that the sensor will perform as calibrated.

To achieve this preload amount the initial preload and voltage were measured using the data acquisition system and a digital voltmeter, respectively. A ratio of the

current preload to the target preload was added to the measured voltage. This calculated value was the desired voltage. A torque was applied to the mounting studs until the desired voltage was achieved, as measured from the digital voltmeter. If necessary, as determined from analyzing the output of the sensors after tests, the load cells were readjusted back to the proper preload value.

For the July 2011 tests the load cell system was held in place on the drop hammer facility's base plate by placing steel plates around it. In April 2012, small steel angles were welded to the drop hammer facility's base plate to hold the load cell system in place. In addition, a hemispherical steel plate was placed on top of the load cell system during tests.

As shown in Figure 3.14, the hemispherical plate is composed of two joining convex and concave hemispherical plates. Reviewing the individual load cell data from the July 2011 tests showed that some force sensors were recording significantly larger loads than others. It was believed that the plate containing the load cells was deflecting unevenly during tests due to concentrated forces. The hemispherical plate was added to the testing configuration to distribute the load more evenly among the load cells, and to prevent the load cell system plates from deflecting unevenly.

3.5. Satec™ Series Instron® Machine

A Satec™ Series Instron® machine was used to test the concrete cylinders statically. The Instron machine applied a constantly increasing load to the cylinders. The American Society for Testing and Materials (ASTM) standard C496/C496M-04e1 Standard Test Method for Splitting Strength of Cylindrical Concrete Specimens (2004) and C39/C39M-10 Standard Test Method for Compressive Strength of Cylindrical Concrete (2010) were

used to determine the appropriate loading rate. The loading rate is a function of the size of cylinder used. Eqns. (3.1) and (3.2) were used to determine the loading rate for split tension and compression, respectively.

$$Tension\ Applied\ Loading\ Rate = 2.5\,psi/sec * \frac{\pi * L * D}{2} \tag{3.1}$$

$$Compression\ Applied\ Loading\ Rate = 40\,psi/sec * \frac{\pi * D^2}{4} \tag{3.2}$$

For the 4 in. diameter by 8 in. high cylinders, the loading rates were 500 pound force per sec (lbf/sec) and 130 lbf/sec for compression and tension, respectively. For 6 in. diameter by 12 in. high cylinders, the loading rate was 1130 lbf/sec and 285 lbf/sec for compression and tension, respectively.

3.6. Despatch Oven

An LBB2-18-1 Despatch oven, with a maximum temperature of 400 °F was used to heat the cylinders for the April 2012 tests. To determine the time required for the cylinder to be placed in the oven, a thermocouple was placed on a normal weight concrete (NWC) 4 in. diameter by 8 in. high cylinder and a NWC 6 in. diameter by 12 in. high cylinder. The resulting rate of temperature increase is shown in Figure 3.15. The maximum interior temperature reached for the 4 in. diameter by 8 in. high cylinders was 386 °F. For the 6 in. diameter by 12 in. high cylinders, the maximum temperature was 381 °F. The 4 in. diameter by 8 in. high cylinder reached its maximum temperature after approximately 5 hours. The 6 in. diameter by 12 in. high cylinder took significantly longer to reach its maximum temperature. From these results, it was decided to allow all cylinders 24 hours of heating before being tested.

Specimen types CN0-400, CN8-400, CN16-400 and TN16-400-1, comprising 15 cylinders, were placed in the oven when it was not preheated. Twenty one additional cylinders, specimen types TN16-400, TN8-400 and CN16-cooled, were added 31 hours later. At 52 hours of heating, specimen types TF16-400, CF16-400 and CF8-400 were added to the oven. At this point in time several of the heated cylinders had been removed and tested but many cylinders still remained in the oven. Two hours later, TF8-400, CF0-400, TN0-400 and TF0-400 were also added to the oven. At this point in time many of the fully heated cylinders had been removed.

The addition of so many room temperature specimens caused the surface temperature of the remaining fully heated cylinders to decrease. The interior temperature of the cylinder was most likely maintained during the addition of the room temperature cylinders. However, since the recorded temperature value was that of the surface temperature, testing was delayed until the surface temperature of all cylinders once again reached the typical maximum readings. This would result in recorded temperatures that were more reflective of the interior temperature of the cylinder. The approximate amount of time each specimen was placed in the oven is shown in Table 3.1. This time varied depending on when the specimens were able to be tested.

The surface temperature of the cylinders was measured using a Fluke® 65 infrared thermometer. Temperatures were recorded as the cylinders came out of the oven and just prior to testing. The temperatures of the cylinders as they were coming out of the oven ranged from 352 ^{o}F to 407 ^{o}F, with an average temperature of 391 ^{o}F. Readings between 323 ^{o}F and 365 ^{o}F, with an average of 353 ^{o}F, were recorded just prior to

testing. By comparison, the room temperature cylinders had an average surface temperature of 63 ^{o}F.

3.7. Data Acquisition System

Personnel from Idaho National Laboratories (INL) provided testing equipment for the drop hammer facility. The load cells were owned and calibrated by INL engineers. A data acquisition system used to collect load cell and strain gauge data was also owned and operated by INL personal. INL engineers programmed the system for acquiring and filtering data.

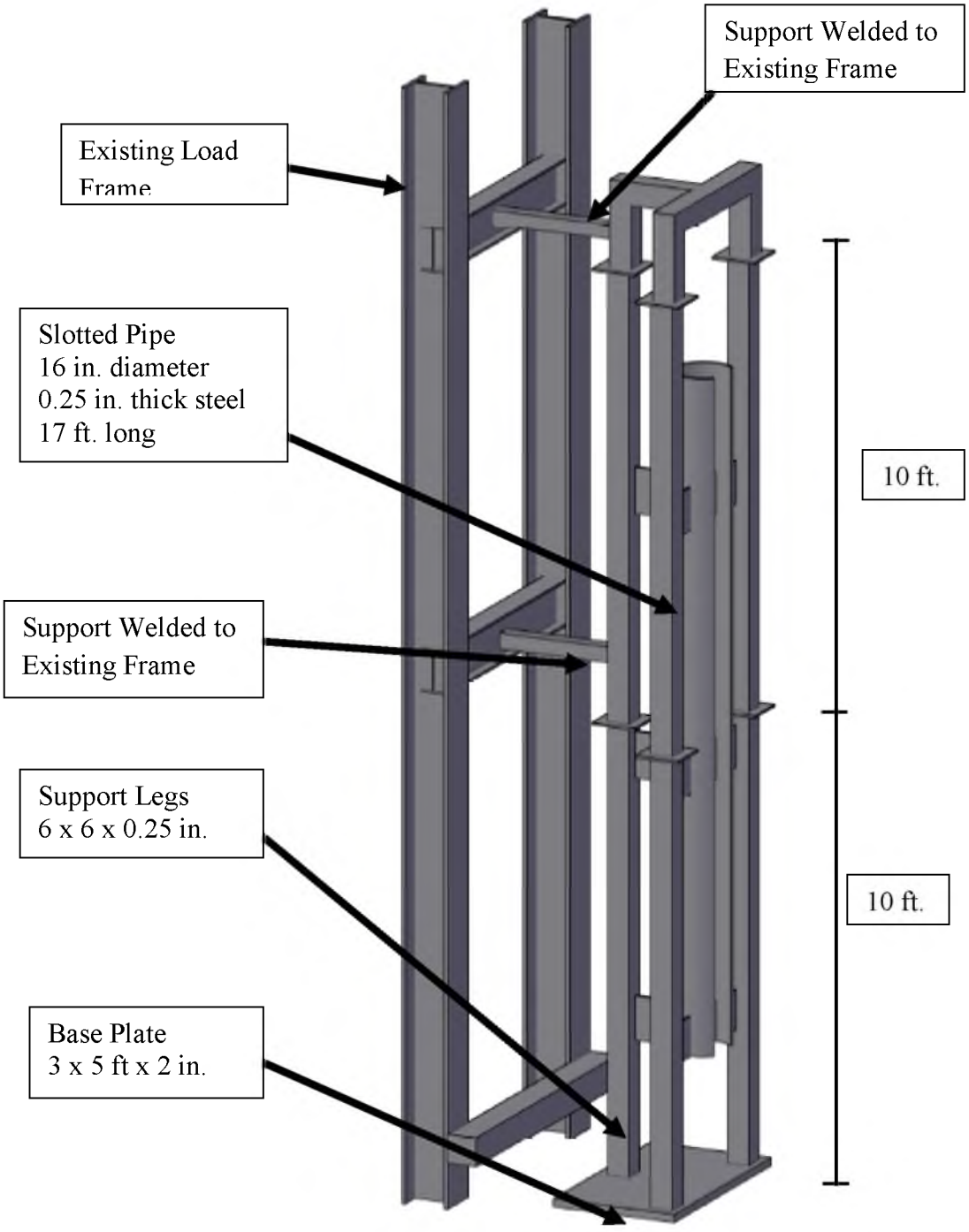

Figure 3.1 - Drop Hammer Facility Model
Courtesy of Timothy Garfield

Figure 3.2 - Drop Hammer Facility

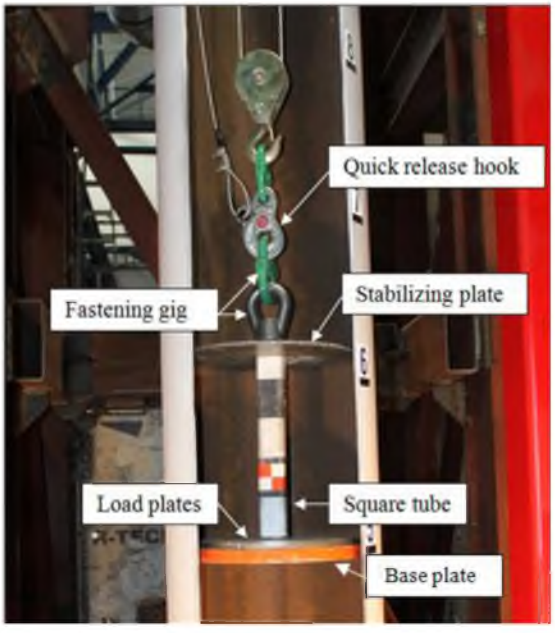

Figure 3.3 - Drop Hammer

Figure 3.4 - Electrical Cable Hoist

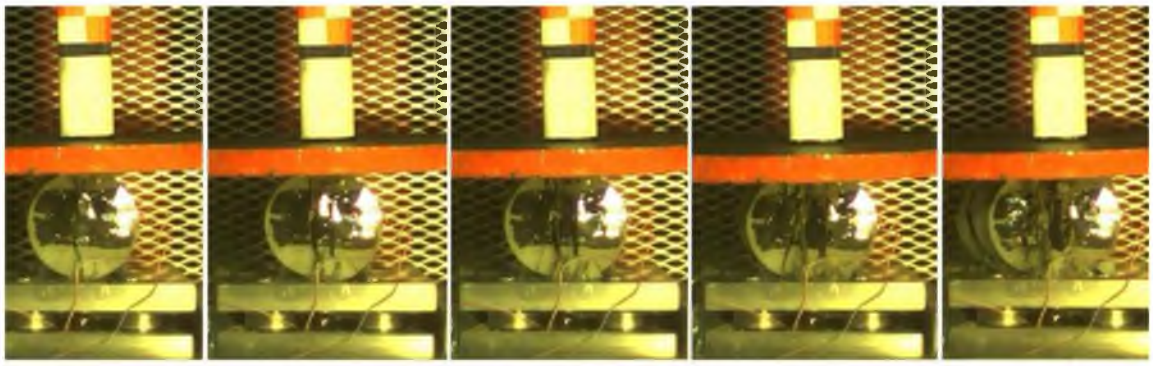

Figure 3.5 – Time-lapse of Tension Tests

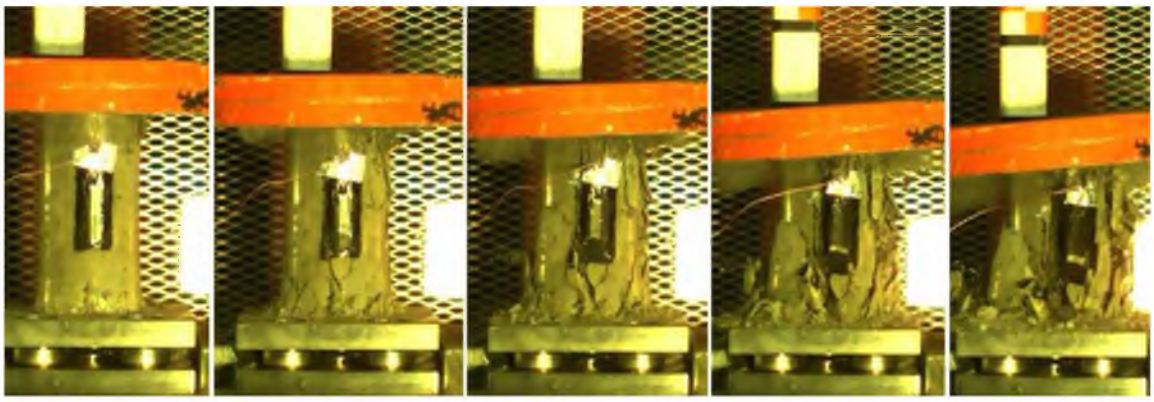

Figure 3.6 – Time-lapse of Compression Test

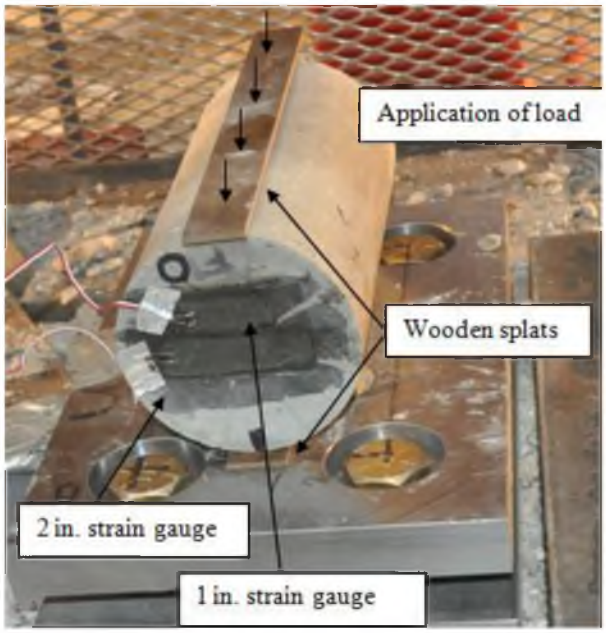

Figure 3.7 – Typical Strain Gauge Location and Cylinder Placement for Split Tension Tests

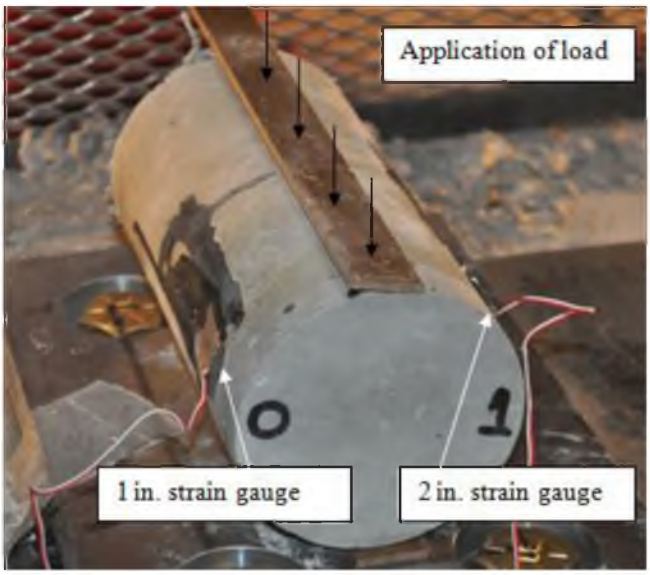

Figure 3.8 - Side Strain Gauge Location for Split Tension Tests

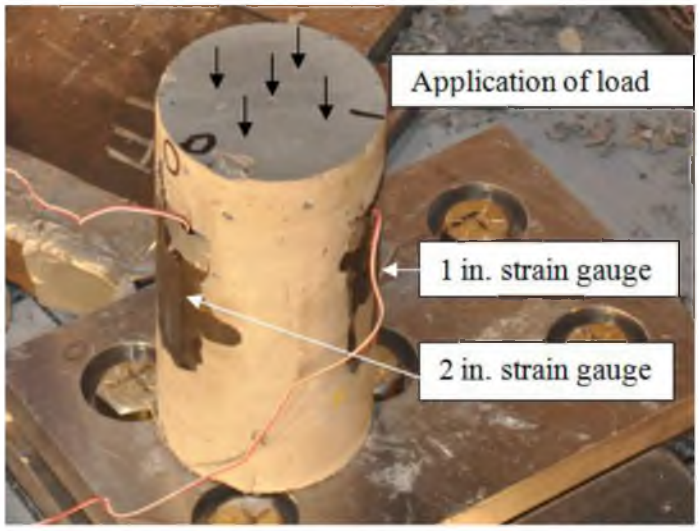

Figure 3.9 - Strain Gauge Location and Cylinder Placement for Compression Tests

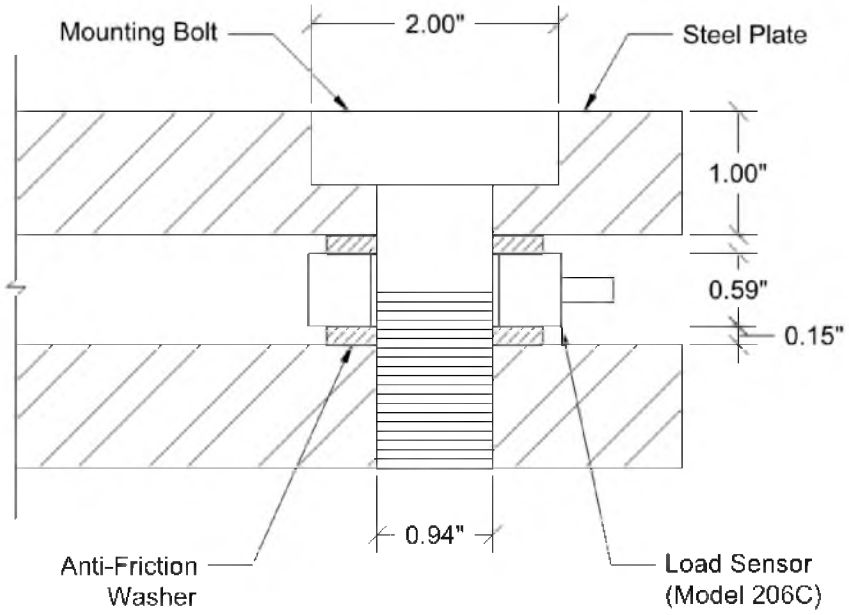

Figure 3.10 - Load Cell System Assembly

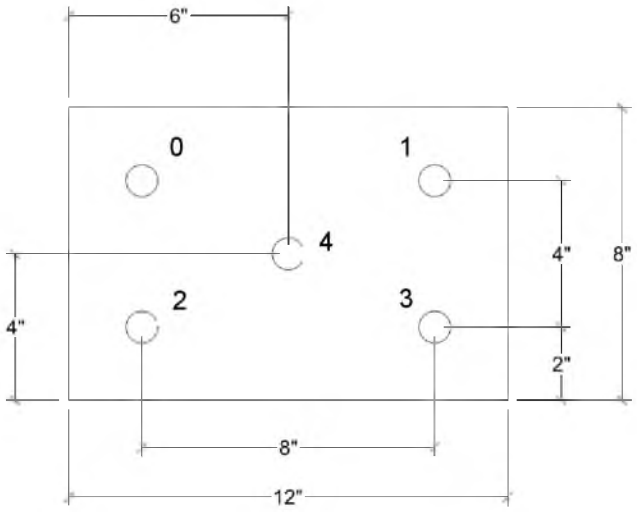

Figure 3.11 - Load Cell Layout

Figure 3.12 - Load Cell System Configuration, July 2011

Figure 3.13 - Model 206C ICP Dynamic Force Sensor

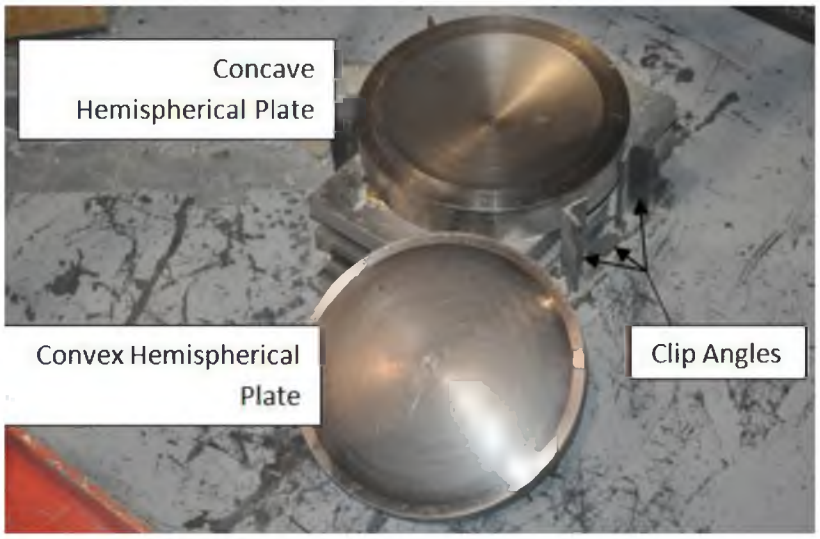

Figure 3.14 - Hemispherical Steel Plate and Load Cell Configuration, April 2012

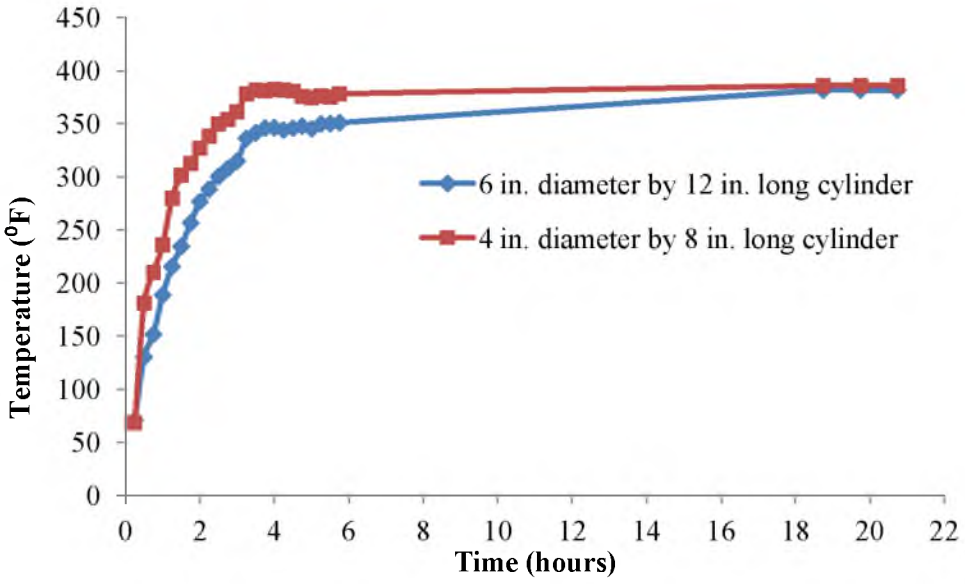

Figure 3.15 – Heating of Cylinders

Table 3.1 - Heating of Specimens

Specimen Type	Approx. Heating Time (hrs)	Specimen Type	Approx. Heating Time (hrs)	Specimen Type	Approx. Heating Time (hrs)
TF8-400	25.0	TF16-400	23.0	TF0-400	45.5
CF8-400	26.0	CF16-400	24.5	CF0-400	45.0
TN8-400	43.0	TN16-400[1]	44.0	TN0-400	45.0
CN8-400	53.0	CN16-400[2]	72.5	CN0-400	51.0
		CN16-cooled	49.0		

1. TN16-400-4-1 was heated for 74 hours
2. CN16-400-4-1 was only heated for 54 hours

4. TEST SETUP AND PROCEDURE

The test setup and procedure are described for the July 2011 and April 2012 dynamic tests. Details are also provided for the static tests that were performed in both July 2011 and April 2012. Information is also provided regarding the composition and casting of the concrete specimens used.

4.1. Concrete Specimens

The concrete cylinders used for drop hammer and static tests were cast following ASTM procedure C31 / C31M-10 Standard Practice for Making and Curing Concrete Test Specimens in the Field (2007). The cylinders were cast at the same time as structural panels used in research by a former University of Utah graduate student. The concrete was mixed by Hanson Structural Precast in Salt Lake City, Utah.

Several 4 in. diameter by 8 in. high cylinders along with 6 in. diameter by 12 in. high cylinders were cast from two batches of concrete. A water-to-cement ratio of 0.46 and 0.47 was used for the two concrete batches. Figure 4.1 shows 2 in. long Macro-synthetic polypropylene fibers that were added to the normal weight concrete. The density of fibers used was 1% by volume. The average 28 day compressive strength for the normal weight concrete and fiber reinforced concrete was 7400 psi and 6600 psi, respectively.

4.2. July 2011 Dynamic Tests

In July 2011 dynamic tests were performed on concrete cylinders considering three parameters: test type, concrete composition and drop height. The test types included compression and tension, the composition was either normal weight concrete (NWC) or fiber reinforced concrete (FRC), and the drop weight was released from either 8 ft or 16 ft. All combinations of parameters were considered and tested as shown in Table 4.1.

The cylinders were placed directly on top of the load cell system. For the tension test the cylinders were placed on their side directly in the middle of the five load cells as shown previously in Figure 3.7 and Figure 3.8. A wooden slat, similar to those used in static tests, was placed above and below the cylinders. Clay, or a small piece of aggregate, was used to stabilize the cylinders during tests and avoid rolling. For the compression tests the cylinders were placed in an upright position directly in the middle of three load cells to best distribute the load (Figure 3.9).

Prior to testing, trial tests were performed to determine what drop weight would be appropriate from a 16 ft and 8 ft drop height. The drop weights listed in Table 4.1 were believed to achieve results that would best represent proper failure of the cylinders.

4.3. April 2012 Dynamic Tests

Additional tests at elevated temperatures, with parameters similar to those used in July 2011 tests, were performed in April 2012. Both normal weight and fiber reinforced concrete was tested at 400 °F for each test type and drop height. The test matrix for the April 2012 dynamic tests is shown in Table 4.2. With the use of the hemispherical plate for the April 2012 tests, the cylinders were simply placed centrally on top of the hemispherical plate as shown in Figure 4.2 and Figure 4.3.

Only NWC cylinders were tested for room temperature tests since FRC specimens were not available. Tests on the same specimen types were performed in July 2011; however, different drop weights were used. The drop weight was modified from the July 2011 test in an effort to be more representative of the static test procedure. This was done be visually inspecting the failure mode of trial tests and determining which weight produced a failure mode most similar to static failure modes.

The change in drop weight was the reason for repeating the same room temperature tests in April 2012 that were performed in July 2011. Even though heated cylinders were not tested in July 2011 it was desirable to know what overall effects the change in drop weight would have on the results. Knowing the effects of the drop weight, it could be determined if it would be appropriate to make comparisons between the FRC room temperature tests performed in July 2011 with FRC heated specimen tests performed in April 2012 at different drop weights. An additional purpose for repeating tests at room temperature is the fact that concrete strength changes over time. For this reason room temperature static tests were also performed.

The results from the July 2011 tests were such that the concrete did not break completely (see Appendix A and Appendix B). This was the case more so for the compression tests than for the tension tests. Therefore, the drop weights were increased significantly for the compression tests and slightly for the tensions tests. It was desirable for each specimen type, and for every height, to have the same drop weight for comparison purposes. For example, every compression test with a drop height of 8 ft had a drop weight of 223 lbf. Table 4.3 shows each test type and its corresponding drop weight for both July 2011 and April 2012 tests.

To better understand and compare the dynamic impact that the different drop hammer weight and drop height combinations had, the potential and kinetic energy were determined. The potential energy (U) was computed by taking into account the weight (W) and height (h) of drop as shown in Eq. (4.1). The delivered kinetic energy (E_K) was calculated using the mass (m = W/g, where g=32.2 ft/sec) of the drop weight and the measured velocity (v) determined from the high speed cameras (as explained in Section 5.2). The velocity for the 8 ft and 16 ft drop heights was 21.2 ft/sec and 30.9 ft/sec, respectively. To determine the kinetic energy Eq. (4.2) was used.

$$U = W * h \tag{4.1}$$

$$E_K = \frac{1}{2} * m * v^2 \tag{4.2}$$

The values for potential and kinetic energy are given for the July 2011 and April 2012 tests in Table 4.4 and Table 4.5, respectively. The average 10% difference between the potential and kinetic energy is from the frictional resistance that occurs when releasing the drop hammer, and from air resistance. The kinetic energy is considered as the impact energy delivered to the test specimen.

4.4. Static Testing

Static tests were performed to establish a basis for comparison with the dynamic drop hammer results. These tests were performed on the same day as the drop hammer tests to reduce any form of variability between specimens. Static tests were performed for both compression and split tension on both normal weight and fiber reinforced concrete. Due to the limited number of FRC specimens available in April 2012, some static tests

utilized 6 in. diameter by 12 in. high cylinders specimens so that all dynamic tests could be performed using 4 in. diameter by 8 in. high cylinders. The static test matrices are shown in Table 4.6 for the July 2011, and Table 4.7 for the April 2012 tests.

The configuration for the static compression test is shown in Figure 4.4. Two steel caps were placed on both ends of the cylinder to distribute the load evenly. The split tension tests were performed using a loading jig that held the cylinder on its side between two wood strips as shown in Figure 4.5. The loading jig held a steel rod directly over the center of the cylinder. A steel plate was then placed on top of the rod to distribute the load and achieve the desired split tension break.

4.5. July 2011 Dynamic Test Procedure

The procedure for the dynamic tests performed in July 2011 was as follows:

1. Test load cells and strain gauge connections periodically. Torque load cells or adjust strain gauge connections if necessary.
2. Prepare data acquisition and camera software.
3. Prepare drop hammer with appropriate weight and connect to electric cable hoist.
4. Connect strain gauges to the data acquisition system. Test wiring periodically with a volt meter to ensure correct readings are being recorded.
5. Raise the drop weight high enough to place the specimen centrally below the weight.
6. Place the cylinder with the correct orientation and in the correct location with respect to the load cell system.

7. Release the safety on the quick release hook and close the protective cage around the base of the drop hammer.
8. Raise drop weight to desired height.
9. Simultaneously begin data acquisition system, trigger camera and pull on quick release hook to drop weight.
10. Visually inspect and record break before removing specimen and debris.
11. Filter and save data collected from data acquisition system and high speed cameras.

4.6. April 2012 Dynamic Test Procedure

The procedure for the dynamic tests performed in April 2012 is listed below. Figure 4.6 through Figure 4.12 show visual implementation of the test procedure.

1. Test load cells and torque if necessary.
2. Prepare drop hammer with appropriate weight and connect to electric cable hoist.
3. Release the safety on the quick release hook and raise drop weight above safety bar location.
4. Insert safety bar into slotted pipe and raise weight to desired height.
5. Prepare data acquisition software.
6. Remove specimen from the oven and record temperature.
7. Place on cart and cover with Styrofoam box. Transport to drop hammer facility.
8. Place the cylinder in the correct orientation on the hemispherical plate and close the protective cage around the base of the drop hammer.

9. Measure and record temperature.
10. Remove safety bar.
11. Simultaneously begin data acquisition system, trigger camera and pull on quick release hook to drop weight.
12. Visually inspect and record break before removing specimen and debris
13. Filter and save data collected from data acquisition system.

4.7. Static Test Procedure

The procedure for static tests performed in July 2011 and April 2012 is listed below. Handling of heated specimens for static tests followed the same procedure as outlined in the April 2012 dynamic test procedure.

1. Set the Satec™ series Instron® machine to the appropriate loading rate
2. Place cylinder on Instron platform.
    a. For compression tests, place steel caps on the top and bottom of the cylinder.
    b. For tension test, place the cylinder in the loading jig.
3. Close the protective cage.
4. Raise the Instron platform until a minimal load is applied.
5. Arm the Instron machine and begin test.
6. Visually inspect and record break before removing specimen and debris
7. Filter and save data collected from data acquisition system.

4.8. Additional Static Tests for Compression Tests

Upon review of the initial test results, it was found that the DIF for the compression tests were much lower than expected. The DIF is inversely proportional to the static strength of the concrete. It is also a ratio of the dynamic to static strength. For the best results, the dynamic and static tests need to be performed in as similar a manner as possible to reduce variability. The static tests were performed using a steel cap, which is the standard method to determine compressive strength of concrete. However, it was not practical to utilize the caps in the dynamic tests.

The steel caps are used to evenly distribute load to the cylinder, which results in a higher strength and a lower DIF. Considering this fact, it was decided to perform additional static tests without using the steel caps. This would result in better uniformity between the dynamic and static test methods. In place of the steel caps, the hemispherical plate used in the dynamic tests was also used in the additional static tests, thus producing the most similar test setup possible.

The additional static tests were done in December 2012 for the nonheated specimens and in February 2013 for the heated specimens. The only cylinders available from the same batch used in the dynamic tests were 6 x 12 in. The compressive strength of a 6 x 12 in. cylinder is comparable with a 4 x 8 in. cylinder when appropriate loading rates are used. However, the DIF is a ratio of maximum loads, which are not comparable between the two cylinder sizes. For this reason, an equivalent maximum load of a 4 x 8 in. cylinder ($P_{4x8\,equi.}$) was calculated using the maximum load of the 6 x 12 in. cylinders (P_{6x12}). The equivalent load is given in Eq. (4.3) for compression. In addition, a small

number of 6 x 12 in. FRC cylinders were used for tension tests in April 2012. An equivalent maximum load for tension tests is given in Eq. (4.4).

$$P_{4x8\ equi.} = \frac{P_{6x12}}{\pi * 6^2/4} * \frac{\pi * 4^2}{4} \tag{4.3}$$

$$P_{4x8\ equi.} = \frac{P_{6x12}}{(\pi * 6 * 12)/2} * \frac{(\pi * 4 * 8)}{2} \tag{4.4}$$

The equivalent load is the only property of these additional static tests that was considered. The original compression static tests performed with capped cylinders in July 2011 and April 2012 were considered for the compressive strength of the concrete. This compressive strength, as discussed later, is used to determine strain rates using elastic theory. This theory considers the compressive strength of the concrete, which is best represented by the capped tests.

Figure 4.1 - Polypropylene Macrosynthetic Fibers

Table 4.1 - July 2011 Dynamic Test Matrix and Specimen Nomenclature

Specimen Notation	Number of Tests	Test Type[1]	Composition	Drop Weight (lbf)	Drop Height (ft)
CN8	3	C	NWC	92	8
CF8	3	C	FRC	158	8
CN16	3	C	NWC	70.5	16
CF16	3	C	NWC	92	16
TN8	8	T	FRC	70.5	8
TF8	9	T	NWC	92	8
TN16	9	T	NWC	49.5	16
TF16	7	T	FRC	49.5	16

1. C = Compression, T= Tension

Table 4.2 - April 2012 Dynamic Test Matrix and Specimen Nomenclature

Specimen Notation	Number of Tests	Test Type[1]	Temper-ature	Composition	Drop Weight (lbf)	Drop Height (ft)
CN8-400	5	C	400°F	NWC	223	8
CF8-400	3	C	400°F	FRC	223	8
CN8-R	3	C	Room	NWC	223	8
CN16-400	5	C	400°F	NWC	136	16
CF16-400	3	C	400°F	FRC	136	16
CN16-R	3	C	Room	NWC	136	16
TN8-400	5	T	400°F	NWC	92	8
TF8-400	3	T	400°F	FRC	92	8
TN8-R	3	T	Room	NWC	92	8
TN16-400	5	T	400°F	NWC	53.5	16
TF16-400	3	T	400°F	FRC	53.5	16
TN16-R	3	T	Room	NWC	53.5	16

1. C = Compression, T= Tension

Figure 4.2 – Specimen Placement for Dynamic Split Tension Tests

Figure 4.3 - Specimen Placement for Dynamic Compression Tests

Table 4.3 - Change in Drop Weights

	Drop Weight (lbf)	
Specimen Type	**July 2011**	**April 2012**
CN8	92	223
CF8	158	
CN16	70.5	136
CF16	92	
TN8	70.5	92
TF8	92	
TN16	49.5	53.5
TF16	49.5	

Table 4.4 - Energy of Drop Hammer for July 2011

Specimen Type	Drop Weight (lbf)	Potential Energy (ft-lbf)	Kinetic Energy (ft-lbf)
CN8	92	736	643
CF8	158	1264	1104
CN16	70.5	1128	1046
CF16	92	1472	1365
TN8	70.5	564	492
TF8	92	736	643
TN16	49.5	792	734
TF16	49.5	792	734

Table 4.5 - Energy of Drop Hammer for April 2012

Specimen Type	Drop Weight (lbf)	Potential Energy (ft-lbf)	Kinetic Energy (ft-lbf)
CN8 **CF8**	223	1784	1558
CN16 **CF16**	136	2176	2018
TN8 **TF8**	92	736	643
TN16 **TF16**	53.5	856	794

Table 4.6 - July 2011 Static Test Matrix

Specimen Notation	Number of Tests	Test Type[1]	Composition
CN	3	C	NWC
CF	3	C	FRC
TN	3	T	NWC
TF	3	T	FRC

1.C = Compression, T = Tension

Table 4.7 - April 2012 Static Test Matrix

Specimen Notation	Number of Tests	Test Type[1]	Temperature	Composition
CN0-R	4	C	Room	NWC
CF0-R[2]	3	C	Room	FRC
CN0-400	4	C	400°F	NWC
CF0-400[3]	3	C	400°F	FRC
TN0-R	4	T	Room	NWC
TF0-R[2]	3	T	Room	FRC
TN0-400	4	T	400°F	NWC
TF0-400[3]	2	T	400°F	FRC

1.C = Compression, T = Tension
2. All specimens were 6 x 12 in. cylinder
3. One of the specimens was a 6 x 12 in. cylinder

Figure 4.4 - Static Compression Test

Figure 4.5 – Static Split Tension Test

Figure 4.6 - Drop Hammer Facility Set Up

Figure 4.7 – Despatch Oven

Figure 4.8 - Heated Cylinder

Figure 4.9 - Cylinder Transport

Figure 4.10 - Cylinder Placement

Figure 4.11 - Temperature Reading

Figure 4.12 - Data Acquisition System

5. DATA REDUCTION

Three software programs were used to reduce the information collected from the test equipment. Diadem, a Labview software program, was used to reduce data collected from the data acquisition system, which recorded data from the load cells and strain gauges. A video review program was used to review high speed camera recordings and take measurements at given time increments. Partner Material Testing software was used to record data for the static tests performed on the Satec series Instron.

5.1. DIAdem

DIAdem version 11.1, a Labview software program from National Instruments, was used to filter data collected from the data acquisition system. For each strain gauge, data was recorded for strain at a given point in time. For the load cells system, a load was recorded for each load sensor. A script was written in DIAdem that combined and filtered the five load sensors giving data for one load at a given point in time for each test.

5.2. Video Program

Phantom Cine Viewer v2.0 software, which allows high speed videos to be played, was used to measure how the cylinder dimensions changed over time. Frames could be viewed approximately every 10^{-4} seconds.

The Cine Viewer has tools that can be used to make measurements on a given frame. Initially, a calibration is made; for the tension test the diameter of the cylinder,

and for the compression test the cylinder height were used to calibrate the measuring tool. The Cine Viewer also provides time information with accuracy of 10^{-6} seconds. Details about how the measurement tool and time were used to determine the strain rate in the Cine Viewer are discussed in the High Speed Camera Method section.

The measuring tool was also used to determine the velocity of the falling drop hammer. For the 8 ft drop hammer tests the average velocity was 21.2 ft/sec. For the 16 ft drop hammer tests the average velocity was 30.9 ft/sec.

5.3. Partner™ Material Testing

The program Partner™ Material Testing for Windows was used to operate and record data from the Satec™ Series Instron®. Partner records the load and corresponding time of the tests. By using the proper areas considering ASTM standard C496/C496M-04e1 (2004) for tension tests and C39/C39M -10 (2010) for compression tests, the compressive strength and strain were calculated. The data recorded could be exported to an Excel file, which could be used for further analysis. This was done to determine the strain rates and to verify the compressive strength using the initial raw data of measured load and time.

6. DATA ANALYSIS

Three main methods of determining the strain rate were explored: the high speed camera method, the load cell method and the strain gauge method. Each method was reviewed to decide which method to consider.

6.1. High Speed Camera Method

During the July 2011 tests, high speed cameras were used to record the tests. The high speed videos of the tests made it possible to visually see how the cylinder responded to dynamic loading. The breaking pattern for the different specimen types was better understood from video recordings. The visual data collected provided information that was used in the high speed camera method of determining strain rates.

The strain rates were calculated by measuring the change in size of the specimen as it was tested. For the tension tests, measurements of the cylinder diameter were taken for each recorded frame, which occurred approximately every 10^{-4} seconds. The change in diameter as the cylinder broke apart was divided by the time in which the change occurred, giving the strain rate. For the compression tests, the same procedure was used by measuring the change in height of the cylinder as it decreased while being loaded dynamically.

The strain rates were computed until the specimen crushed to a point where the diameter or height could no longer be measured from the video image. On average, this lasted $1.5\ x\ 10^{-3}$ seconds. Individual strain rates were computed over this time range for each specimen. That is, a strain rate was computed every 10^{-4} seconds for $1.5\ x\ 10^{-3}$ seconds. The maximum strain rate, which was considered to be the strain rate of the concrete specimen, generally occurred within $0.75\ x\ 10^{-3}$ seconds.

The high speed camera method introduces some error when measuring the width or height of the specimen. This was especially true for the compression tests which were difficult to measure because the drop weight obstructed the image of the cylinder. Also, the strain rate will be different depending on which location on the cylinder the measurement is made. Generally, the center of the specimen was found to better represent the specimen; however, it is difficult to guarantee that you are measuring the same portion of the cylinder as it breaks. Measuring the change in length on the end (considered for tension tests) or side (considered for compression tests) of the specimen corresponds to a local strain rate. Therefore, the high speed camera method does not represent the overall strain rate of the specimen.

6.2. Load Cell Method

The load cell method considers the data collected from the load cells and then applies elastic theory to determine the strain rate for each specimen. This method was employed by Millard et al. (2010). The first step in this method is to determine the loading rate. This was done by plotting the filtered load data. For example, Figure 6.1 shows the filtered load versus time data for a fiber reinforced specimen tested in tension

at a drop height of 16 ft (TF16). The load versus time plots show the individual loads for each load sensor (see Figure 3.11 for load sensor layout), the total load for all load sensors and the filtered load, which was considered during analysis (see Appendix C and Appendix D). The only portion of the graph considered when determining the loading rate was from initial loading to peak load. The point of initial loading was not always definitive and required some judgment as to where it should begin.

To determine the loading rate, various methods were explored. First, the loading rate in between each data point was determined. For this approach, the loading rate was considered to be the average of the individual loading rates. Second, a linear regression line was computed, in which the loading rate was taken as the slope of the regression line. Lastly, only the maximum value of the individual loading rates in between each data point was determined. The first two methods depend on the point of initial loading; the last method does not, making it a more standardized approach. Using the maximum value also proved to be the most consistent among various tests, therefore, this was the approach used to determine the loading rate for all specimens.

Once the loading rate (P_R) was determined, elasticity theory was applied. This method assumes that the relationship between stress and strain is linear. To compute the strain rate the compressive strength (f_c') was determined for NWC and FRC specimens. For the July 2011 tests the average compressive strength for CN and CF static tests were computed. For the April 2012 tests the average compressive strength for CF0-R and CN0-R were computed. These specimens were tested at room temperature; their compressive strengths are most representative of the concrete material and are therefore used to calculate the modulus of elasticity. Assuming the weight of concrete to be normal

weight (145 pcf), and f_c' is given in ksi units, Eq. (6.1) was used to determine the modulus of elasticity for NWC and FRC for both July 2011 and April 2012 tests.

$$E_c = 1746\sqrt{f_c'} \tag{6.1}$$

The stress rate was then determined using the measured loading rate and the appropriate area according to ASTM standard C496/C496M-04e1 Standard Test Method for Splitting Strength of Cylindrical Concrete Specimens (2004) and C39/C39M -10 Standard Test Method for Compressive Strength of Cylindrical Concrete (2010). The area used for tension is half of the side surface area, as shown in Figure 6.2 (a). The area used for compression is the cross sectional area of the cylinder as shown in Figure 6.2 (b). The stress rate was then determined using the calculated modulus of elasticity and appropriate area. Eq. (6.2) was used for the tension tests and Eq. (6.3) was used for the compression tests. For both equations, D is the cylinder diameter and L is the cylinder height; these equations give the stress rate in (ksi/in.). Finally, stress-strain properties were used to determine the strain rate in (in./in./sec) using Eq. (6.4).

$$\sigma_{R,Tension} = \frac{P_R}{A_{Tension}} = \frac{P_R}{(\pi * D * L)/2} \tag{6.2}$$

$$\sigma_{R,Compression} = \frac{P_R}{A_{Compression}} = \frac{P_R}{(\pi * D^2)/4} \tag{6.3}$$

$$\varepsilon_R = \frac{\sigma_R}{E_c} \tag{6.4}$$

6.3. Strain Gauge Method

Depending on the specimen type, compression versus tension test, and 16 versus 8 ft drop, the strain gauge data varied greatly. Examples of different plots of strain versus time are shown in Figure 6.3 through Figure 6.6. See Appendix E for each specimen type.

Some approaches initially taken included: (a) using a moving average from the initial strain to the peak, (b) using an average of the moving average of the first and second portions (shown in Figure 6.3), (c) using an overall average from initial to peak strain, and (d) using the average of the two slopes where the plot changes from the first to the second portion. In some tests, different approaches were taken depending on the type of data available. The various methods used produced drastically different results within a single specimen and were not repeatable for any given specimen type.

After considering the load cell and high speed camera methods, it was observed that the peak plateau seen in a majority of the strain data was a result of the strain gauge reaching capacity. It was also determined that the data collected, after the strain began to decrease, was representative of the strain rate. For this reason, two new methods for determining the strain rate were considered. First, the strain rate was taken from the point in time when the strain began increasing significantly, up to the peak strain. Similarly, the strain rate was determined using the strain rate of the decreasing strain after the plateau was reached. The average of the absolute value of the two strain rates before and after the plateau was then considered to be the true strain rate.

The second method also considered the strain rates before and after the plateau. However, it considered the absolute average of single strain rates one data point prior to and after the plateau. That is, it only considered the second portion of the data. Both of

these methods required judgment to determine which time values should be considered and which peak values were most appropriate in cases where the strain gauge did not reach capacity (when there was no plateau). There were also graphs that varied greatly as was shown in Figure 6.3 through Figure 6.6. This made it difficult to take a consistent approach in the analysis of the data. However, the first approach had the most consistent results and was determined to be the best method; it was used to determine the strain rate.

Once refined, comparisons between the three methods of determining strain rates were made. Values determined for each method are shown in Table 6.1 for tests with an 8 ft test height. Tests done with a 16 ft test height are shown in Table 6.2. These results are also shown graphically in Figure 6.7, which is a plot of strain rates versus the ratio of dynamic to static load.

From Figure 6.7 it can be seen that the strain gauge and high speed camera methods for determining the strain rate produced very similar results. This is expected, since both methods represent a local strain rate measured at a similar location on the cylinder. The load cell method had strain rates that were significantly lower than the other two methods. It was also the method that best represented the cylinder as a whole. As a whole, the cylinder would be able to better resist the dynamic impact, thus having a lower strain rate.

For the purpose of these tests, a global representation of the dynamic impact effect is desired. Therefore, the load cell method was used to further analyze the effects of reinforcement and temperature under dynamic loading.

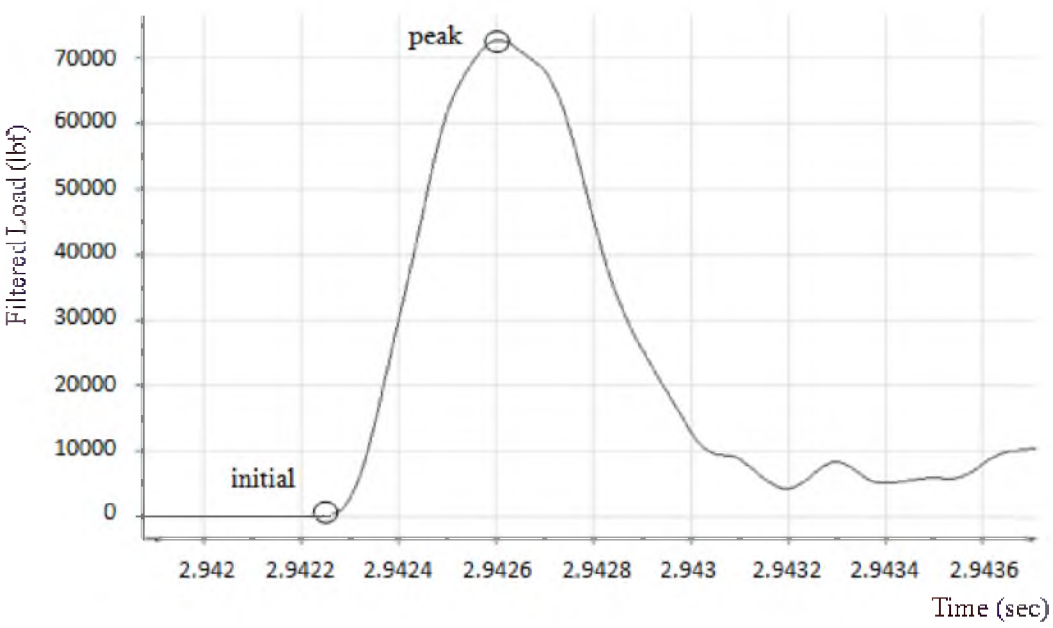

Figure 6.1 - TF16 Load Data

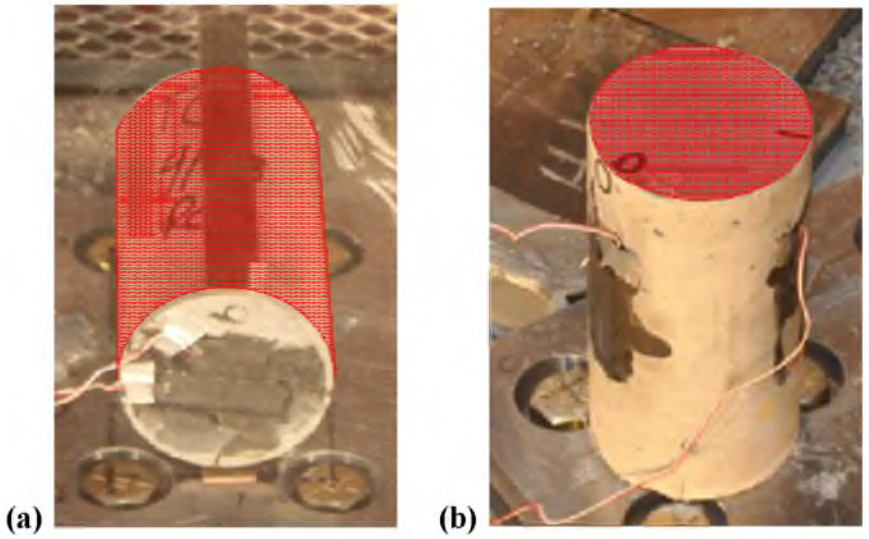

Figure 6.2 - Area Considered for (a) Tension and (b) Compression

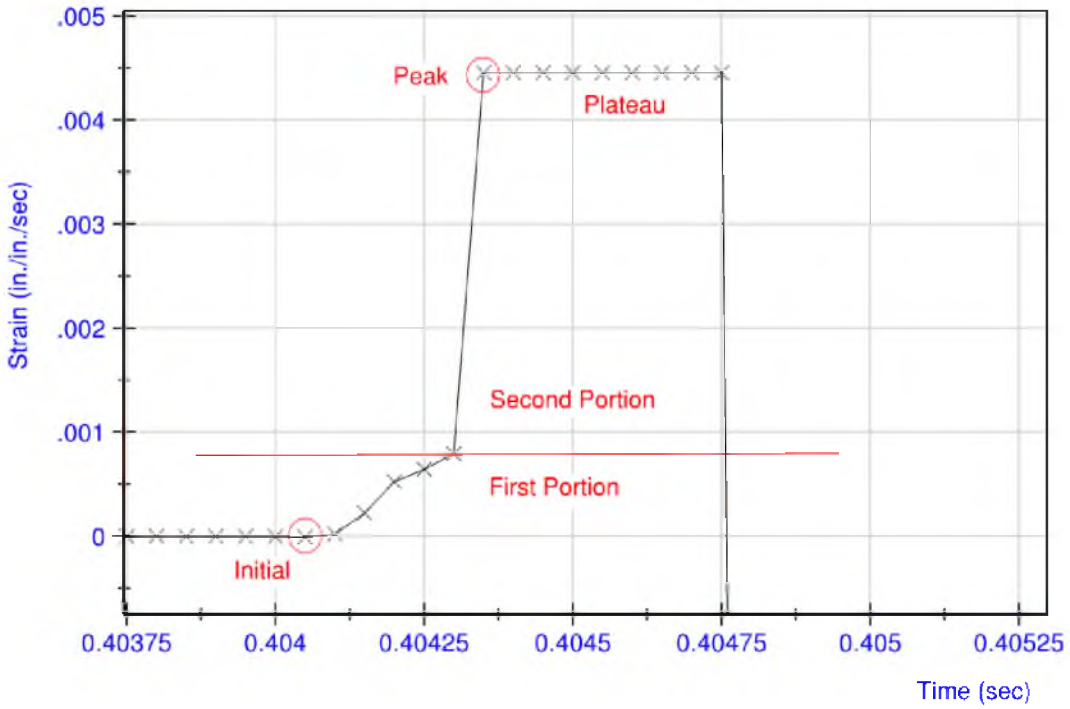

Figure 6.3 – TF16 Strain Data

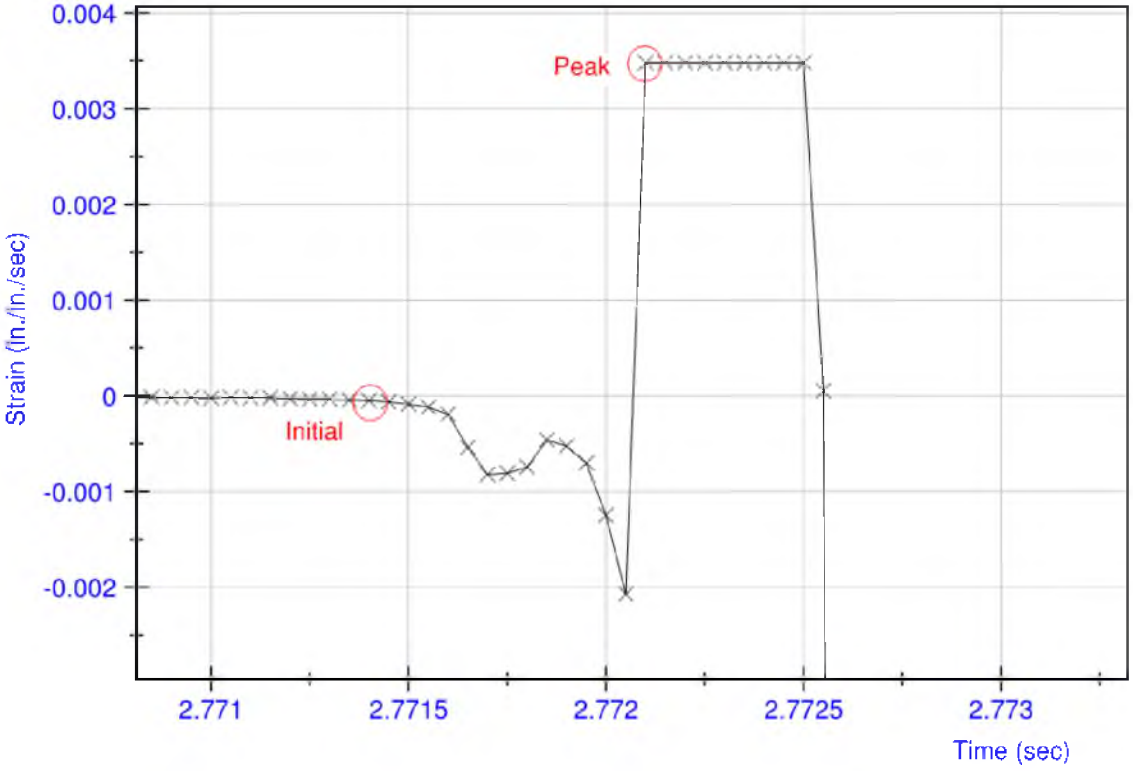

Figure 6.4 - CF16 Strain Data

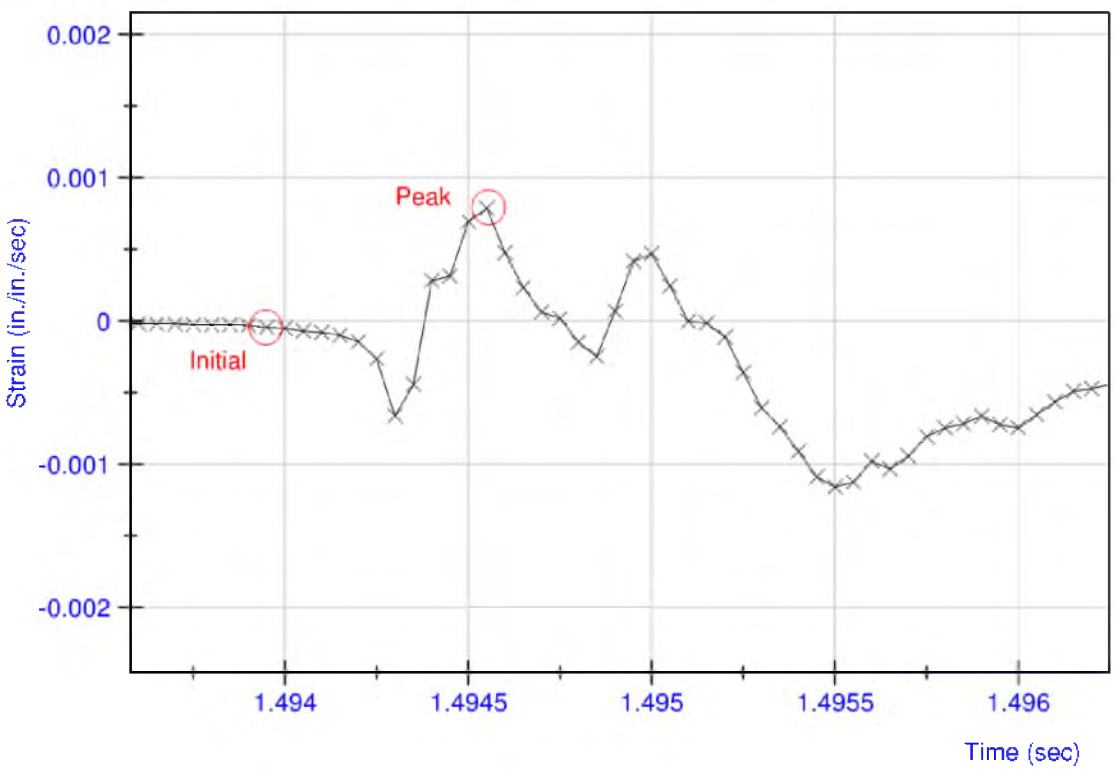

Figure 6.5 - CN16 Strain Data

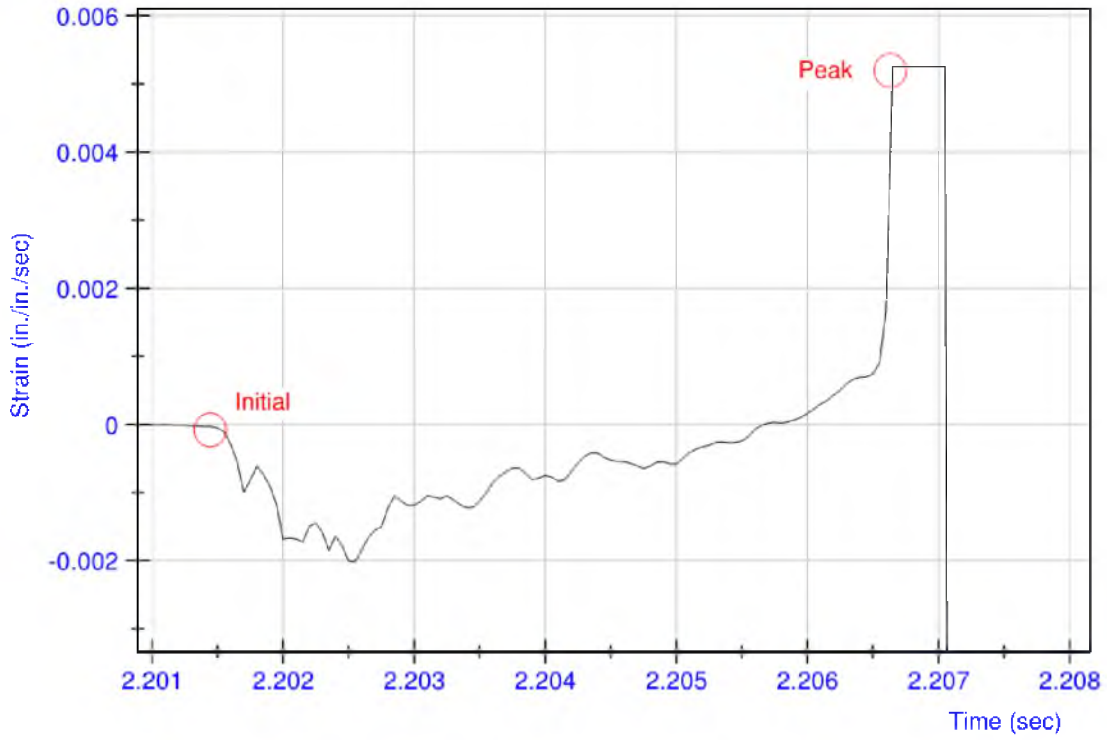

Figure 6.6 - CF8 Strain Data

Table 6.1 – Comparison of Strain Rate Methods for 8 ft Drop Height

	Strain Rates (1/sec)				
Specimen	**Camera**	**Strain Gauge 0**	**Strain Gauge 1**	**Load Cells**	**Maximum Filtered Load vs. Average Static Load**
TF8-1	94	N.A.	N.A.	N.A.	N.A.
TF8-2	95	385	201	1.411	2.432
TF8-3	65	199	199	1.165	2.305
TF8-4	63	386	318	1.115	2.303
TF8-5	95	390	751	1.159	2.348
TF8-6	62	197	N.A.	0.868	1.922
TF8-7	95	N.A.	206	1.105	1.932
TF8-8	63	64	388	1.103	1.812
TF8-9	95	387	N.A.	1.223	1.852
CF8-1	51	308	N.A.	2.206	1.738
CF8-2	25	378	N.A.	4.152	1.528
CF8-3	47	N.A.	202	4.961	1.740
TN8-1	94	208	208	0.512	1.500
TN8-2	126	193	193	0.548	1.987
TN8-3	119	192	192	0.610	2.670
TN8-4	94	200	200	0.872	2.563
TN8-5	95	386	385	0.610	2.768
TN8-6	158	202	202	0.697	2.211
TN8-7	95	198	198	0.883	2.553
TN8-8	94	389	387	0.941	2.546
CN8-1	N.A.	216	N.A.	0.886	0.933
CN8-2	47	392	N.A.	3.152	1.193
CN8-3	31	235	235	1.881	1.205

Table 6.2 – Comparison of Strain Rate Methods for 16 ft Drop Height

	Strain Rates (1/sec)				
Specimen	**Camera**	**Strain Gauge 0**	**Strain Gauge 1**	**Load Cells**	**Maximum Filtered Load vs. Average Static Load**
TF16-1	95	201	204	0.619	1.621
TF16-2	95	196	N.A.	1.274	2.384
TF16-3	127	386	N.A.	1.225	2.243
TF16-4	96	386	200	1.541	2.694
TF16-5	95	383	198	1.096	2.307
TF16-6	94	202	368	1.237	2.109
TF16-7	95	389	391	0.755	1.766
CF16-1	47	191	191	5.293	2.013
CF16-2	19	252	N.A.	9.429	2.328
CF16-3	48	209	243	5.551	1.893
TN16-1	157	388	N.A.	0.845	2.310
TN16-2	126	202	235	1.780	4.031
TN16-3	95	202	392	1.231	4.124
TN16-4	94	379	193	1.599	3.757
TN16-6	157	N.A.	N.A.	N.A.	N.A.
TN16-7	119	214	209	N.A.	N.A.
TN16-8	95	217	204	1.339	2.970
TN16-9	125	199	200	1.112	3.262
CN16-1	46	209	N.A.	3.761	1.536
CN16-2	24	543	203	4.945	1.979
CN16-3	47	342	363	5.259	1.977

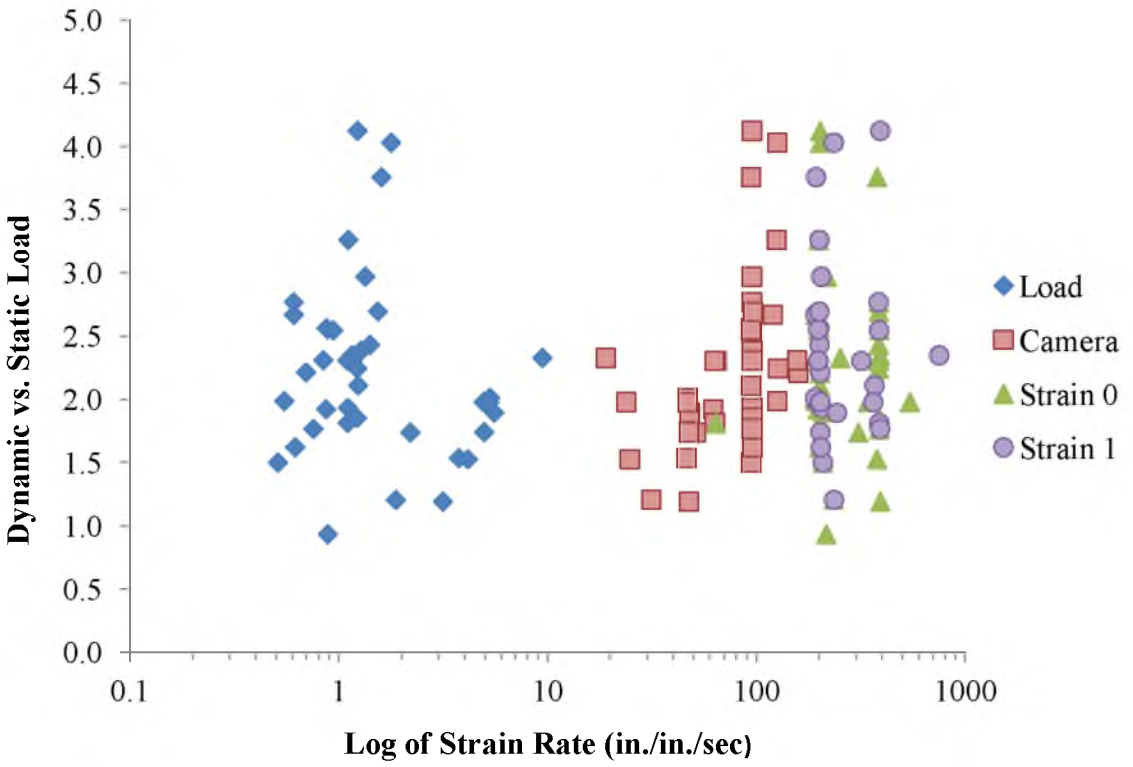

Figure 6.7 – Comparison of Strain Rate Methods

7. RESULTS

In several cases, comparisons had to be made between tests with different drop weights. For example, the drop weight for CN8 was 92 lbf in July 2011, whereas it was 223 lbf in April 2012. To evaluate the effect of the drop weight, the NWC room temperature tests from July 2011 were compared to the same tests performed in April 2012. For all tests the drop weights were increased from July 2011 to April 21012. It is important to know the significance of the change in drop weight to determine if proper comparisons can be made where only one variable is present.

The static compression test specimens in July 2011 had a compressive strength of 10900 psi, whereas the April 2012 test specimens had a compressive strength of 11000 psi. Similarly, the tension test strengths were 520 psi in July 2011 and 470 psi in April 2012. The strength of the concrete did not change significantly between the two test dates and is therefore not considered to be a variable. Similar results were also found for the FRC specimens.

The CN8 test drop weights increased from 92 lbf in July 2011 to 223 lbf in April 2012 and the average DIF increased from 1.1 to 1.5. For the CN16 specimens the drop weight increased from 70.5 to 136 lbf and the average DIF increased from 1.8 to 2.8.

The changes in drop weight for the tension tests were less extensive than the compression tests. For the TN8 tests the drop weight increased from 70.5 to 92 lbf. This

decreased the average DIF from 2.4 to 1.4. For the TN16 tests the drop weight increased from 49.5 to 53.5 lbf; this decreased the DIF from 3.4 to 2.2.

The result of increasing the drop weight by 142% for the CN8 tests had a similar effect as increasing the drop weight by 8% for the TN16 tests. Since a direct correlation between drop weights and resulting DIF and strain rates was not observed between July 2011 and April 2012, test types with different drop weight are believed to be comparable. To better compare test results and demonstrate the testing conditions, the kinetic energy is given along with the test results.

To summarize the dynamic test results, the DIFs are compared visually with the strain rates in Figure 7.1 for the July 2011 tests and in Figure 7.2 for the April 2012 tests. Similar dynamic research has been conducted to determine the relationship between strain rate and DIF as described in the literature review. It is important to note that the data available from previous research are from tests performed on a variety of different specimen sizes, none of which were concrete cylinders. These specimens were also tested using different mechanisms to deliver the dynamic force, one of which was the split-Hopkinson pressure bar.

Models for determining DIFs based on strain rates have been produced as previously reviewed by Malvar and Ross (1998). One model for compression was formulated by the CEB and is given in Eq. (1.1) through (1.4). This model is shown along with compression test results from July 2011 and April 2012 in Figure 7.3. For the tension tests, two models were proposed: the CEB model, given in Eq. (1.5) through (1.8), and the Modified CEB model by Ross, given in Eq. (1.9) through (1.12). Both of

these models, and the tension results for July 2011 and April 2012, are given in Figure 7.4.

For the tension tests, it can be seen that the majority of the data follows closely the trend of the Modified CEB model. The Modified CEB model is a much better representation of the results than the CEB Model. The Modified CEB model conservatively predicts lower DIF than those determined from the test results. This is true with the exception of several heated test specimens. A couple of TN16-400 and TN8-400 specimens had lower DIF than what was predicted by the model. However, it can be seen that specimens of these same categories had DIF well above the model prediction. This shows the wide variability of results produced by the heated cylinders. A single TF8-400 specimen even had a DIF lower than 1.0, which in this case is considered to be an outlier.

The results of the dynamic compression tests, when compared to the static compression tests performed without steel caps, follow the trend of increasing DIF with increasing strain rate given by the CEB model for compression. The results show that the CEB model is much more conservative than the Modified CEB model for tension. However, in some instances, at lower strain rates, the model is slightly unconservative. The single CN8 specimen with a DIF less than 1.0 is considered to be an outlier.

See Appendix F for additional DIF versus strain rate graphs. A plot of the tension tests at 400 ^{o}F is given to compare the results of NWC and FRC, thus comparing the effects of fiber reinforcement at elevated temperatures. Graphs can be used to better understand the results for each individual variable, and also show the CEB and Modified CEB (Ross) models for further comparison.

To review the results of the drop hammer tests more extensively, comparisons were made between drop heights of 8 ft and 16 ft for NWC and FRC at room temperature and between a drop height of 8 ft and 16 ft for NWC and FRC at elevated temperatures. Comparisons were also made between NWC and FRC at room temperature and between NWC and FRC at elevated temperatures. Finally, comparisons were made between room and elevated temperatures for both NWC and FRC. See Appendix C for July 2011 and Appendix D for April 2012 dynamic load data. See Appendix A for July 2011 and Appendix B for April 2012 static and dynamic test results.

7.1. Drop Height Comparison at Room Temperature

Results for the July 2011 tests are shown in Table 7.1 for static tests, and Table 7.2 for dynamic tests with an 8 ft drop height and Table 7.3 for dynamic tests with a 16 ft drop height. Also included in Table 7.1 are the results of additional room temperature compression tests performed without steel caps in December 2012. When comparing results, average DIFs are reported for each specimen type. Note that in some cases this average is taken from the results of only three tests. Therefore, the range of values can be significant; refer to the results tables for more comprehensive comparisons.

The impact energy, as discussed in Section 4.3, is a function of drop height and drop weight. It is used to better understand and compare the test parameters for each specimen type. To determine the effect of the impact energy on DIF at room temperature, results from NWC specimens are compared. The TN8 specimens, having an impact energy of 492 ft-lbf, had an average DIF of 2.4. For the TN16 specimens, which had an impact energy of 734 ft-lbf, the average DIF increased to 3.4.

The CN8 specimens, having an impact energy of 643 ft-lbf, had an average DIF of 1.1. For the CN16 specimens, which had an impact energy of 1046 ft-lbf, the average DIF was 1.8.

The DIF for tension increased by 45% when the impact energy increased by 49%. Likewise, the DIF for compression increased by 65% when the impact energy increased by 62%. From these results, it can be seen that the increase in DIF is nearly equivalent to the increase in impact energy for both compression and tension NWC specimens.

The change in impact energy is also compared for FRC specimens. The TF8 specimens, having an impact energy of 643 ft-lbf, had an average DIF of 2.1. The TF16 specimens, having an impact energy of 734 ft-lbf, had a similar average DIF of 2.2. The increase in impact energy from the TF8 to the TF16 specimens was about 14%, which, as can be seen had little effect on the average strain rate and DIF. From these results it can be concluded that similar impact energies produce similar results. Thus, it is important to consider both drop height and drop weight when comparing results of drop hammer tests.

The CF8 specimens, having an impact energy of 1104 ft-lbf, had an average DIF of 1.7. For the CF16 specimens, which had an impact energy of 1364 ft-lbf, the average DIF increased to 2.1. The increase in impact energy from the CF8 to the CF16 specimens was about 24%; this resulted in a 25% increase in the average DIF. Similar to the NWC results, the increase in impact energy is nearly equivalent to the increase in DIF for FRC compression specimens. In Figure 7.5 and Figure 7.6 plots of impact energy versus DIF are given for compression and tension tests, respectively. These plots summarize the relationships that have been discussed in this section.

7.2. Drop Height Comparison at Elevated Temperature

Results for the April 2012 tests are shown in Table 7.4 and Table 7.5 for static tests, and Table 7.6 for dynamic tests with an 8 ft drop height and Table 7.7 for dynamic tests with a 16 ft drop height. Also included in Table 7.4 and Table 7.5, are the results of the additional elevated temperature compression tests performed without steel caps in February 2013. To determine the effects of the drop height at elevated temperature, NWC concrete specimens are compared. The TN8-400 specimens, which had an impact energy of 643 ft-lbf, had an average DIF of 1.7. For the TN16-400 specimens, which had an impact energy of 794 ft-lbf, the average DIF increased to 2.0.

The CN8-400 specimens, which had an impact energy of 1558 ft-lbf, had an average DIF of 2.0. Comparatively, for the CN16-400 specimens, which had an impact energy of 2018 ft-lbf impact energy, the average DIF decreased to 1.5 in./in./sec.

For heated NWC tension specimens, a 24% increase in impact energy resulted in a 20% increase in DIF. The increase in DIF was similar to the increase in impact energy for the room temperature NWC tension specimens. In contrast, for the heated NWC compression specimens, the DIF decreased by 25% when the impact energy increased by 30%. Therefore, heated NWC specimens when tested in compression have lower strength results at higher impact energies. This behavior is unexpected; it is recommended that additional tests are performed to verify the repeatability of these results.

The change in drop height is also compared for elevated temperature FRC specimens. The TF8-400 specimens, having an impact energy of 643 lbf, had a DIF of 1.3. For the TF16-400 specimens, which had an impact energy of 794 ft-lbf, the average DIF increased to 1.8.

The CF8-400 specimens, having an impact energy of 1558 ft-lbf, had an average DIF of 1.8. For the CN16-400 specimens, which had an impact energy of 2018 ft-lbf, the average DIF increased slightly to 1.9 in./in./sec.

For heated FRC tension specimens, a 24% increase in impact energy resulted in a 32% increase in average DIF. For the heated FRC compression specimens, a 30% increase in impact energy resulted in a 11% increase in average DIF. In comparison, when similar increases in impact energy were applied, the strength results for the heated FRC tension specimens increased at a higher percentage than the compression specimens. This was also true for the NWC, which actually had a reduction in strength.

Comparing test drop heights, and thus impact energies, is another way of comparing the effects of strain rate. The results explained in these last two sections on the effect of impact energy are similar to explaining how the strain rate affects the DIF. The CEB, and modified CEB models, as shown in Figure 7.3 and Figure 7.4, provide a correlation between strain rates and DIFs for both compression and tension. In addition, Figure 7.7 and Figure 7.8 show the relationship of strain rate versus impact energy for compression and tension tests, respectively.

7.3. Concrete Composition Comparison at Room Temperature

To compare the results of FRC specimens with NWC specimens, compression tests performed at room temperature are evaluated. For CN8 specimens the average DIF was 1.1, which increased by 50% to 1.7 for CF8 specimens. This increase may in part be due to the increased impact energy from 643 ft-lb for NWC specimens to 1104 ft-lbf for FRC specimens; an increase of 72%.

The change in impact energy was less extensive for compression tests with a drop height of 16 ft. The impact energy increased from 1046 ft-lbf for CN16 specimens to 1365 ft-lbf for CF16; an increase of 30%. The CN16 specimens had an average DIF of 1.8, which increased by 14% to 2.1 for CF16 specimens.

To draw a conclusion regarding the effects of FRC when tested in compression, comparisons must be made between the percent increase in DIF and impact energy. In the case of the 8 ft drop height specimens, the DIF increased by only 50% from NWC to FRC, whereas the impact energy increased by 72%. In the case of the 16 ft drop height specimens, the DIF increased by only 14% from NWC to FRC, whereas the impact energy increased by 30%. In both cases the increase in DIF is less than the increase in impact energy. Therefore, it can be concluded that FRC specimens tested in compression have lower DIF than NWC specimens.

Comparisons regarding concrete composition are also made for tension specimens. The TN8 specimens had an impact energy of 492 ft-lbf, which increase by 31% to 643 ft-lbf for TF8 specimens. The TN8 specimens had an average DIF of 2.4, which decreased by 13% to 2.1 for TF8 specimens. This decrease in DIF is even more prominent when it is considered that the impact energy actually increased between tests.

The same impact energy of 734 ft-lbf was used for the TN16 and TF16 specimens. The TN16 specimens had an average DIF of 3.4, which decreased by 37% to 2.2 for TF16 specimens.

Overall, for tension tests the average DIFs decreased when FRC was used in place of NWC. It is emphasized that the comparisons between concrete composition results for

both compression and tension specimens are not ideal since, in most cases, different impact energies were used.

7.4. Concrete Composition Comparison at Elevated Temperature

For elevated temperature compression tests an 8 ft drop height with a 1558 ft-lbf impact energy was used for both NWC and FRC. The average DIF decreased by 13% from 2.0 for CN8-400 to 1.8 for CF8-400. Additional elevated temperature compression tests were performed using a 16 ft drop height, which had an impact energy of 2018 ft-lbf. The average DIF increased by 30% from 1.5 for CN16-400 to 1.9 for CF16-400. Overall, when tested in compression at a lower impact energy, the addition of fibers to heated specimens caused a slight reduction in strength results. The opposite was true when tested at a higher impact energy, in which case the strength results increased with the addition of fibers.

For elevated temperature tension tests an 8 ft drop height with a 643 ft-lbf impact energy was used. The average DIF decreased by 19% from 1.7 for TN8-400 to 1.4 for TF8-400. For elevated temperature tension tests with a 16 ft drop height a 794 ft-lbf impact energy was used. The average DIF decreased by 11% from 2.0 for TN16-400 to 1.8 for TF16-400.

Overall, for both impact energies, the FRC specimens had lower strength results than the NWC specimens when heated and tested in tension. The decrease in strength results for the specimens tested with the higher impact energy was slightly less than the specimens tested with the lower impact energy. This can be related to the results of the compression tests, which had an increase in strength when tested at a higher impact energy. Therefore, it is concluded that FRC specimens generate lower strength results

than NWC when heated, but improve as the impact energy increases, especially when subjected to compressive forces.

7.5. Temperature Comparison for Normal Weight Concrete

For NWC specimens tested in compression, the average static strength decreased by 28% from 10919 psi at room temperature to 7905 psi when heated to 400 °F. For a list of all average static strengths from April 2012, refer to Table 7.8. More detailed static results are given in Table 7.1 for July 2011 tests and Table 7.4 and Table 7.5 for April 2012 tests.

For the dynamic tests, an 8 ft drop height having an impact energy of 1558 ft-lbf was used for elevated temperature compression tests on NWC. Heating the specimens increased the average DIF by 33% from 1.5 for CN8-R to 2.0 for CN8-400. For elevated temperature NWC compression tests with a 16 ft drop height a 2018 ft-lbf impact energy was used. Heating the specimen decreased the average DIF by 47% from 2.8 for CN16-R to 1.5 for CN16-400.

When comparing room temperature DIFs to elevate temperature DIFs, it is noted that the average static strength used to determine the DIF for the two temperature types is different. Therefore, the comparison between DIFs is a simultaneous comparison between both the dynamic strength and static strength. To determine how the different specimen types perform dynamically, the maximum dynamic loads can be compared instead of the DIF.

When average maximum dynamic loads are compared between room temperature and heated specimens with an 8 ft drop height, the results are nearly equivalent. CN8-R

and CN8-400 had average maximum dynamic loads of 72359 lbf and 73201 lbf, respectively. The results for the CN8-400 specimens had a large variability, ranging from 46496 lbf to 101491 lbf and only three cylinders were tested to determine the average maximum dynamic load for CN8-R specimens. Therefore, the comparisons between these tests are inconclusive and more specimens should be tested to determine the effects of temperature on NWC at elevated temperatures for lower strain rates.

The average maximum dynamic loads for CN16-R and CN16-400 specimens were 135267 lbf and 54589 lbf, respectively. Three CN16-R specimens were tested; their average maximum dynamic load ranges from 114367 lbf to 153630 lbf. Five CN16-400 specimens were tested; their average maximum dynamic loads ranging from 46374 lbf to 63759 lbf. From these results, it can be concluded the dynamic strength of CN16-400 specimens is lower than CN16-R specimens.

For NWC specimens tested in tension, the average static strength decreased by 24% from 521 psi at room temperature to 396 psi when heated to 400 ^{o}F. An 8 ft drop height with an impact energy of 643 ft-lbf was used for dynamic tests on NWC tension specimens at elevated temperatures. Heating the specimens increased the DIF by 21% from 1.4 for TN8-R to 1.7 for TN8-400. For NWC tension tests at 16 ft drop heights a 794 ft-lbf impact energy was used. Heating these specimens decreased the averages DIF by 10% from 2.2 for TN16-R to 2.0 for TN16-400.

Similar to the compression results, when average maximum dynamic loads are compared between room temperature and heated specimens tests in tension with an 8 ft drop height, the results are nearly equivalent. CN8-R and CN8-400 specimens had average maximum dynamic loads of 35736 lbf and 32883 lbf, respectively. Both

specimen types had similar variability in results. Three TN8-R specimens were tested with maximum dynamic loads ranging from 26799 lbf to 52990 lbf; five TN8-400 specimens were tested with maximum dynamic loads ranging from 20689 lbf to 54574 lbf. These results show that there is a slight decrease in dynamic strength when the specimens are heated.

The average maximum dynamic loads for TN16-R and TN16-400 specimens were 57494 lbf and 39278 lbf, respectively. Three TN16-R specimens were tested; their average maximum dynamic load ranges from 38653 lbf to 69992 lbf. Five TN16-400 specimens were tested; their average maximum dynamic loads ranging from 20896 lbf to 63753 lbf. From these results, it can be concluded that the dynamic strength of TN16-400 specimens is lower than TN16-R specimens.

Reviewing the NWC results for both compression and tension specimens, it is observed that when higher impact energies are applied, the maximum dynamic load is also higher. When heated, the decrease in maximum dynamic load was larger for specimens with higher impact energies, meaning that the strength of heated specimens is more negatively influenced when tested at higher impact energies.

A few additional compression tests with a drop height of 16 ft and a 2018 ft-lbf impact energy were performed for NWC specimens that were allowed to cool. Static tests were not performed on uncapped, cooled cylinders and therefore, DIF comparisons cannot be made. However, maximum dynamic load data is available for each CN16 specimen type. The average maximum dynamic load for the CN16-cooled, CN16-400 and CN16-R specimens was 98270 lbf, 54589 lbf, and 135267 lbf, respectively.

From the maximum dynamic load results it can be concluded that the cooled specimens perform better than the heated specimens, but do not perform as well as the room temperature specimens. It is recommended that additional cooled specimen tests be performed to determine the effects of additional variables, such as the use of FRC.

7.6. Temperature Comparison for Fiber Reinforced Concrete

For FRC specimens tested in compression, the average static strength at room temperature was 9338 psi. This strength decreased by 44% to 5253 psi when heated to 400 ^{o}F. For FRC specimens tested in tension, the average static strength decreased by 27% from 605 psi at room temperature to 443 psi when tested at 400 ^{o}F.

For elevated temperature FRC dynamic tests, comparisons are made between July 2011 (room temperature) and April 2012 (heated) tests since no room temperature tests were done on FRC specimens in April 2012. Impact energies of 1104 and 1558 ft-lbf (a 41% difference) were used for CF8 and CF8-400 specimens, respectively. The average DIF increased by 5% from 1.7 for CF8 to 1.8 for CF8-400 and the average maximum dynamic load decreased by 39% from 77422 lbf for CF8 to 47040 lbf for CF8-400 Impact energies of 1365 and 2018 ft-lbf (a 48% difference) were used for CF16 and CF16-400 specimens, respectively. The average DIF decreased by 6% from 2.1 for CF16 to 1.9 for CF16-400 and the average maximum dynamic load decreased by 46% from 96416 lbf for CF16 to 52321 lbf for CF16-400.

For elevated temperature FRC tension tests, similar drop weights were used in July 2011 and April 2012. An impact energy of 643 ft-lbf was used for both TF8 and TF8-400. The average DIF decreased from 2.1 for TF8 to 1.3 for TF8-400, a decrease of

37%. The average maximum dynamic load decrease by 54% from 64472 lbf for TF8 to 29711 lbf for TF8-400. Impact energies of 734 and 794 ft-lbf were used for TF16 and TF16-400 specimens, respectively. The average DIF decreased by 19% from 2.2 for TF16 to 1.8 for TF16-400. The average maximum dynamic load decreased by 41% from 65922 lbf for TF16 to 39114 lbf for TF16-400. For FRC tension tests at elevated temperatures the DIF decreased for both 8 ft and 16 ft drop heights when compared with corresponding room temperature test results.

In general, for the tension tests, similar impact energies were used when comparing the room temperature and heated specimens. It can be concluded that the increase in temperature reduces the DIF for tension members with fiber reinforcement. For the compression tests, not all of the comparisons are exact since different impact energies were used.

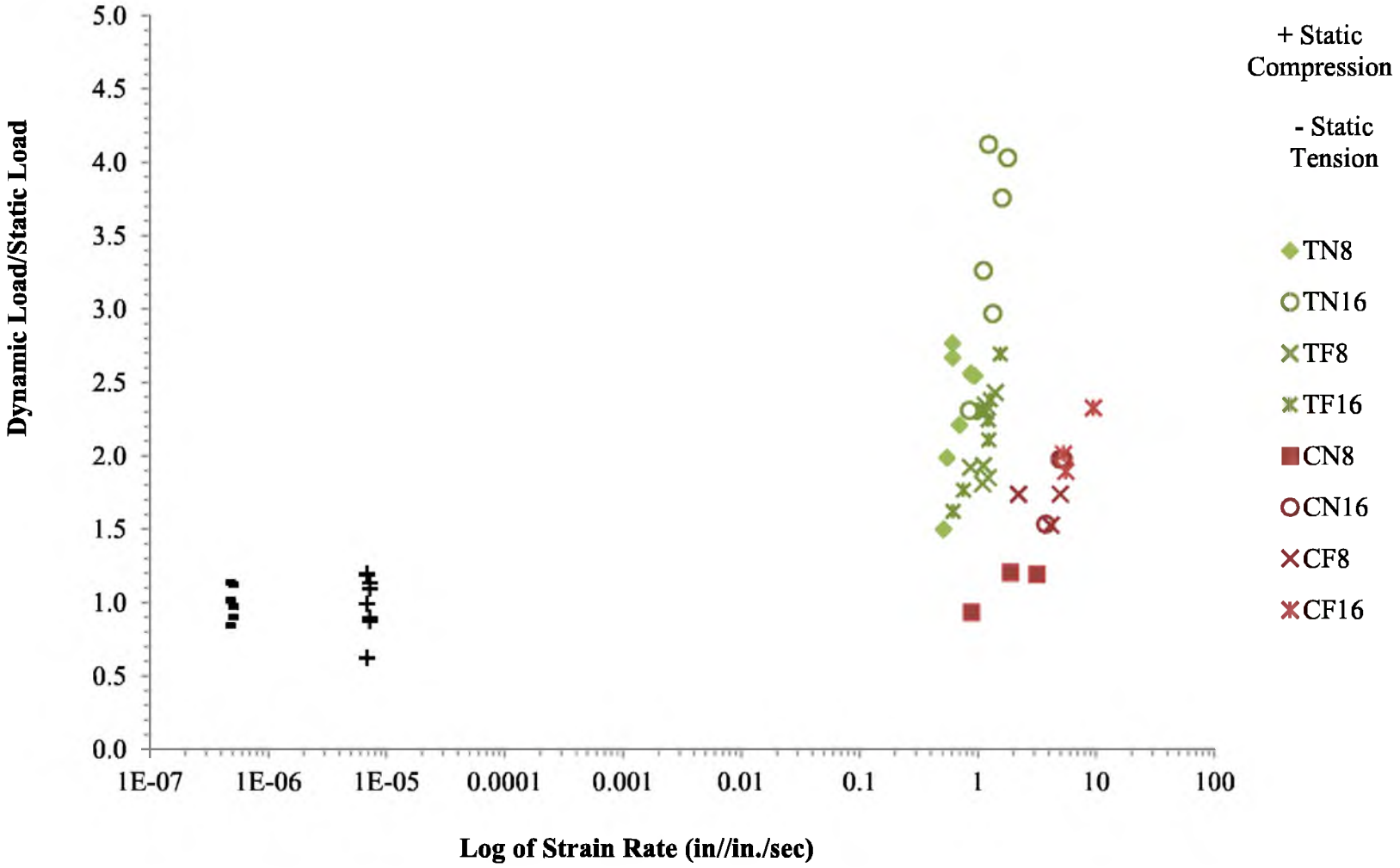

Figure 7.1 - Dynamic Increase Factor vs. Strain Rate for July 2011

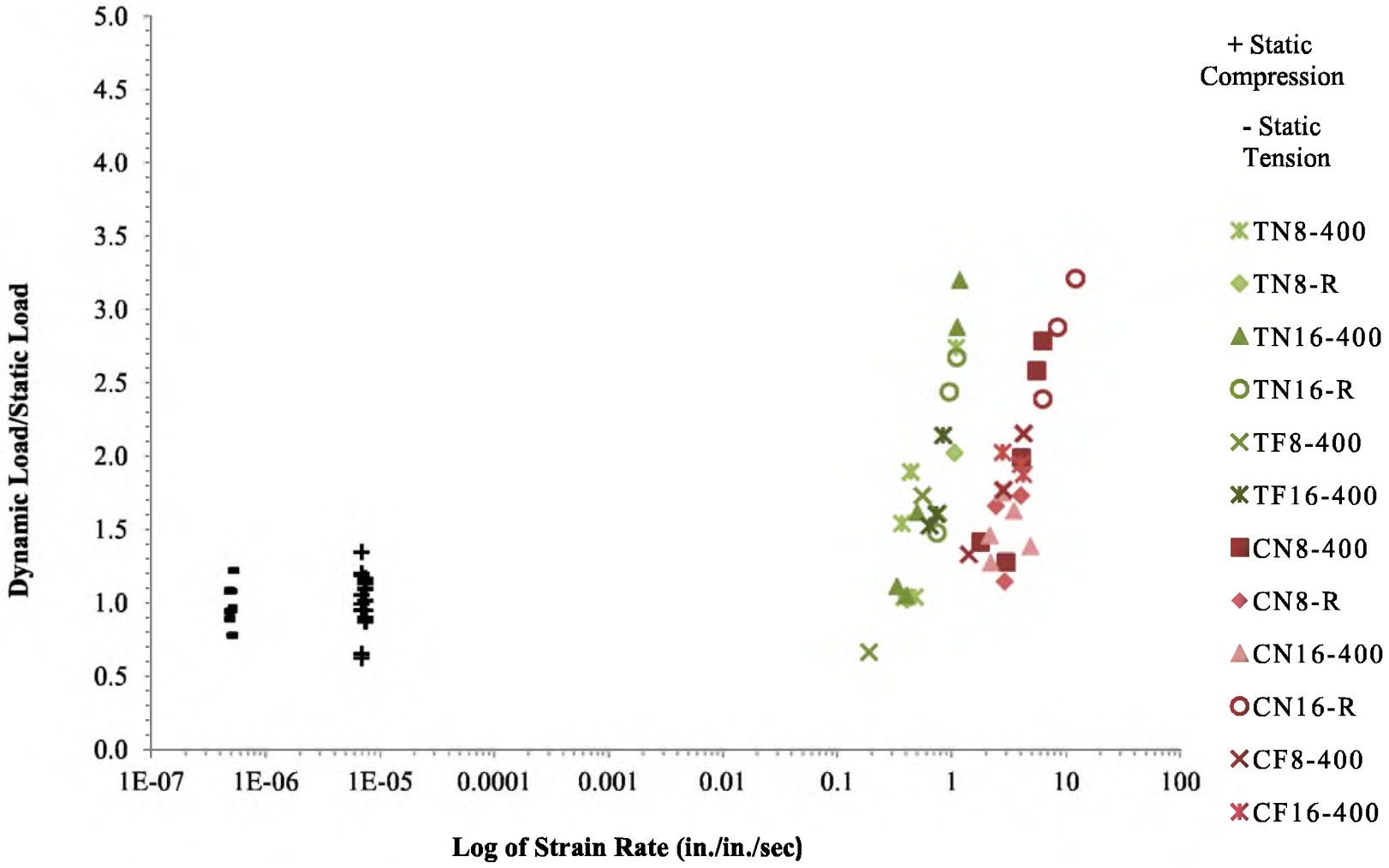

Figure 7.2 - Dynamic Increase Factor vs. Strain Rate for April 2012

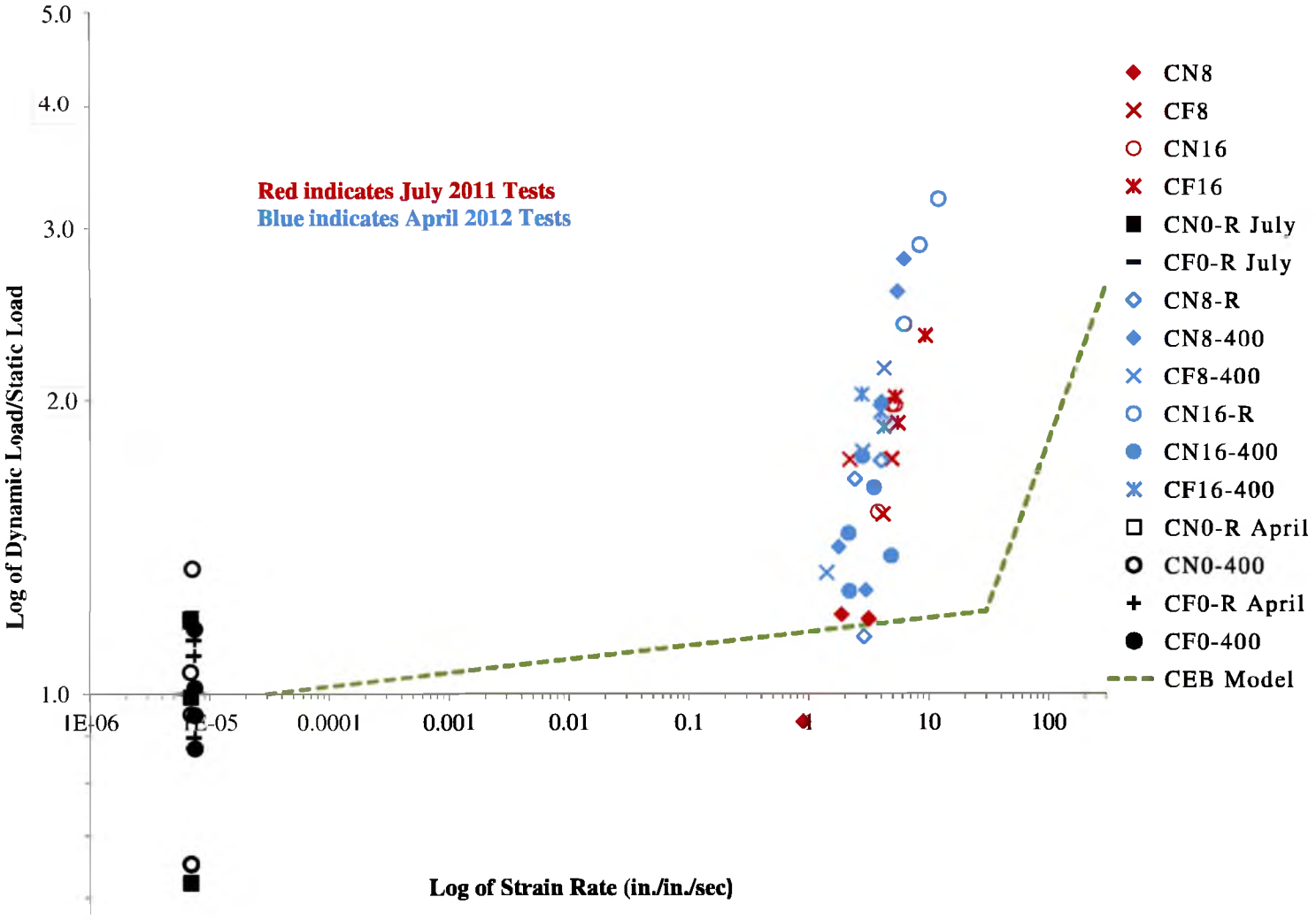

Figure 7.3 - Compression Dynamic Increase Factor vs. Strain Rate

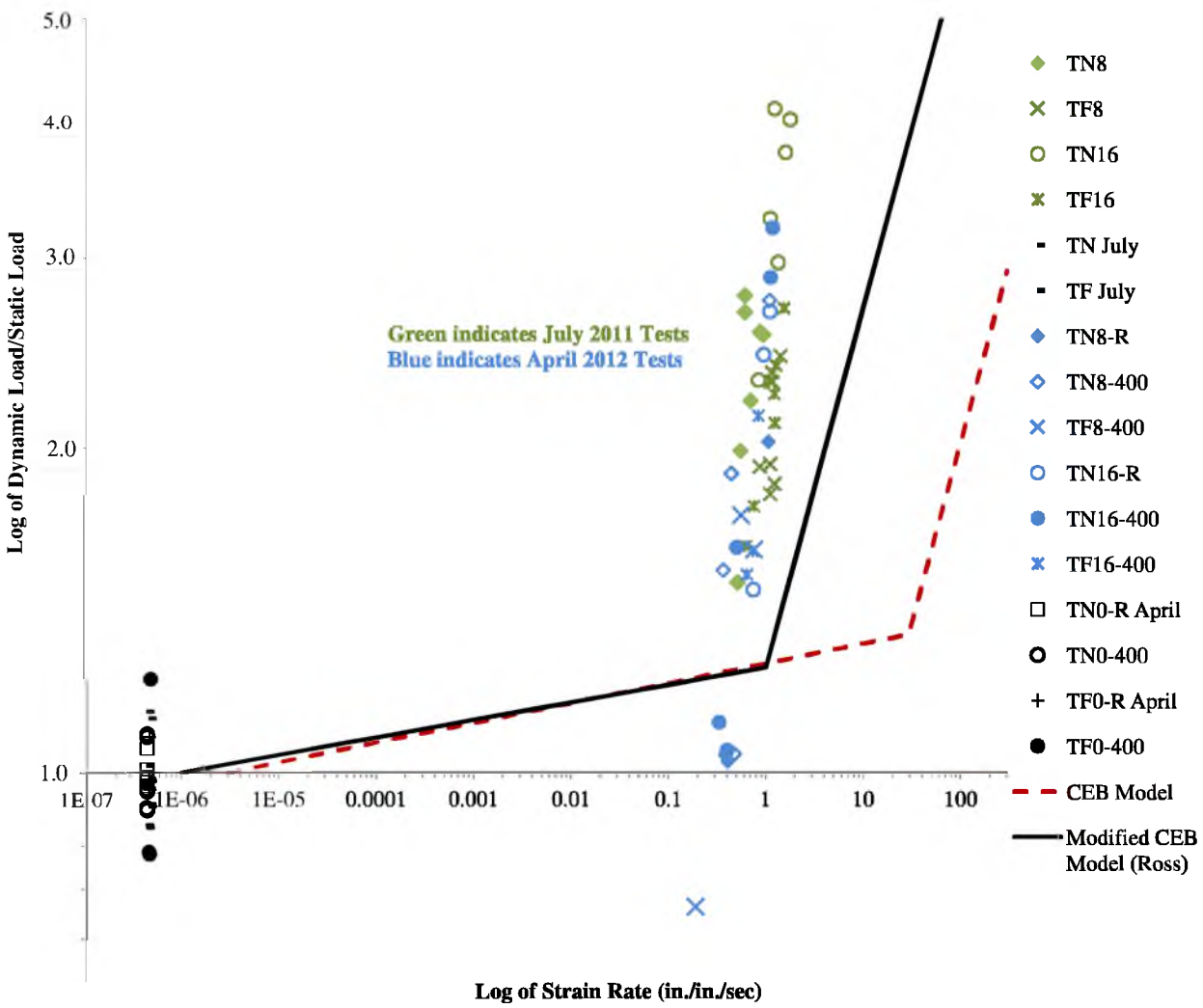

Figure 7.4 – Tension Dynamic Increase Factor vs. Strain Rate

Table 7.1 - July 2011, Static Test Results

Specimen ID	Strain Rates (in/in/sec)	Strength (psi)	Maximum Load (lbf)	Equivalent 4x8 Maximum Load (lbf)	Maximum Load/Maximum Average Load
TF-1	4.70E-07	592	29737	N.A.	0.975
TF-2	4.70E-07	682	34260	N.A.	1.123
TF-3	4.70E-07	548	27531	N.A.	0.902
Average		**607**	**30509**		
CF-1	-	9706	-	-	-
CF-2	-	9863	-	-	-
CF-3	-	10207	-	-	-
Average		**9926**			
CF0-R-6-1*	7.27E-06	4042	114290	50796	1.095
CF0-R-6-2*	7.27E-06	3312	93636	41616	0.897
CF0-R-6-3*	7.27E-06	4191	118504	52669	1.135
CF0-R-6-4*	7.27E-06	3225	91194	40531	0.873
Average		**3693**	**104406**	**46403**	
TN-1	4.46E-07	399	20071	N.A.	0.846
TN-2	4.46E-07	479	24093	N.A.	1.015
TN-3	4.46E-07	538	27024	N.A.	1.139
Average		**472**	**23729**		
CN-1	-	11130	-	-	-
CN-2	-	10951	-	-	-
CN-3	-	11008	-	-	-
Average		**11030**			
CN0-R-6-1*	6.89E-06	4563	129014	57340	1.198
CN0-R-6-2*	6.89E-06	2370	67007	29781	0.622
CN0-R-6-3*	6.89E-06	3776	106774	47455	0.992
CN0-R-6-4*	6.89E-06	4520	127804	56802	1.187
Average		**3807**	**107650**	**47844**	

*Tested without steel caps in December 2012

Table 7.2 - July 2011, 8 ft Test Results

Specimen ID	Strain Rate (in./in./sec)	Maximum Dynamic Load (lbf)	Average Maximum Static Load (lbf)	Dynamic/Static Load
TF8-1	N.A.	N.A.	30509	N.A.
TF8-2	1.411	74207		2.432
TF8-3	1.165	70312		2.305
TF8-4	1.115	70267		2.303
TF8-5	1.159	71637		2.348
TF8-6	0.868	58642		1.922
TF8-7	1.105	58950		1.932
TF8-8	1.103	55272		1.812
TF8-9	1.223	56488		1.852
CF8-1	2.206	80629	46403	1.738
CF8-2	4.152	70883		1.528
CF8-3	4.961	80755		1.740
TN8-1	0.512	35595	23729	1.500
TN8-2	0.548	47150		1.987
TN8-3	1.111	63353		2.670
TN8-4	0.872	60822		2.563
TN8-5	0.610	65674		2.768
TN8-6	0.697	52474		2.211
TN8-7	0.883	60578		2.553
TN8-8	0.941	60412		2.546
CN8-1	0.886	44634	47844	0.933
CN8-2	3.152	57063		1.193
CN8-3	1.881	57661		1.205

Table 7.3 - July 2011, 16 ft Test Results

Specimen ID	Strain Rate (in./in./sec)	Maximum Dynamic Load (lbf)	Average Maximum Static Load (lbf)	Dynamic/Static Load
TF16-1	0.619	49465	30509	1.621
TF16-2	1.274	72727		2.384
TF16-3	1.225	68444		2.243
TF16-4	1.541	82205		2.694
TF16-5	1.096	70384		2.307
TF16-6	1.237	64349		2.109
TF16-7	0.755	53882		1.766
CF16-1	5.293	93409	46403	2.013
CF16-2	9.429	108006		2.328
CF16-3	5.551	87833		1.893
TN16-1	0.845	54825	23729	2.310
TN16-2	1.780	95652		4.031
TN16-3	1.231	97850		4.124
TN16-4	1.599	89158		3.757
TN16-6	N.A.	N.A.		N.A.
TN16-7	N.A.	N.A.		N.A.
TN16-8	1.339	70477		2.970
TN16-9	1.112	77400		3.262
CN16-1	3.761	73496	47844	1.536
CN16-2	4.945	94661		1.979
CN16-3	5.259	94585		1.977

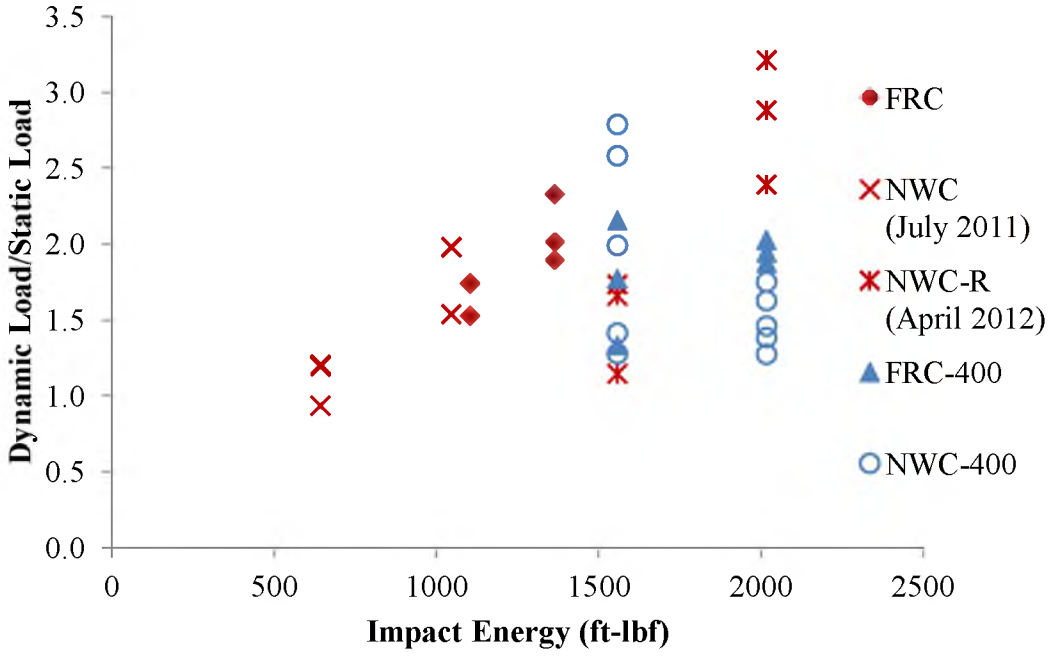

Figure 7.5 - Compression Dynamic Increase Factor vs. Impact Energy

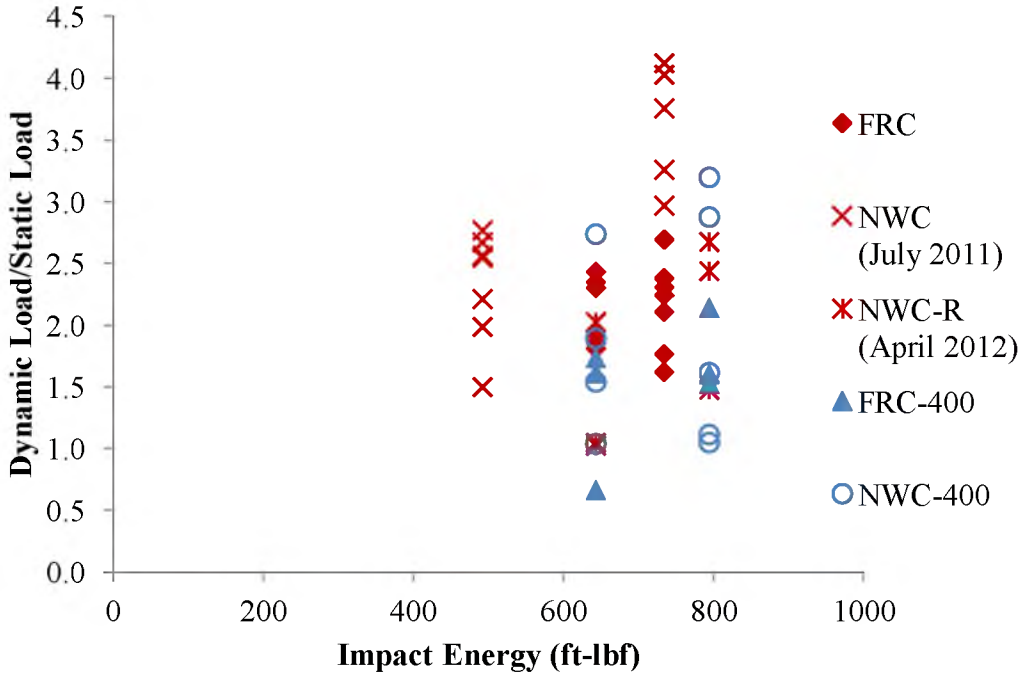

Figure 7.6 - Tension Dynamic Increase Factor vs. Impact Energy

Table 7.4 - April 2012, Static Test Results for Fiber Reinforced Concrete

Specimen ID	Strain Rates (in./in./sec)	Strength (psi)	Maximum Load (lbf)	Equivalent 4x8 Maximum Load (lbf)	Maximum Load/Maximum Average Load
TF0-400-4-1	4.85E-07	541	27173	N.A.	1.221
TF0-400-6-1	4.72E-07	345	39028	17346	0.779
Average		**443**	**33101**	**22259**	
TF0-R-6-1	4.72E-07	588	66462	29539	0.972
TF0-R-6-2	4.72E-07	574	64951	28867	0.949
TF0-R-6-3	4.72E-07	653	73822	32810	1.079
Average		**605**	**68412**	**30405**	
CF0-400-4-1	-	5107	-	-	-
CF0-400-4-2	-	5316	-	-	-
CF0-400-6-1	-	5336	-	-	-
Average		**5253**			
CF0-400-6-1**	7.49E-06	2166	61251	27223	1.014
CF0-400-6-2**	7.49E-06	1863	52687	23416	0.872
CF0-400-6-3**	7.49E-06	2026	57272	25454	0.948
CF0-400-6-4**	7.49E-06	2490	70403	31290	1.166
Average		**2136**	**60403**	**26846**	
CF0-R-6-1	-	9468	-	-	-
CF0-R-6-2	-	9791	-	-	-
CF0-R-6-3	-	8756	-	-	-
Average		**9338**			
CF0-R-6-1*	7.49E-06	4042	114290	50796	1.095
CF0-R-6-2*	7.49E-06	3312	93636	41616	0.897
CF0-R-6-3*	7.49E-06	4191	118504	52669	1.135
CF0-R-6-4*	7.49E-06	3225	91194	40531	0.873
Average		**3693**	**104406**	**46403**	

*Tested without steel caps in December 2012

**Tested without steel caps in February 2013

Table 7.5 – April 2012, Static Test Results for Normal Weight Concrete

Specimen ID	Strain Rates (in./in./sec)	Strength (psi)	Maximum Load (lbf)	Equivalent 4x8 Maximum Load (lbf)	Maximum Load/Maximum Average Load
TN0-400-4-1	4.48E-07	430	21637	N.A.	1.086
TN0-400-4-2	4.48E-07	374	18811	N.A.	0.944
TN0-400-4-3	4.48E-07	428	21505	N.A.	1.079
TN0-400-4-4	4.48E-07	353	17764	N.A.	0.891
Average		**396**	**19929**		
TN0-R-4-1	4.48E-07	525	26375	N.A.	1.008
TN0-R-4-2	4.48E-07	548	27554	N.A.	1.053
TN0-R-4-3	4.48E-07	513	25786	N.A.	0.985
TN0-R-4-4	4.48E-07	496	24956	N.A.	0.954
Average		**521**	**26168**		
CN0-400-4-1	-	8270	-	-	-
CN0-400-4-2	-	8154	-	-	-
CN0-400-4-3	-	7021	-	-	-
CN0-400-4-4	-	8174	-	-	-
Average		**7905**			
CN0-400-6-1**	6.93E-06	3051	86264	38340	1.053
CN0-400-6-2**	6.93E-06	1892	53493	23775	0.653
CN0-400-6-3**	6.93E-06	3897	110187	48972	1.344
CN0-400-6-4**	6.93E-06	2754	77873	34610	0.950
Average		**2899**	**81954**	**36424**	

Table 7.5 – Continued

Specimen ID	Strain Rates (in./in./sec)	Strength (psi)	Maximum Load (lbf)	Equivalent 4x8 Maximum Load (lbf)	Maximum Load/Maximum Average Load
CN0-R-4-1	-	9939	-	-	-
CN0-R-4-2	-	10872	-	-	-
CN0-R-4-3	-	11145	-	-	-
CN0-R-4-4	-	11718	-	-	-
Average		**10919**			
CN0-R-6-1*	6.93E-06	4563	129014	57340	1.198
CN0-R-6-2*	6.93E-06	2370	67007	29781	0.622
CN0-R-6-3*	6.93E-06	3776	106774	47455	0.992
CN0-R-6-4*	6.93E-06	4520	127804	56802	1.187
Average		**3807**	**107650**	**47844**	

*Tested without steel caps in December 2012

**Tested without steel caps in February 2013

Table 7.6 - April 2012, 8 ft Test Results

Specimen ID	Strain Rate (in./in./sec)	Maximum Dynamic Load (lbf)	Average Maximum Static Load (lbf)	Dynamic/Static Load
TF8-400-4-1	0.757	35821	22259	1.609
TF8-400-4-2	0.189	14770		0.664
TF8-400-4-3	0.553	38541		1.731
CF8-400-4-1	2.829	47549	26846	1.771
CF8-400-4-2	1.415	35723		1.331
CF8-400-4-3	4.271	57847		2.155
TN8-400-4-1	0.366	30687	19929	1.540
TN8-400-4-2	0.385	20689		1.038
TN8-400-4-3	0.441	37728		1.893
TN8-400-4-4	0.475	20738		1.041
TN8-400-4-5	1.090	54574		2.738
TN8-R-4-1	0.405	26799	26168	1.024
TN8-R-4-2	1.059	52990		2.025
TN8-R-4-3	0.406	27420		1.048
CN8-400-4-1	6.251	101491	36424	2.786
CN8-400-4-2	1.781	51476		1.413
CN8-400-4-3	5.530	94046		2.582
CN8-400-4-4	4.060	72496		1.990
CN8-400-4-5	2.987	46496		1.277
CN8-R-4-1	2.880	54744	47844	1.144
CN8-R-4-2	4.024	82929		1.733
CN8-R-4-3	2.430	79404		1.660

Table 7.7 - April 2012, 16 ft Test Results

Specimen ID	Strain Rate (in./in./sec)	Maximum Dynamic Load (lbf)	Average Maximum Static Load (lbf)	Dynamic/Static Load
TF16-400-4-1	0.735	35715	22259	1.605
TF16-400-4-2	0.840	47664		2.141
TF16-400-4-3	0.639	33964		1.526
CF16-400-4-1	2.792	54394	26846	2.026
CF16-400-4-2	4.250	50369		1.876
CF16-400-4-3	4.012	52201		1.944
TN16-400-4-1	0.400	20896	19929	1.049
TN16-400-4-2	0.331	22187		1.113
TN16-400-4-3	1.172	63753		3.199
TN16-400-4-4	0.500	32222		1.617
TN16-400-4-5	1.117	57333		2.877
TN16-R-4-1	0.951	63837	26168	2.440
TN16-R-4-2	0.744	38653		1.477
TN16-R-4-3	1.102	69992		2.675
CN16-400-4-1	4.865	50390	36424	1.383
CN16-400-4-2	3.495	59244		1.626
CN16-400-4-3	2.184	46375		1.273
CN16-400-4-4	2.147	53176		1.460
CN16-400-4-5	2.794	63759		1.750
CN16-R-4-1	12.103	153630	47844	3.211
CN16-R-4-2	6.254	114367		2.390
CN16-R-4-3	8.429	137804		2.880
CN16-cooled-4-1	4.006	87321	N/A	N/A
CN16-cooled-4-2	4.843	109316		N/A
CN16-cooled-4-3	4.794	98173		N/A

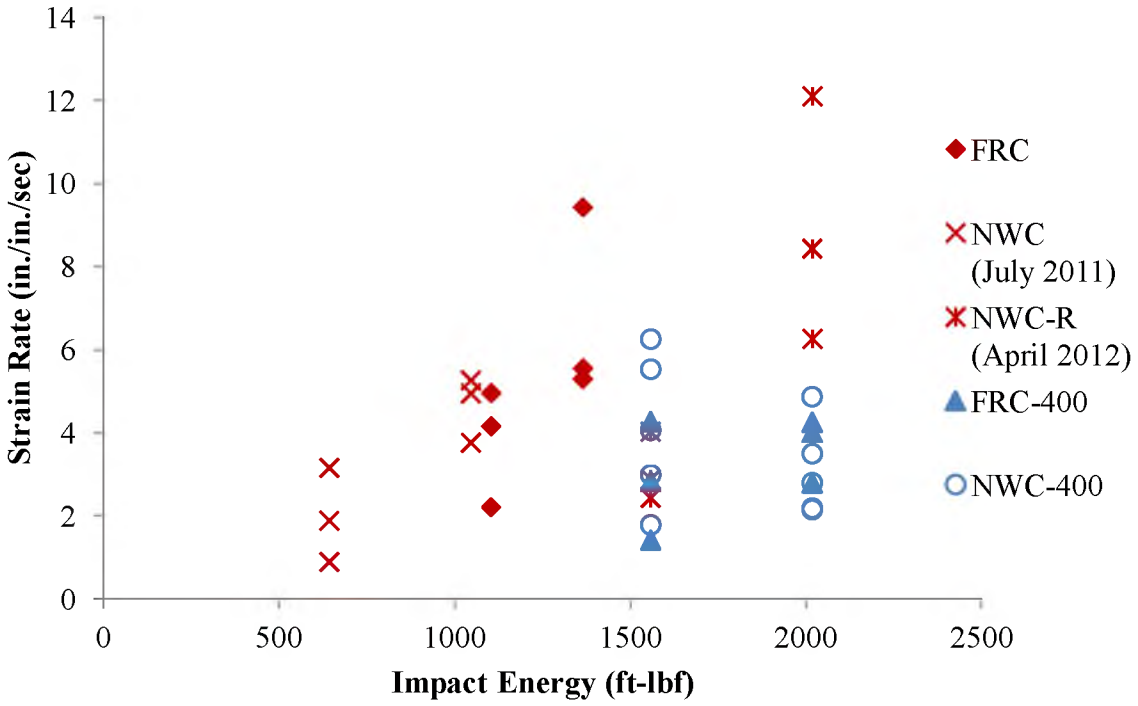

Figure 7.7 - Compression Strain Rate vs. Impact Energy

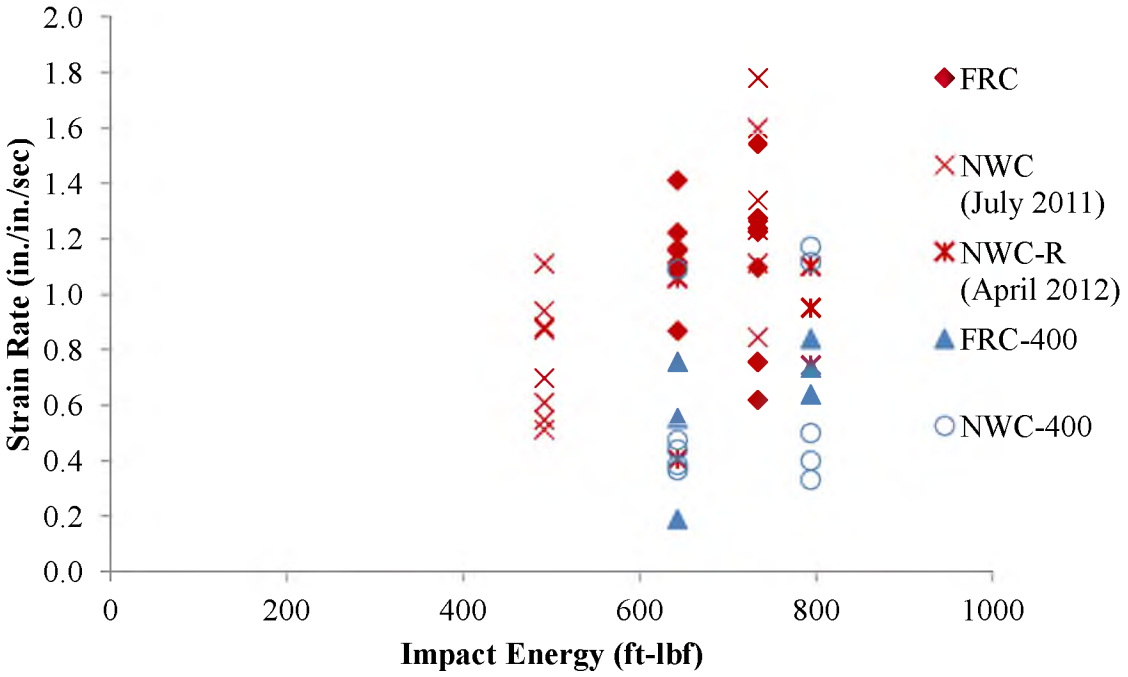

Figure 7.8 - Tension Strain Rate vs. Impact Energy

Table 7.8 - Average Static Strength

		Strength (psi)	
Test Type	**Composition**	**Room Temperature**	**400 °F**
Tension	FRC	605	443
Tension	NWC	521	396
Compression	FRC	9338	5253
Compression	NWC	10919	7905

8. CONCLUSIONS

To determine how concrete is affected by dynamic loads, 4 in. diameter by 8 in. high cylinders were tested with various concrete materials, loading types and drop heights. Dynamic increase factors and strain rates were calculated to compare the results of these tests. The dynamic increase factor is the ratio of maximum dynamic load to the corresponding average maximum static load.

To determine the appropriate strain rate three methods were explored: the high speed camera, load cell and strain gauge methods. The high speed camera method and load cell method gave strain rates that were up to 100% higher than the load cell method. These two methods are representative of a local strain rate, whereas the load cell method provides an average (global) result. To compare different specimen types, the load cell method was used to determine the strain rates.

Once the appropriate DIFs and strain rates were determined, they were compared with models based on previous research. The following conclusions and recommendations can be drawn from the results:

- The combined effect of the drop weight and height can be summarized by calculating an impact energy, which is equivalent to the kinetic energy at impact. As a general trend of all data, for both compression and tension tests, increasing the impact energy results in an increase in DIF. This followed the trends proposed by the CEB and Modified CEB models. The results also show

that tension tests are more affected by the increase in impact energy than compression tests.

- The strain rates were calculated using the modulus of elasticity determined from static compressive strength. Watstein (1953) stated that the modulus of elasticity increases between 13% to 85% (depending on the type of concrete) when loaded dynamically. Additional tests should be performed to determine the mechanical properties of concrete under dynamic loading. This possible change in modulus of elasticity only affects the strain rate; the DIF is independent of the test method used.
- A small number of tests were performed on NWC that had been heated and then cooled before testing. It was found that the maximum dynamic load increased by 80% when compared to the heated concrete, but was still 27% less than the room temperature concrete. Similar results were found when cooled specimens were tested statically by Behnood and Ghandehari (2009); the strength was reduced by 30% compared to room temperature concrete when tested statically. Additional testing may be performed to further analyze the effects of cooling on concrete specimens with both NWC and FRC under dynamic loading.
- For compression tests, different impact energies were used for FRC and NWC specimens. Because of this difference, it was difficult to determine how FRC concrete performed compared to NWC. However, by comparing the percent increase in impact energy to the percent increase in DIF, it is concluded that the FRC performed worse than NWC. For better comparisons, additional

testing can be performed using the same impact energy for FRC and NWC specimens. The same can be said for the tension tests. However, for tension tests with a 16 ft drop height, the same impact energy was used. In this case, the same conclusion was drawn: FRC specimens had lower strength than NWC specimens. This is the opposite result obtained from static tests, in which fibers add strength when the cylinders are tested in tension. Therefore, it is recommended that additional dynamic tests are performed to verify the repeatability of these results.

- For compression and tension tests at low impact energies, FRC specimens heated to 400 ^{o}F had lower DIFs than NWC specimens heated to 400 ^{o}F. For tension tests, FRC specimens at high impact energies also had lower DIFs than NWC, but the decrease in DIFs was not as large as that experienced when a lower impact energy was used. For compression tests at high impact energies, the DIFs actually increased when FRC was used in place of NWC. Therefore, FRC specimens generally have lower strength results compared to NWC when heated, but improve as the impact energy increases, especially when tested in compression. Similarly, both Lam et al. (2012) and Behnood and Ghandehari (2009) found that at 400 ^{o}F roughly a 25% drop of the static compressive strength was observed for both NWC and FRC.
- For NWC compression and tension specimens heated to 400 ^{o}F the average maximum dynamic load decreased when compared to specimens tested at room temperature when a higher impact energy was used. The average

maximum dynamic load also decreases when lower impact energies are used, but the decrease was nearly negligible.

- Increasing the test temperature reduces the DIF for tension members with fiber reinforcement. This is similar to static results achieved by Behnood and Ghandehari (2009).

In summary, a standardized method for testing dynamic properties of concrete is needed. There are many contributing factors that need to be considered, including test specimen size, test configuration and the measurement of impact load and strain rate. A limited number of test results were available for certain specimen types that have been reviewed and summarized. It is recommended that additional tests are performed to verify the consistency of all results that have been presented herein.

APPENDIX A

JULY 2011 – PHOTOGRAPHS OF TESTED SPECIMENS

Figure A.1 - TF Specimens after Static Tests

Figure A.2 - TN Specimens after Static Test

Figure A.3 - Specimen TF8-2 after Dynamic Test

Figure A.4 – Specimen CF8-2 after Dynamic Test

Figure A.5 - Specimen TN8-2 after Dynamic Test

Figure A.6 - Specimen CN8-2 after Dynamic Test

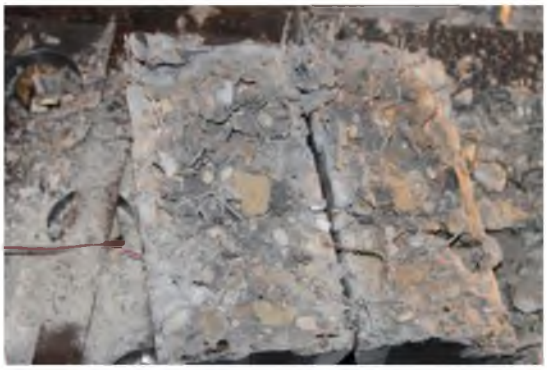

Figure A.7 - Specimen TF16-2 after Dynamic Test

Figure A.8 - Specimen CF16-2 after Dynamic Test

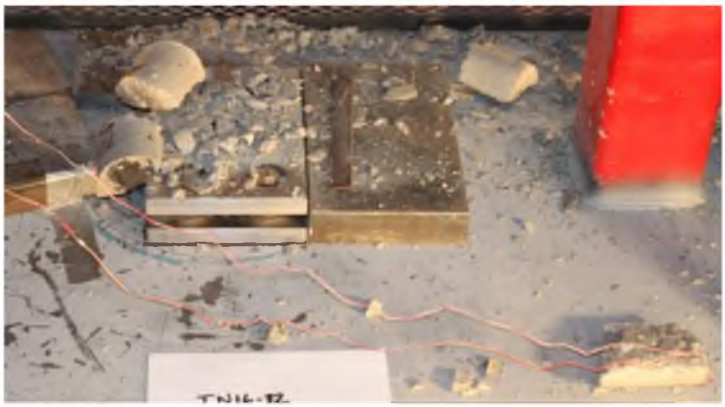

Figure A.9 - Specimen TN16-2 after Dynamic Test

Figure A.10 - Specimen CN16-2 after Dynamic Test

APPENDIX B

APRIL 2012 – PHOTOGRAPHS OF TESTED SPECIMENS

Figure B.11 - CF0-0-4 after Static Test

Figure B.12 - CN0-0-4 after Static Test

Figure B.13 - TF0-400-4 after Static Test

Figure B.14 - CF0-400-4 after Static Test

Figure B.15 - TN0-400-4 after Static Test

Figure B.16 - CN0-400-4 after Static Test

Figure B.17 – Specimen TF8-400-4-1 after Dynamic Test

Figure B.18 – Specimen CF8-400-4-1 after Dynamic Test

Figure B.19 – Specimen TN8-400-4-1 after Dynamic Test

Figure B.20 - Specimen TN8-0-4-3 after Dynamic Test

Figure B.21 - Specimen CN8-400-4-4 after Dynamic Test

Figure B.22 - Specimen CN8-0-4-3 after Dynamic Test

Figure B.23 - Specimen TF16-400-4-1 after Dynamic Test

Figure B.24 – Specimen TF16-400-4-3 with Melted Fibers after Dynamic Test

Figure B.25 - Specimen CF16-400-4-1 after Dynamic Test

Figure B.26 – Specimen TN16-400-4-4 after Dynamic Test

Figure B.27 - Specimen TN16-0-4-1 after Dynamic Test

Figure B.28 – Specimen CN16-400-4-4 after Dynamic Test

Figure B.29 - Specimen CN16-0-4-1 after Dynamic Test

Figure B.30 - Specimen CN16-cooled-4-3

APPENDIX C

JULY 2011 – LOAD DATA GRAPHS

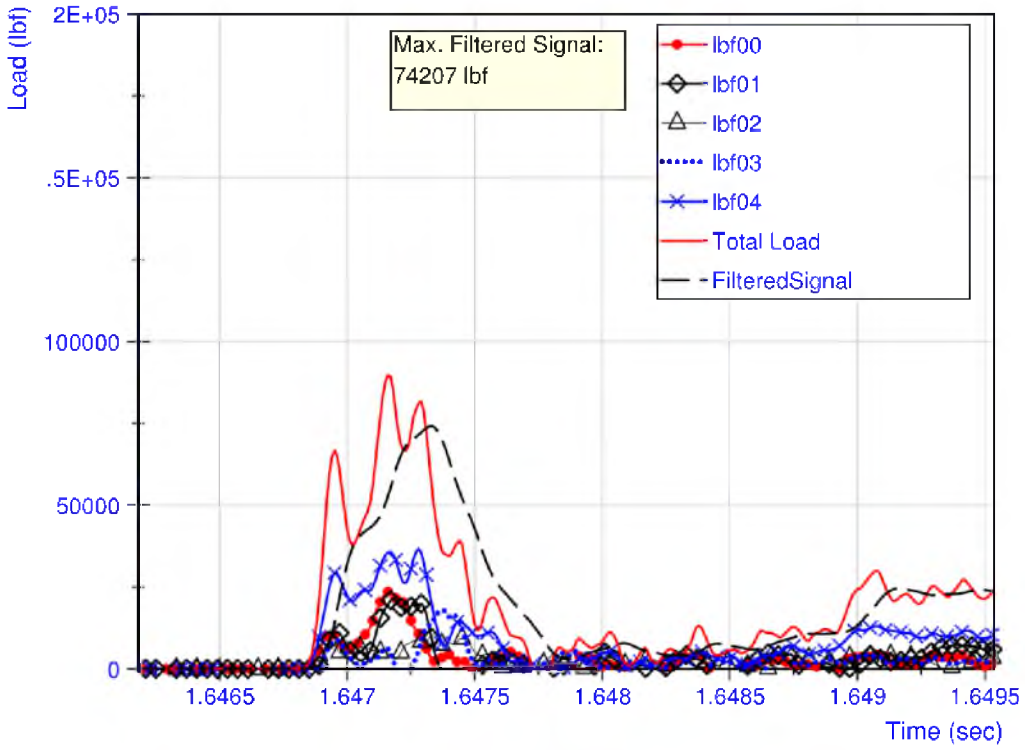

Figure C.31 – TF8-2 Load Data

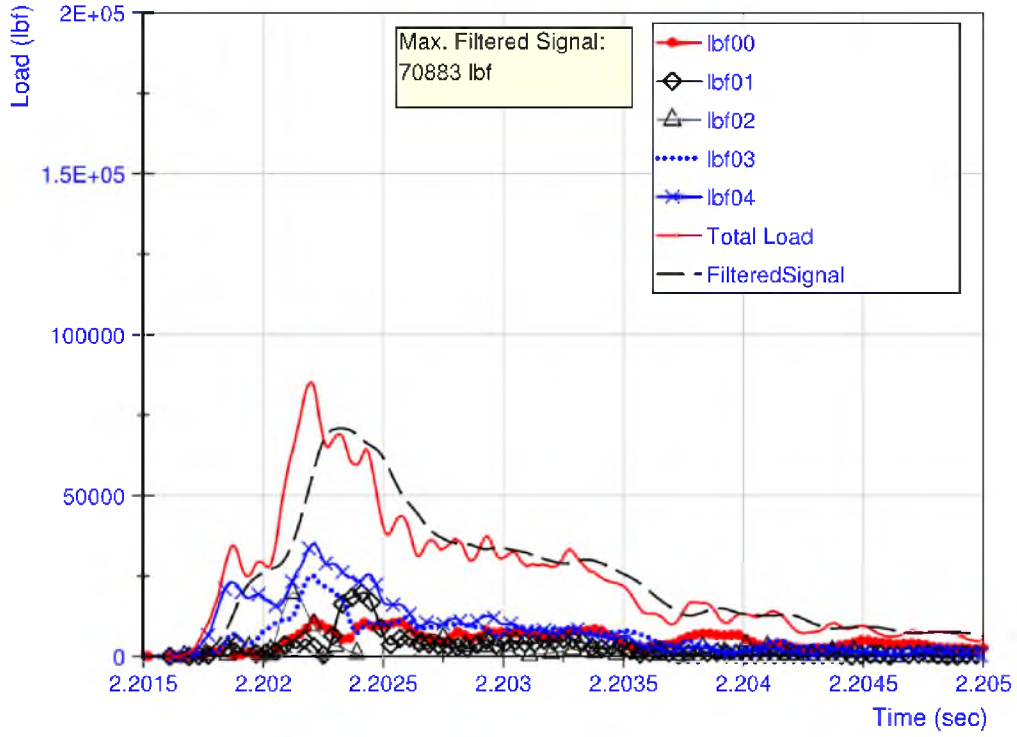

Figure C.32 - CF8-2 Load Data

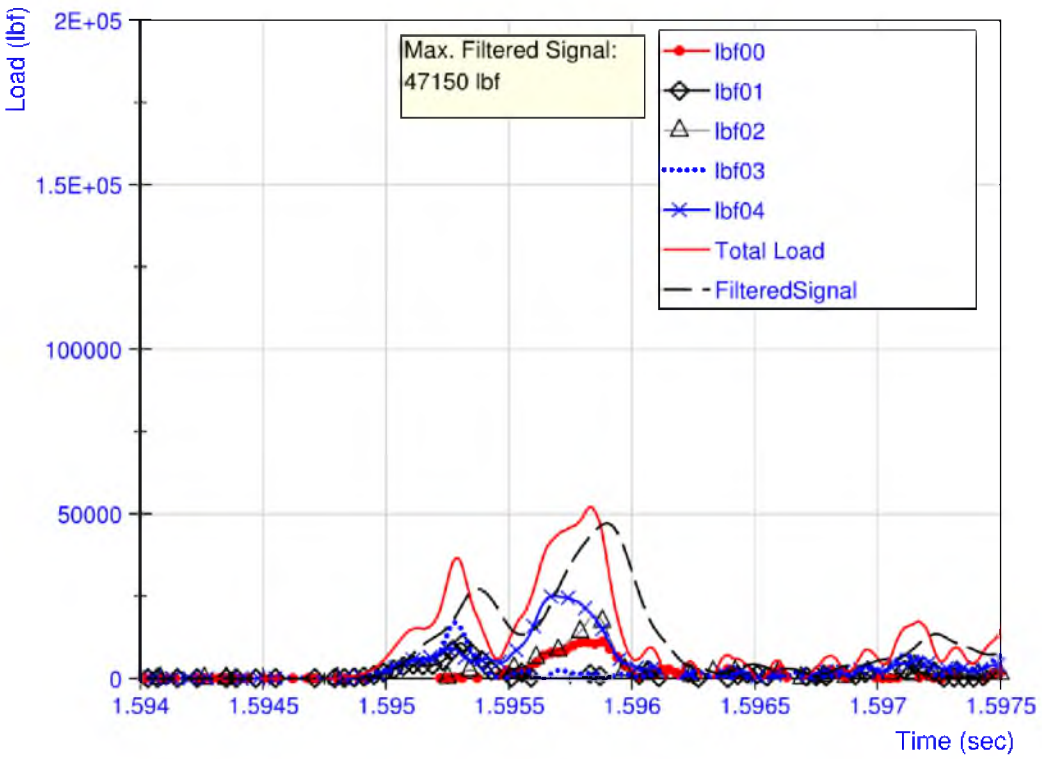

Figure C.33 - TN8-2 Load Data

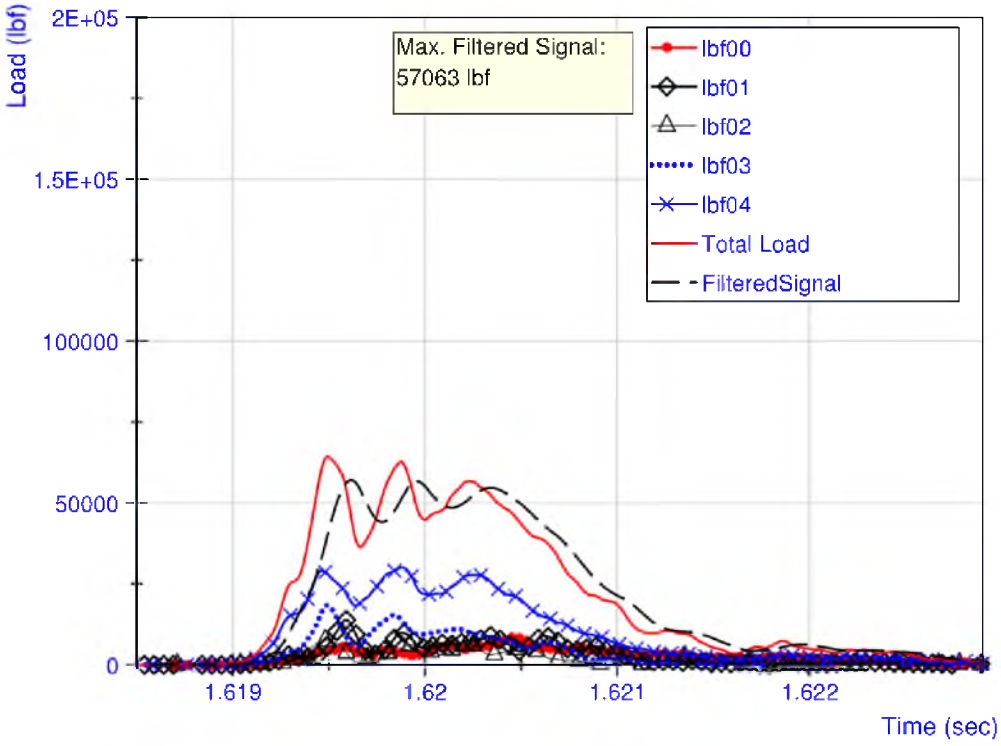

Figure C.34 - CN8-2 Load Data

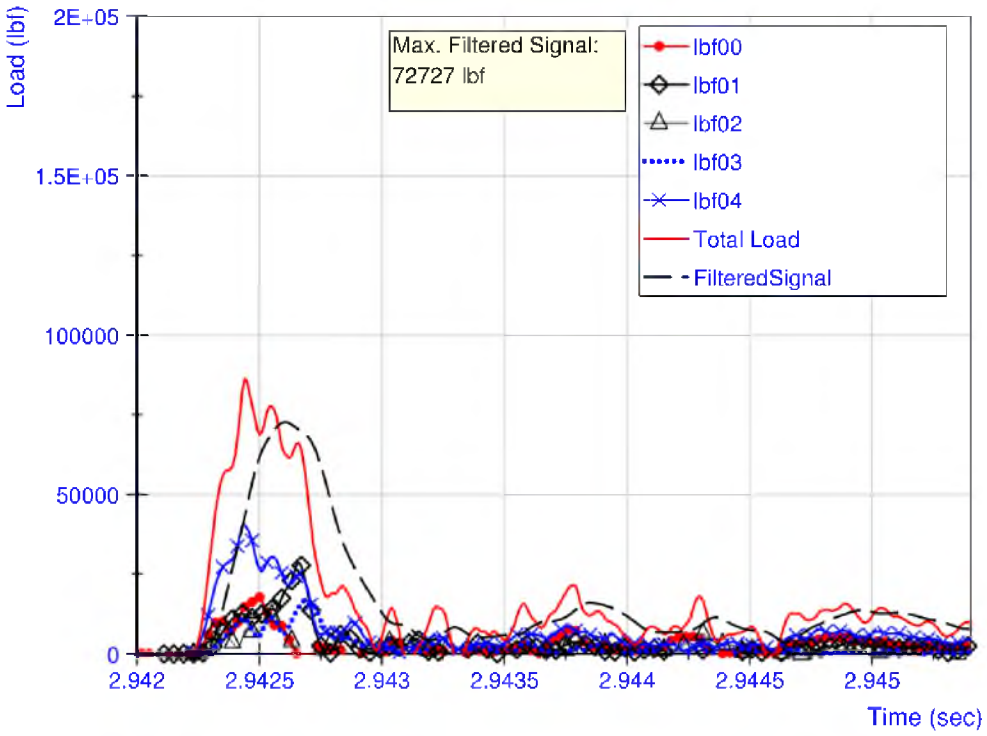

Figure C.35 - TF16-2 Load Data

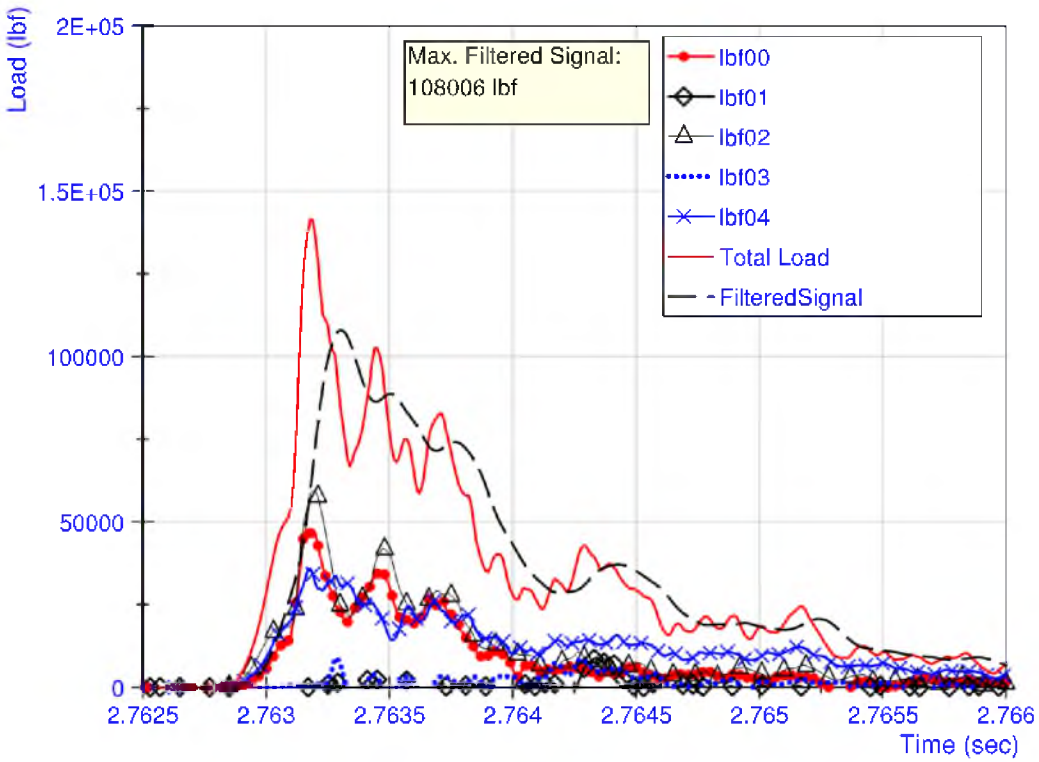

Figure C.36 - CF16-2 Load Data

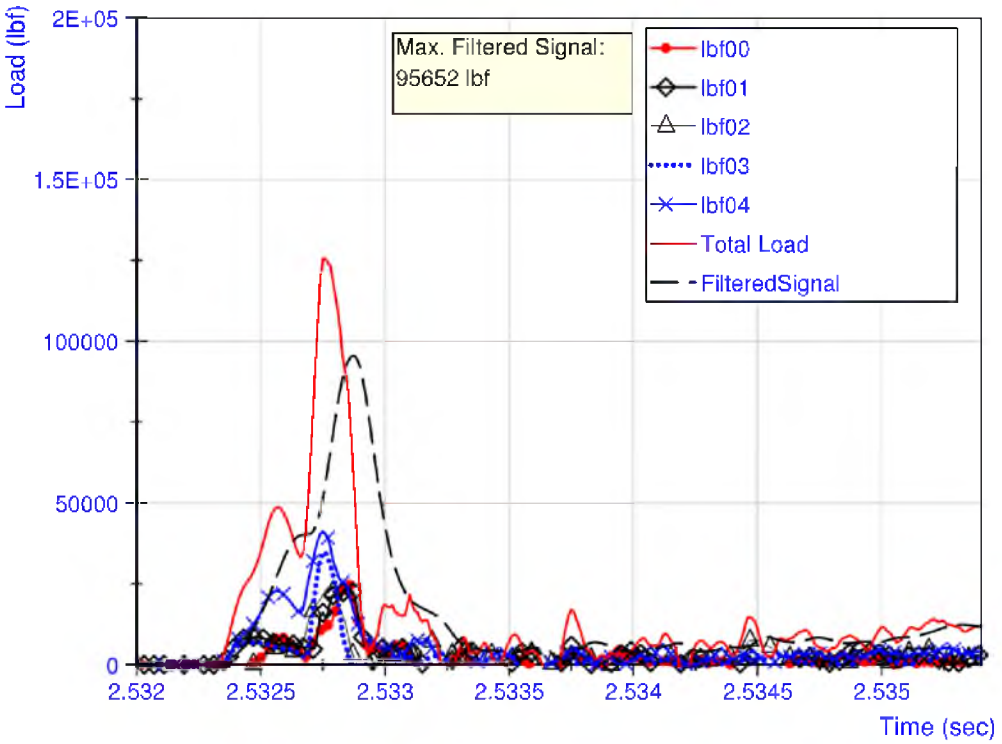

Figure C.37 - TN16-2 Load Data

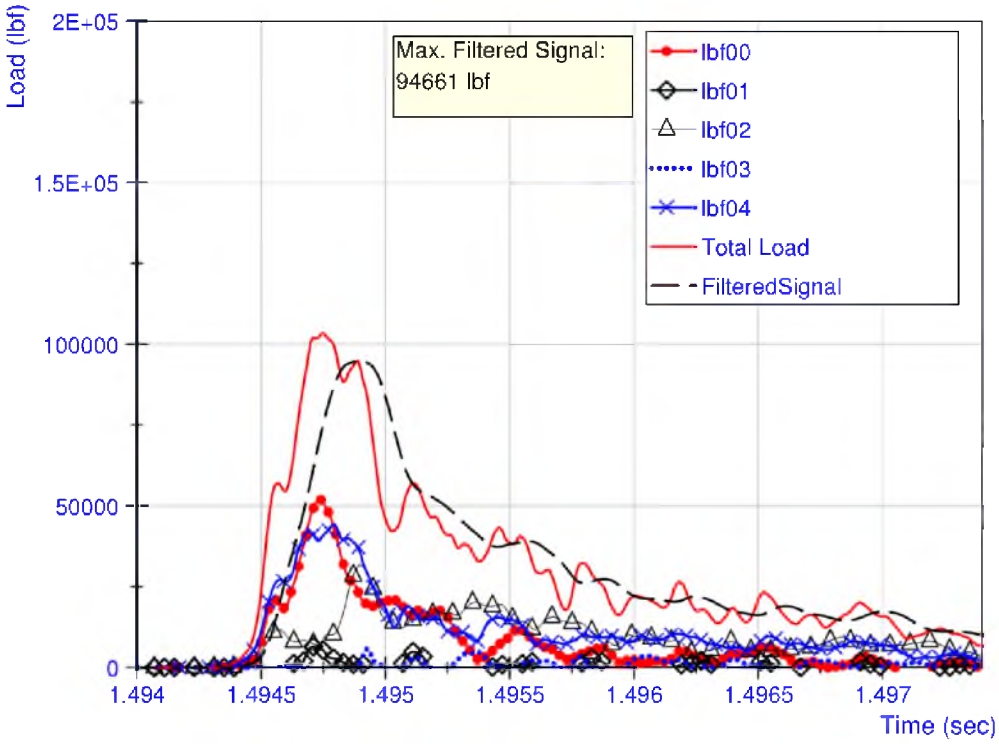

Figure C.38 - CN16-2 Load Data

APPENDIX D

APRIL 2012 – LOAD DATA GRAPHS

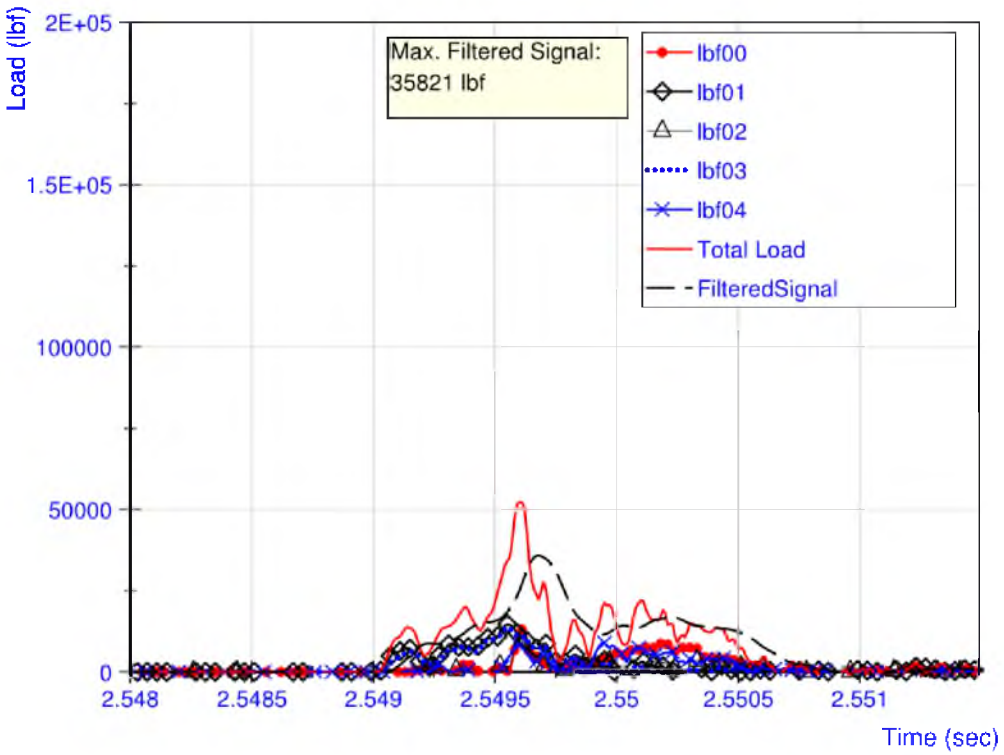

Figure D.39 - TF8-400-4-1 Load Data

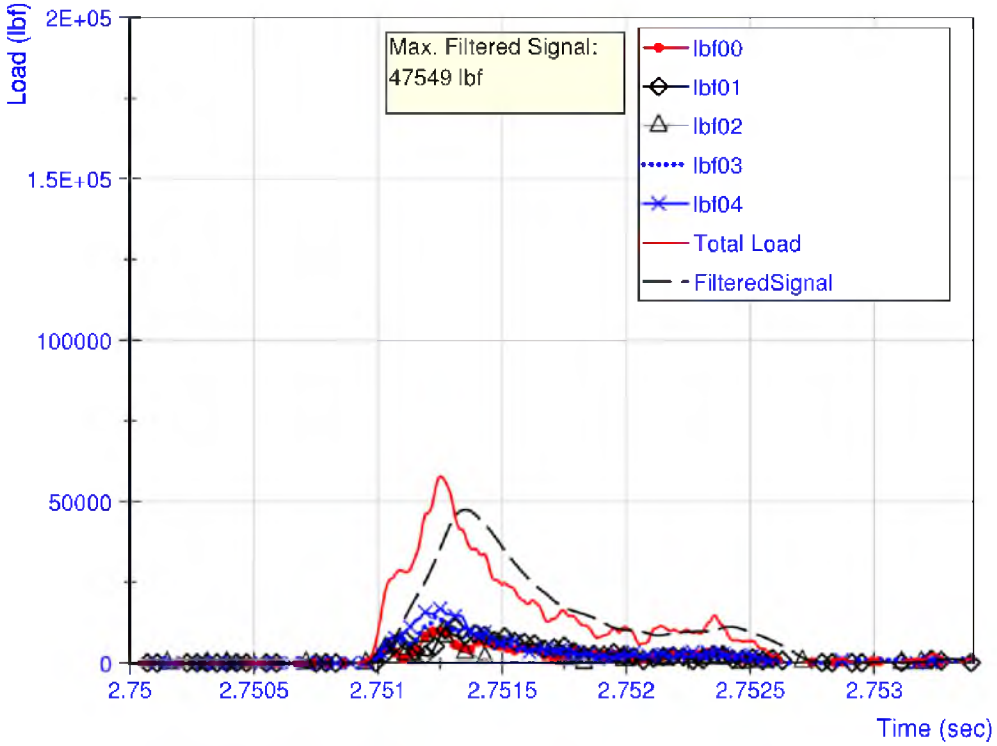

Figure D.40 - CF8-400-4-1 Load Data

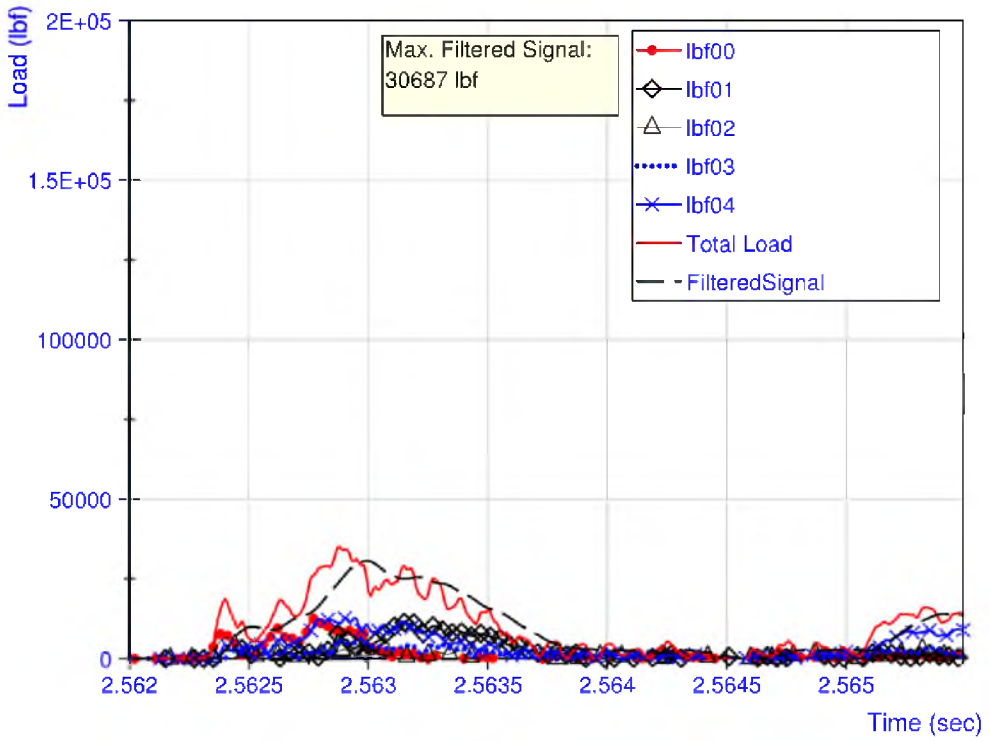

Figure D.41 - TN8-400-4-1 Load Data

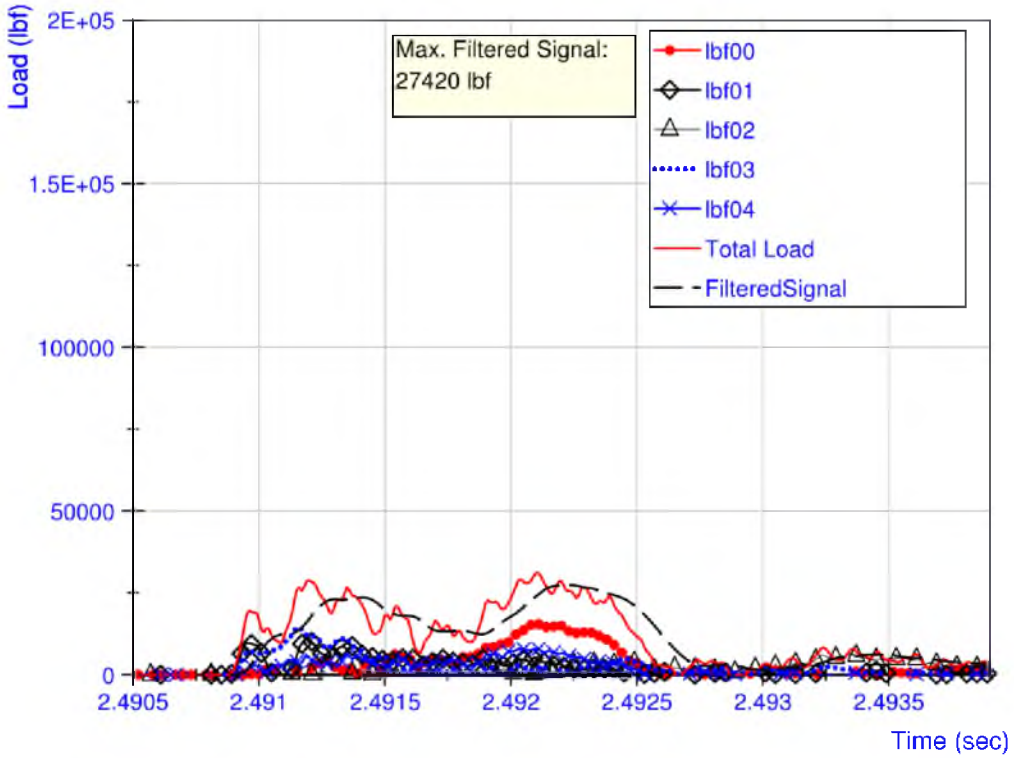

Figure D.42 - TN8-0-4-3 Load Data

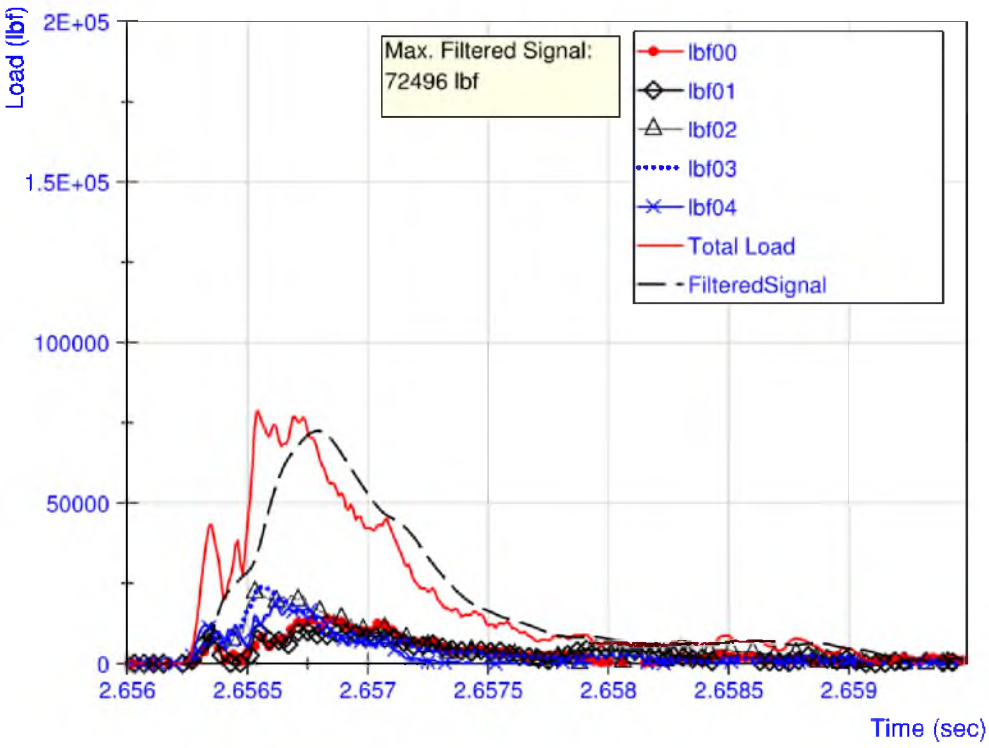

Figure D.43 - CN8-400-4-4 Load Data

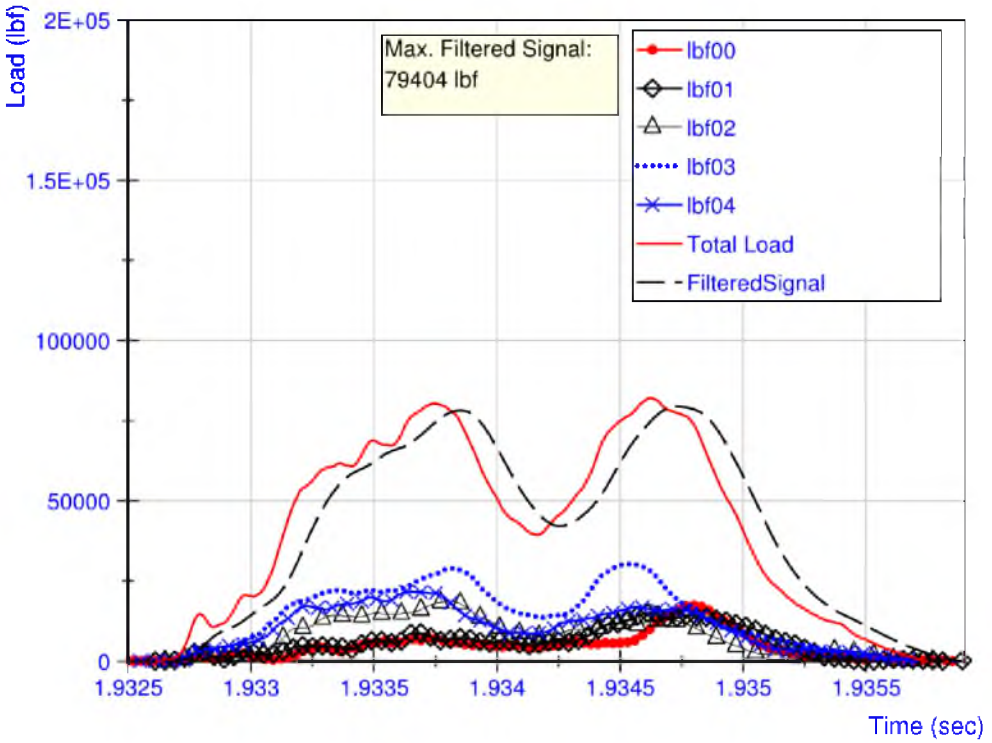

Figure D.44 - CN8-0-4-3 Load Data

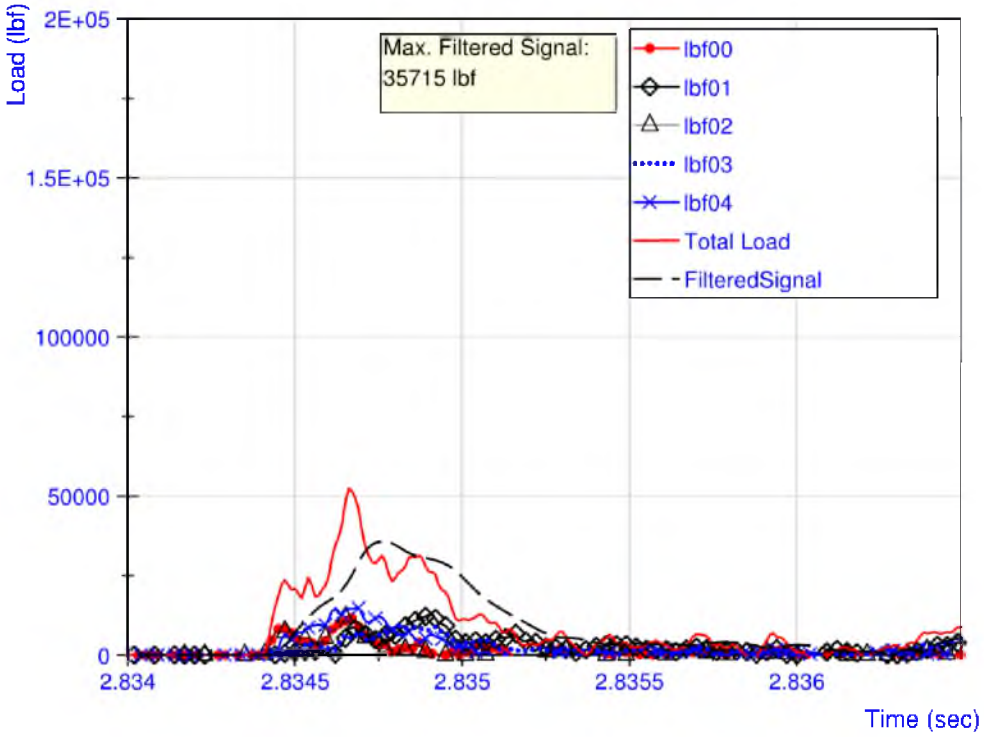

Figure D.45 - TF16-400-4-1 Load Data

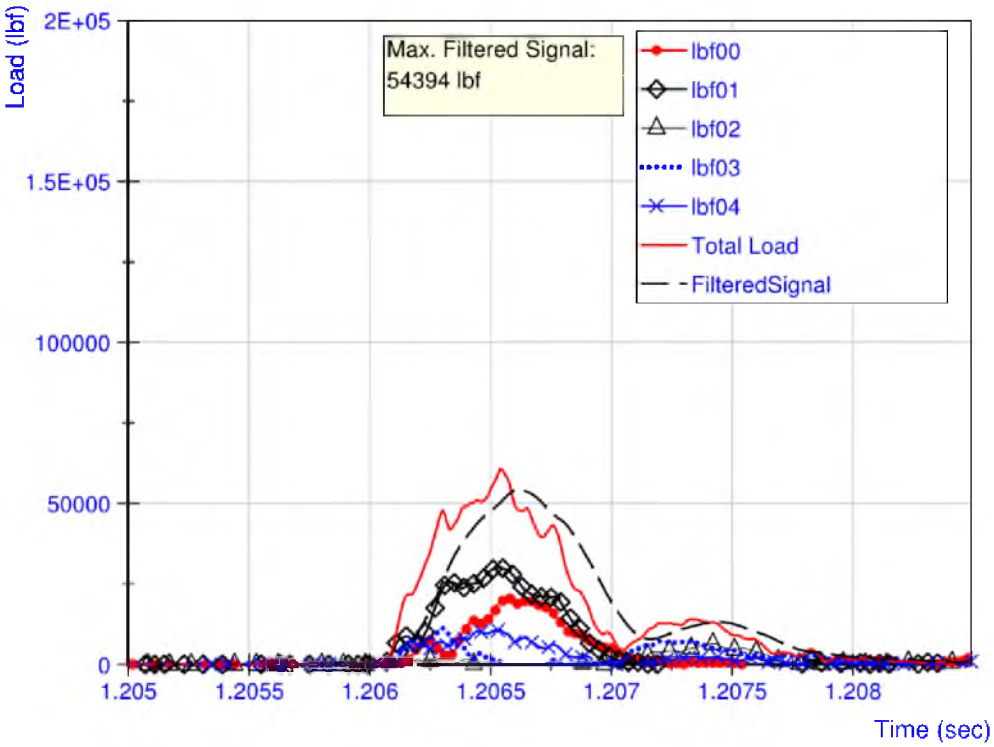

Figure D.46 - CF16-400-4-1 Load Data

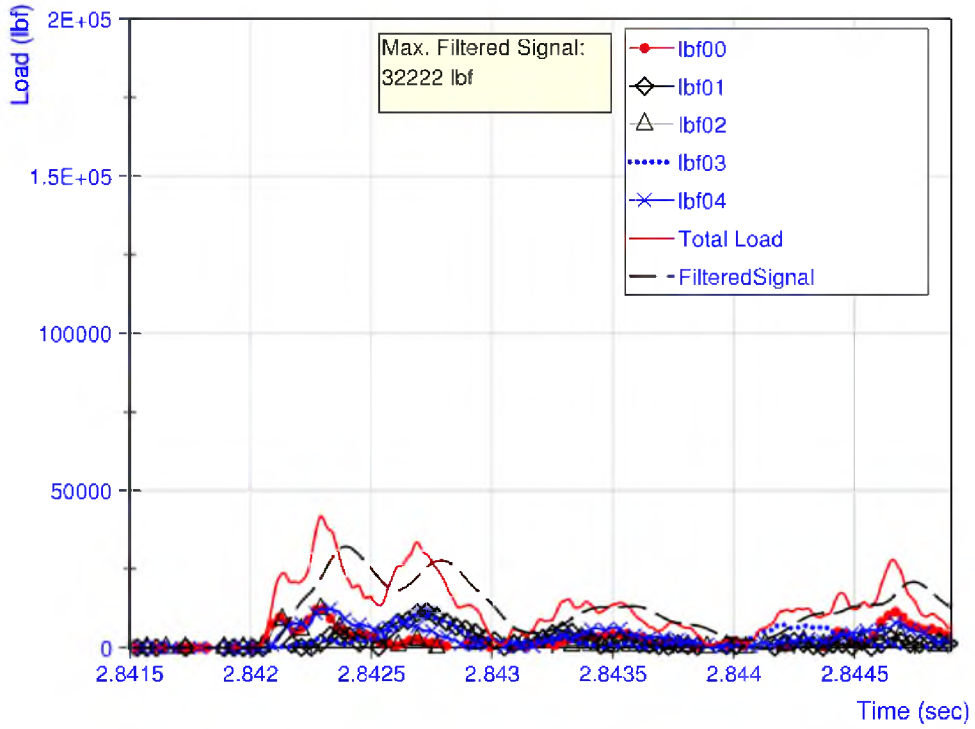

Figure D.47 - TN16-400-4-4 Load Data

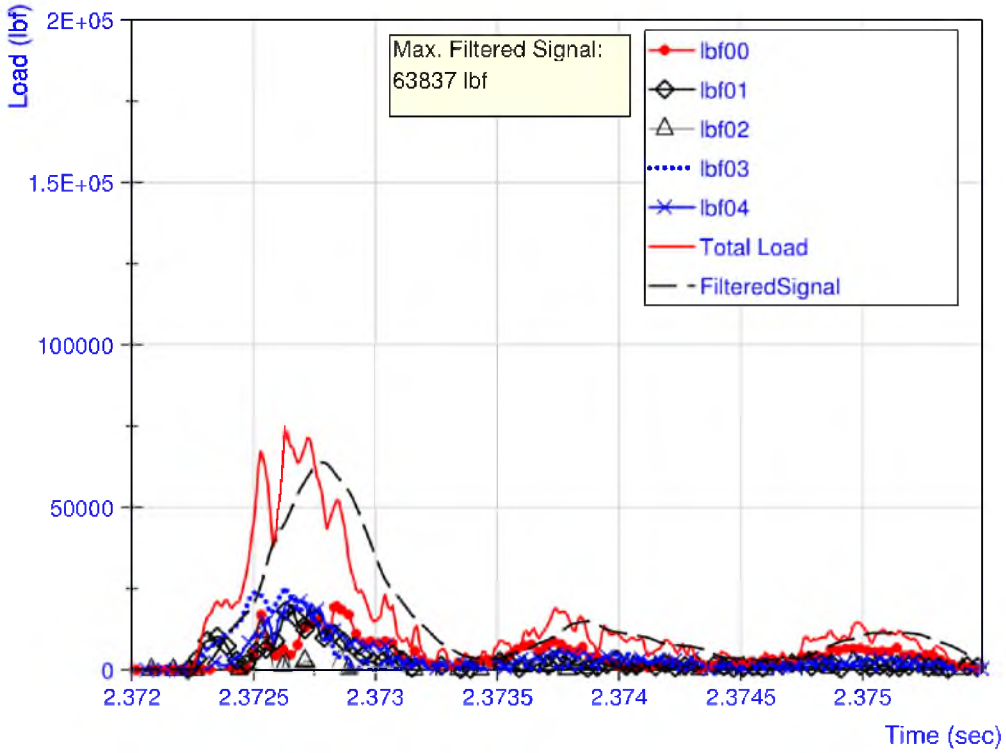

Figure D.48 - TN16-0-4-1 Load Data

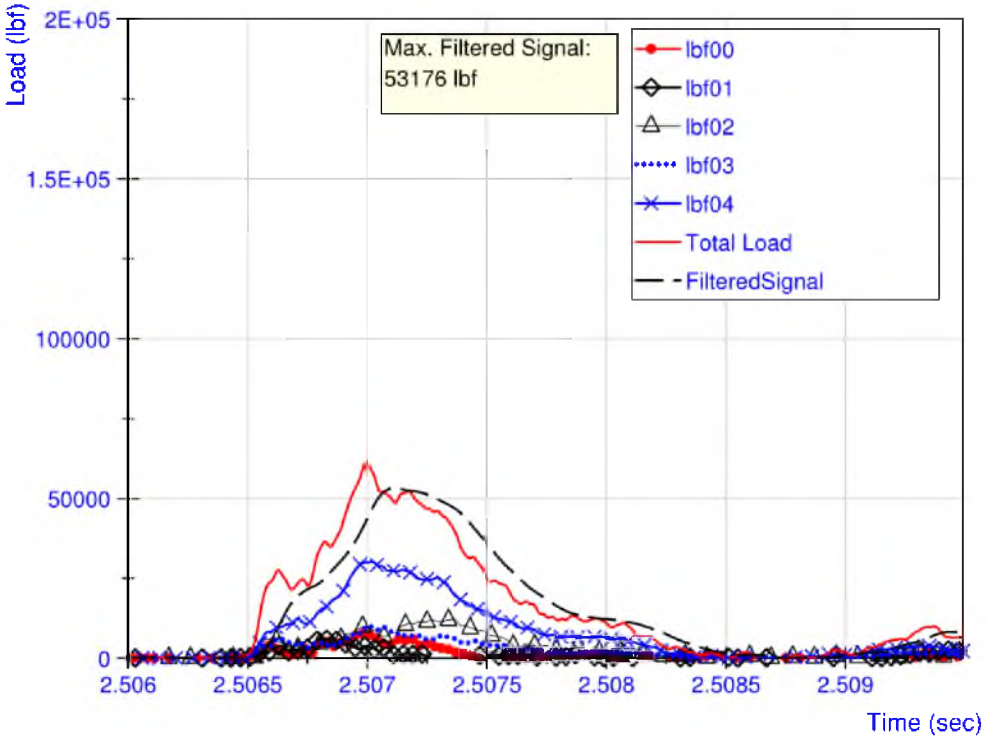

Figure D.49 - CN16-400-4-4 Load Data

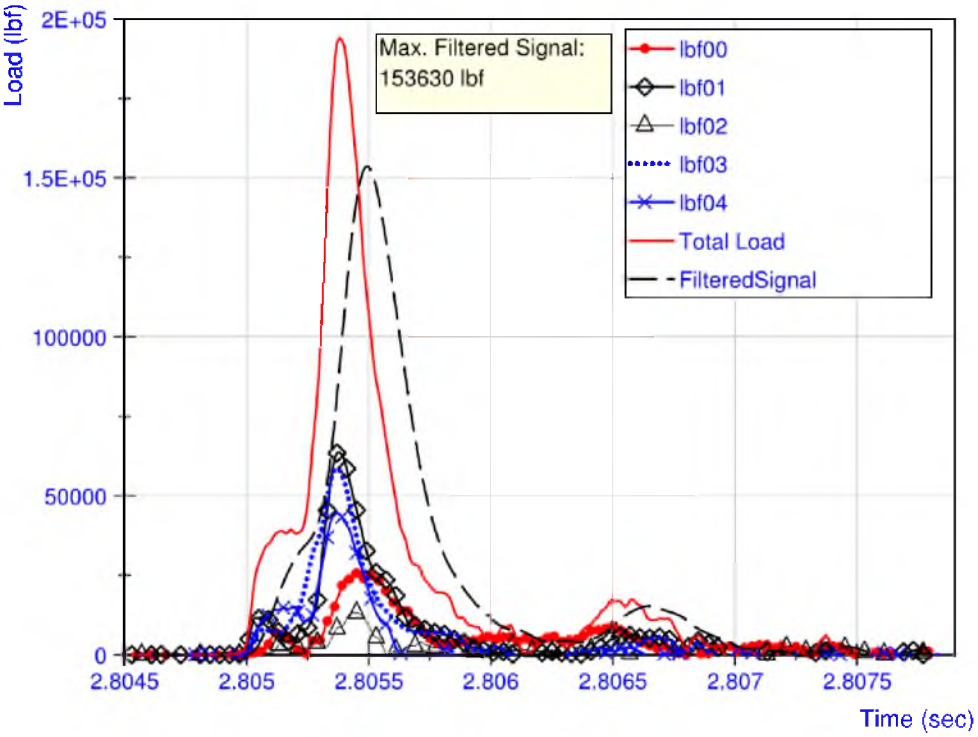

Figure D.50 - CN16-0-4-1 Load Data

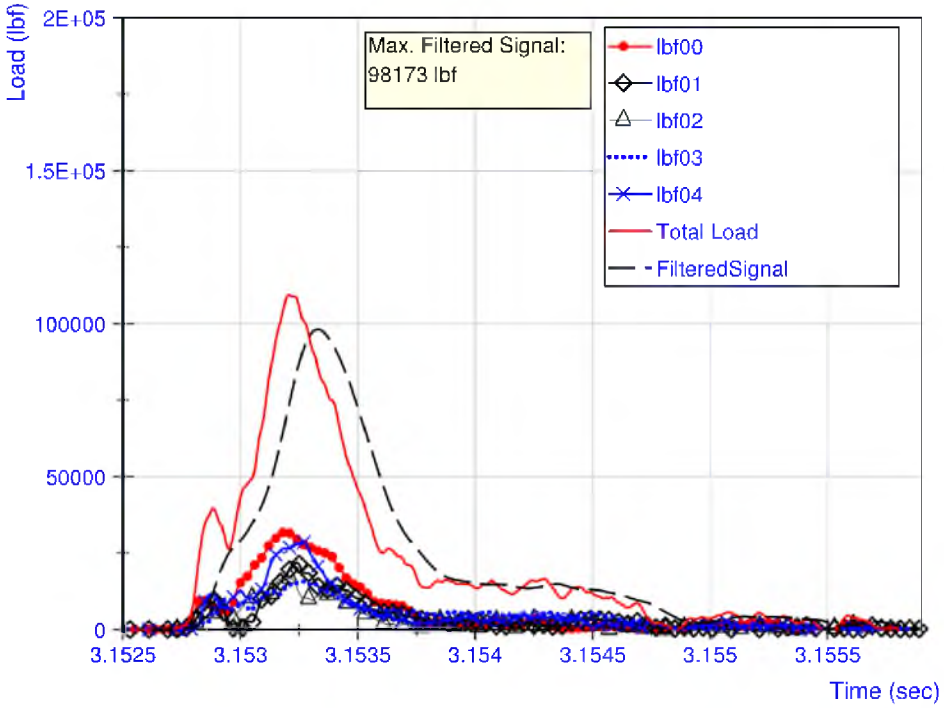

Figure D.51 - CN16-cooled-4-3 Load Data

APPENDIX E

JULY 2011 – STRAIN DATA GRAPHS

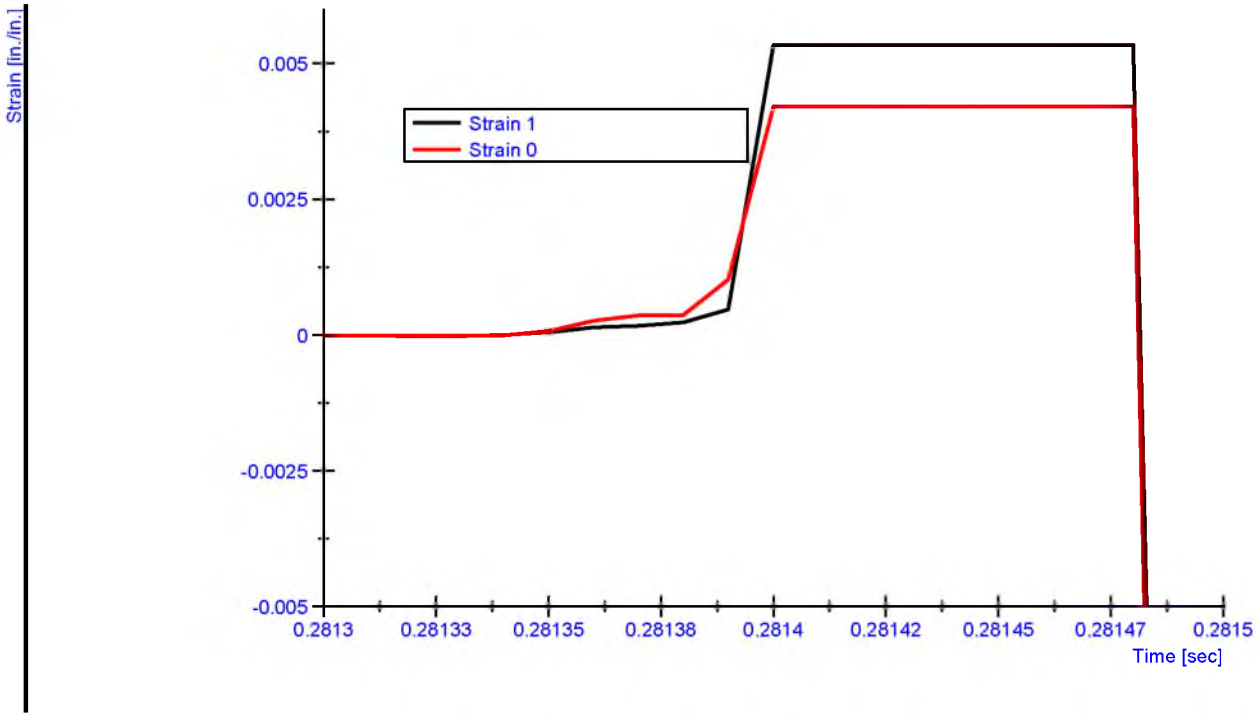

Figure E.52 – Specimen TN8-2 Strain Data for Dynamic Test

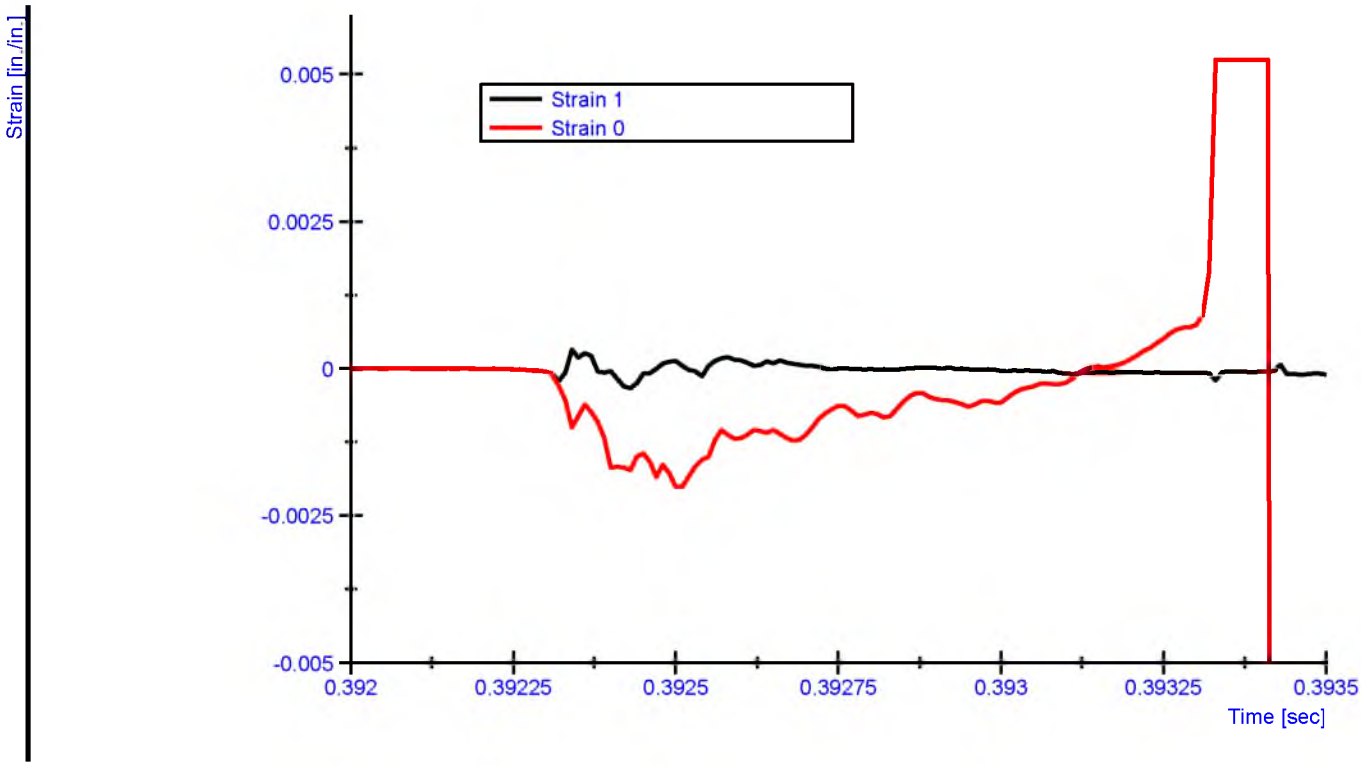

Figure E.53 – Specimen CF8-2 Strain Data for Dynamic Test

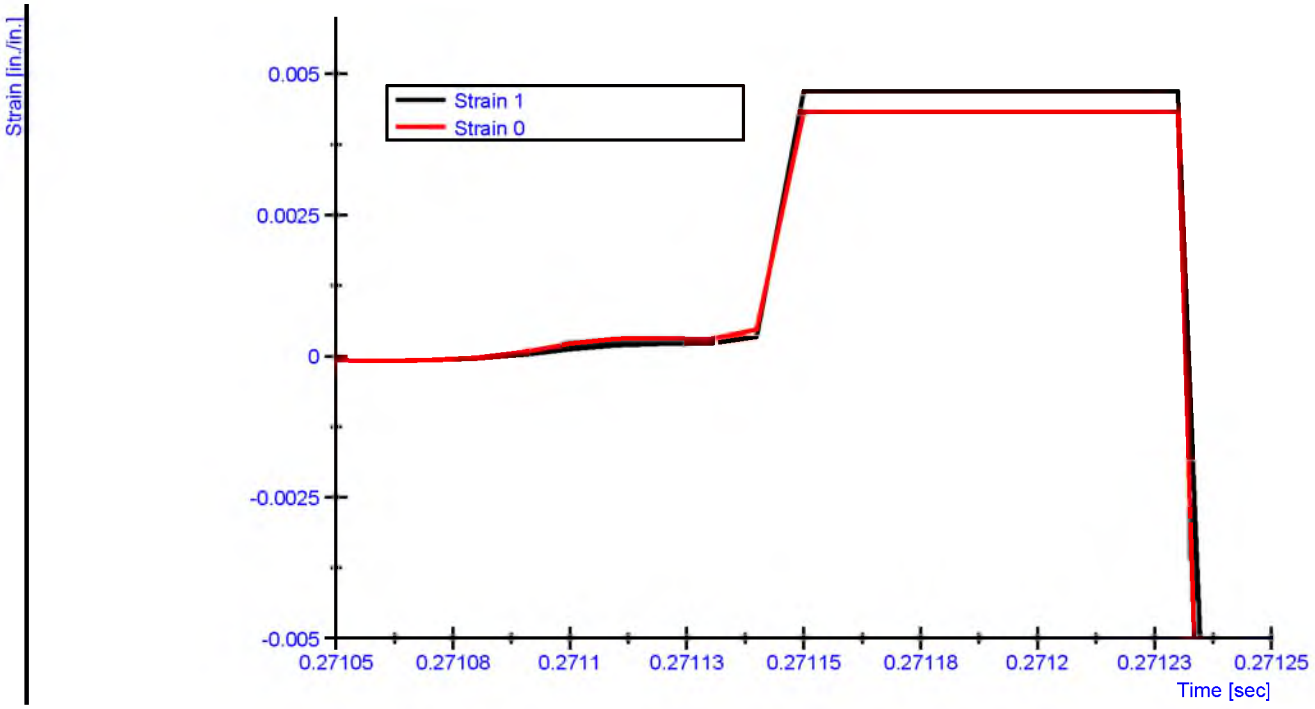

Figure E.54 – Specimen TN8-2 Strain Data for Dynamic Test

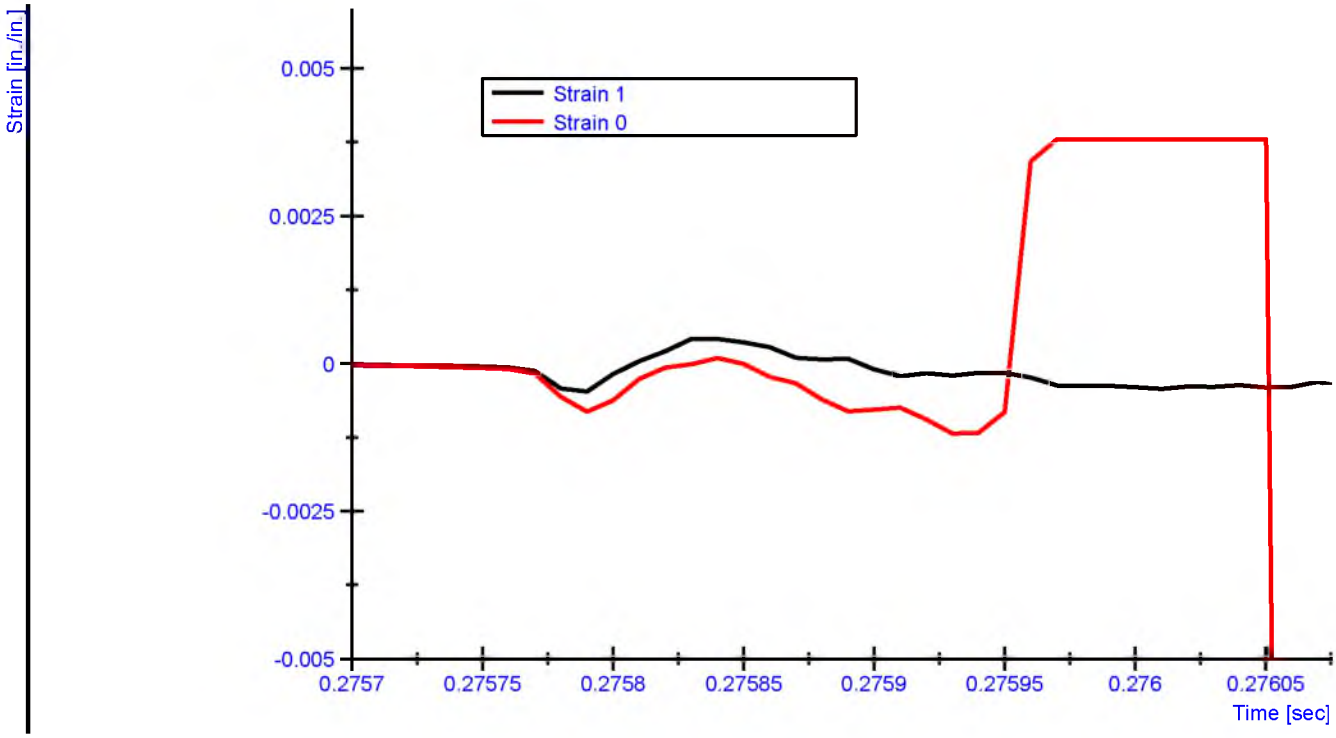

Figure E.55 – Specimen CN8-2 Strain Data for Dynamic Test

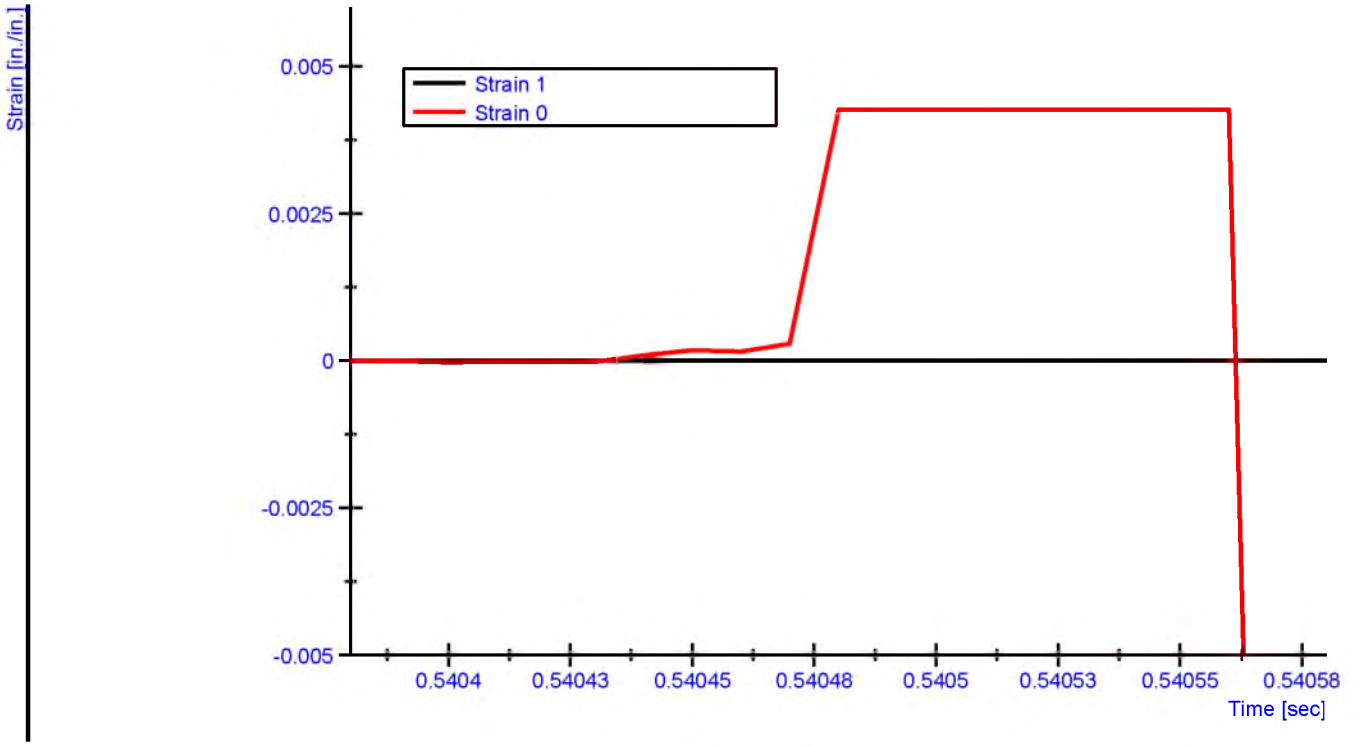

Figure E.56 – Specimen TF16-2 Strain Data for Dynamic Test

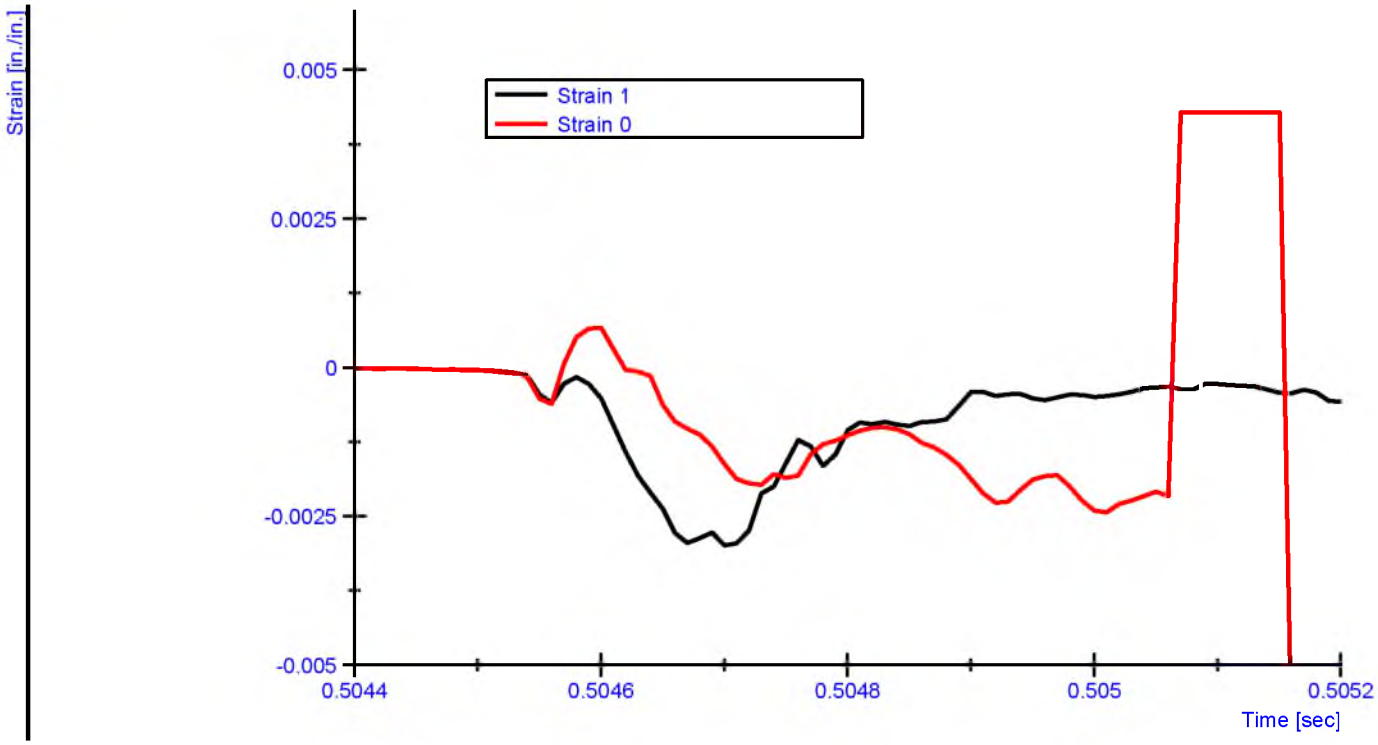

Figure E.57 – Specimen CF16-2 Strain Data for Dynamic Test

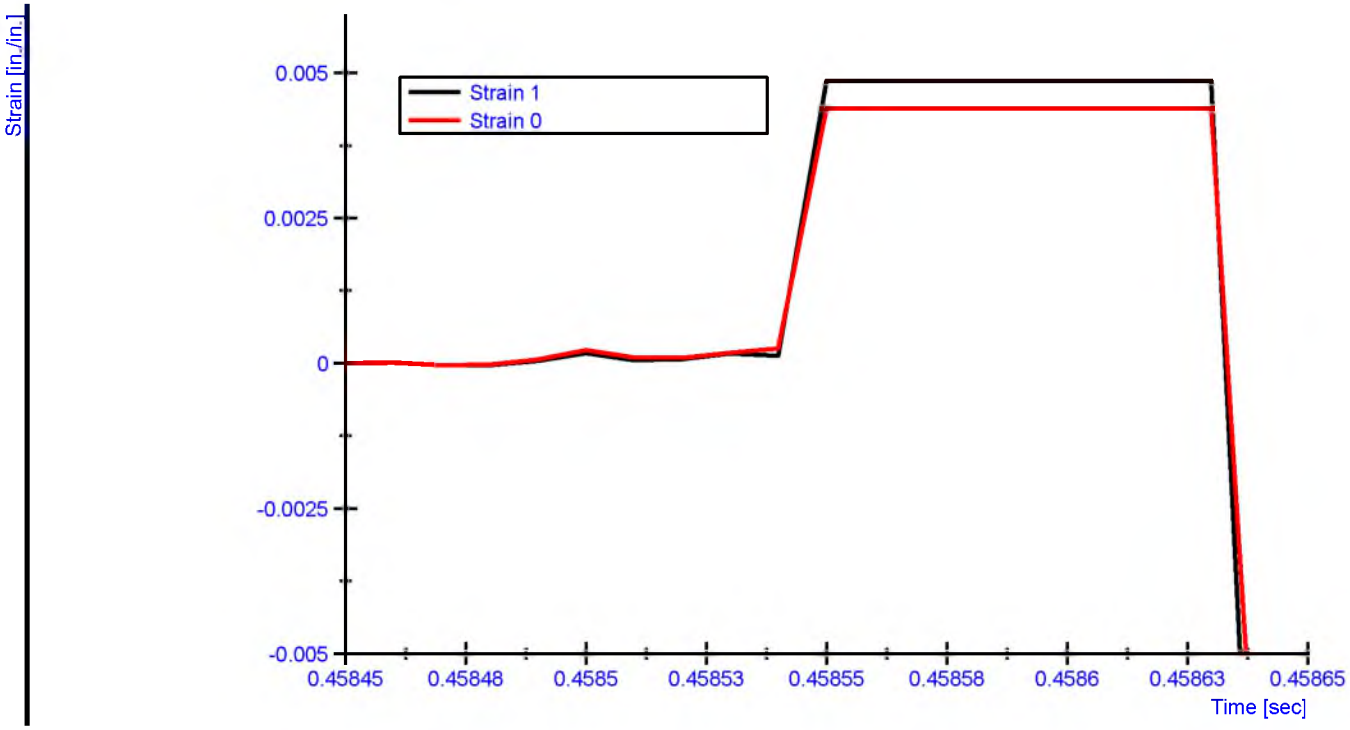

Figure E.58 – Specimen TN16-2 Strain Data for Dynamic Test

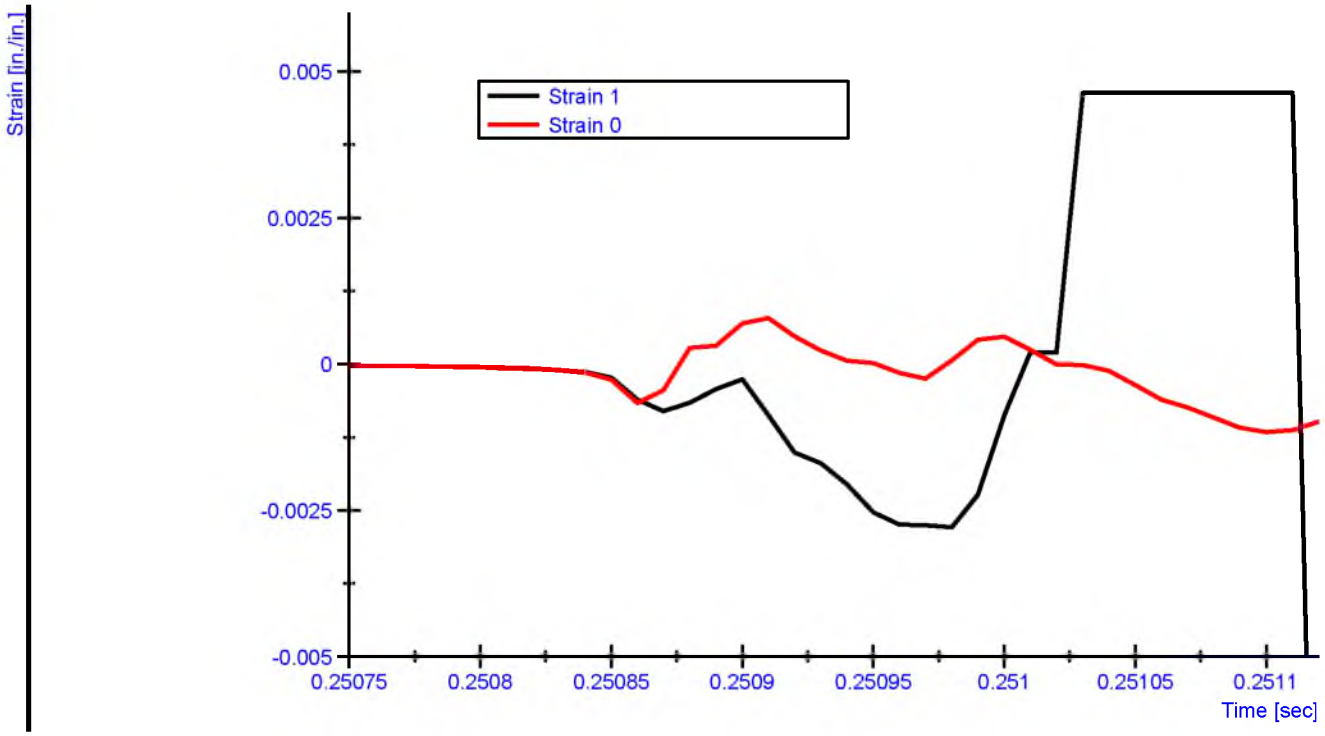

Figure E.59 – Specimen CN16-2 Strain Data for Dynamic Test

APPENDIX F

DIF VERSUS STRAIN RATE PLOTS

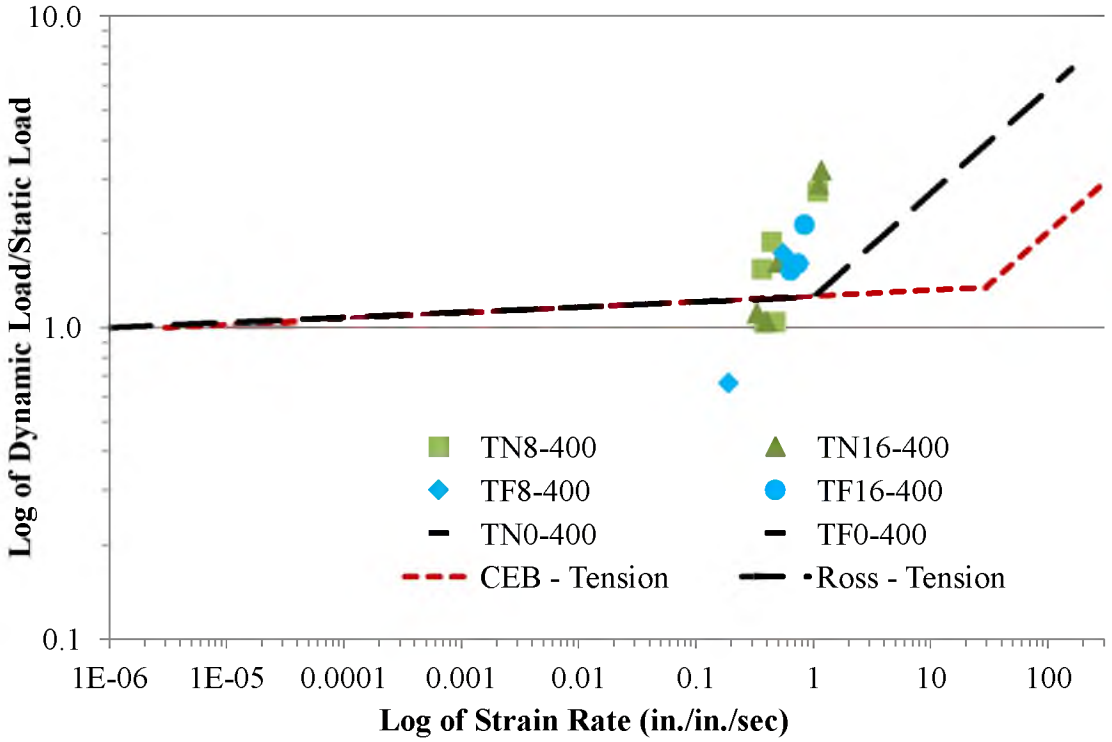

Figure F.1 – Tension at 400 °F

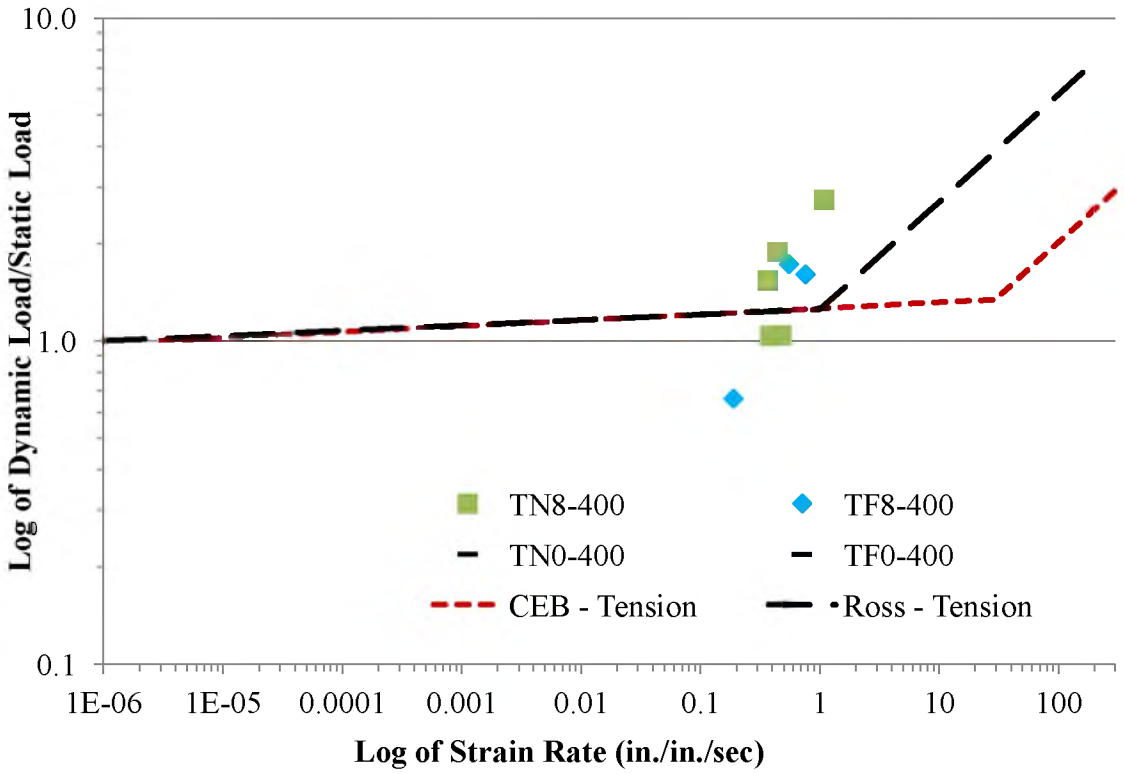

Figure F.2 – Tension, 8 ft at 400 °F

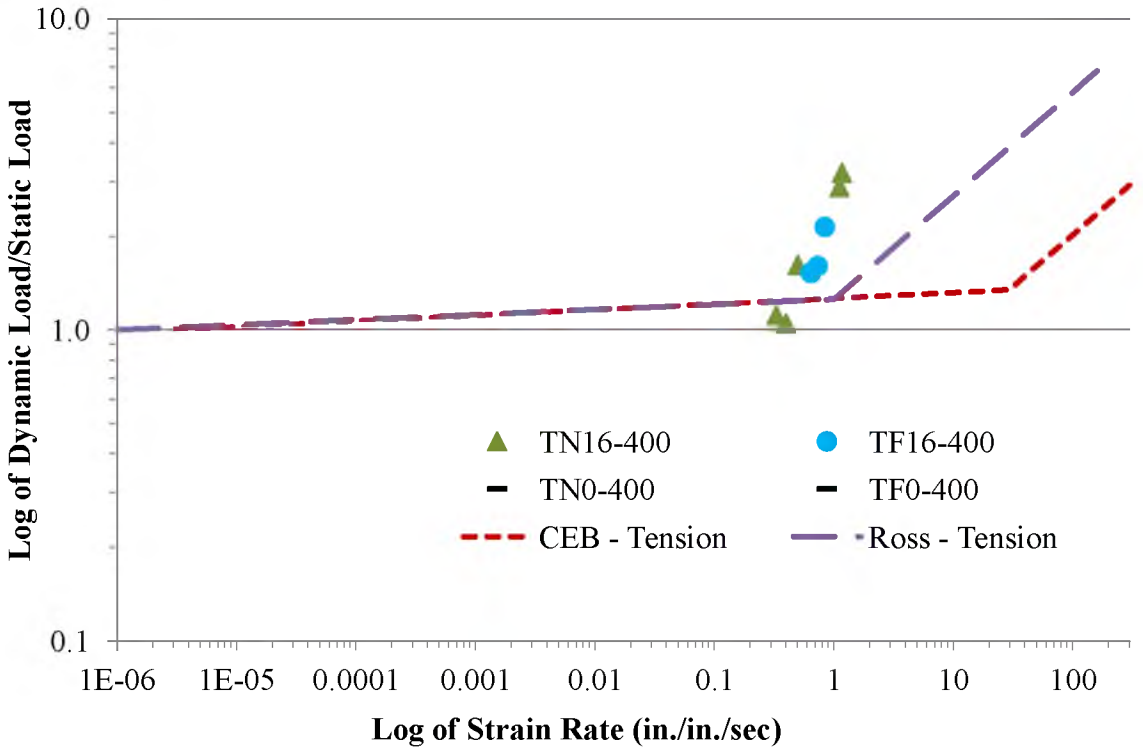

Figure F.3 – Tension, 16 ft at 400 °F

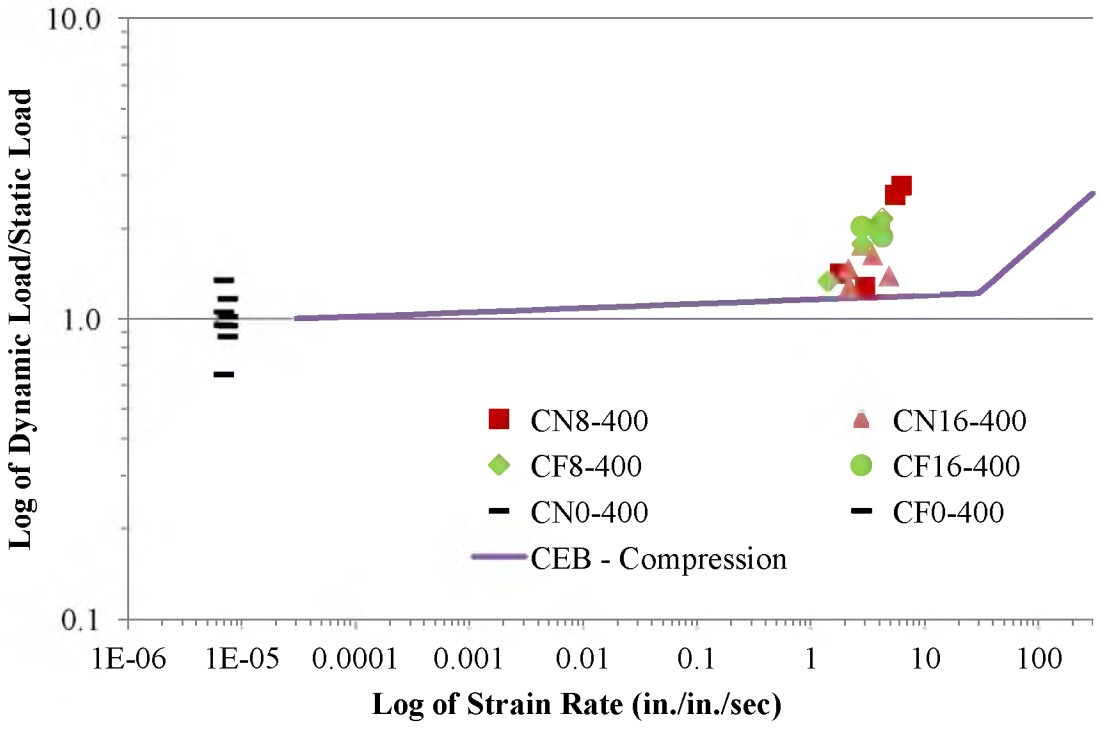

Figure F.4 – Compression at 400 °F

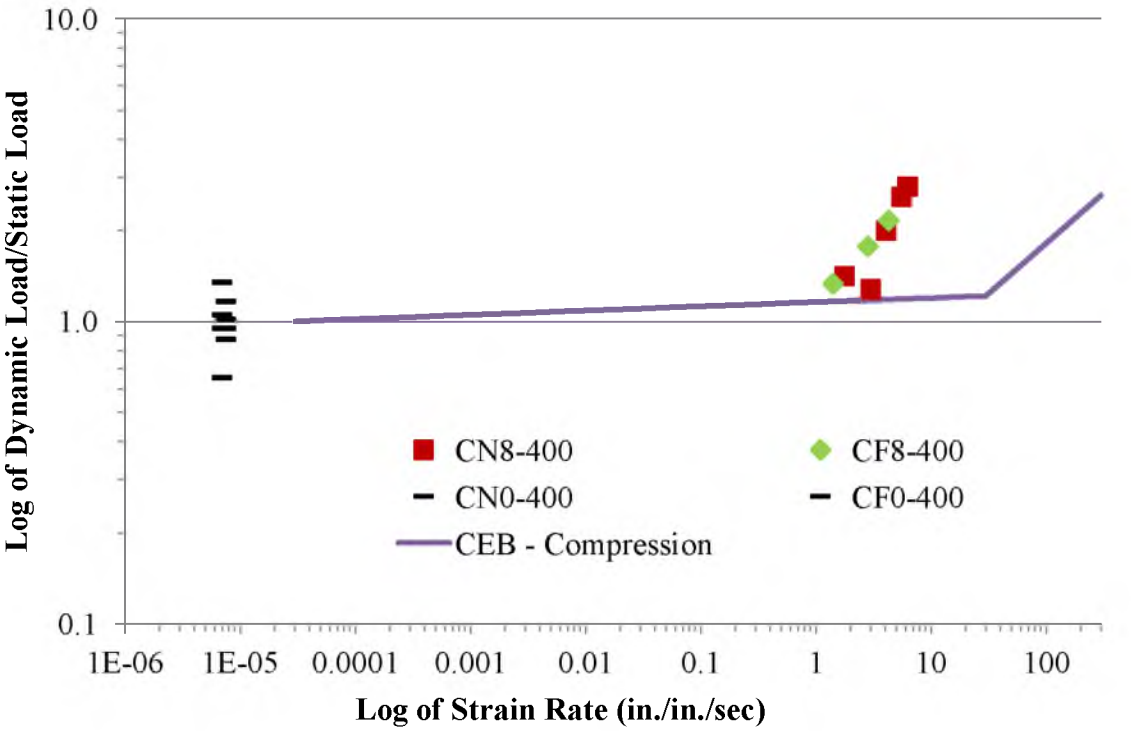

Figure F.5 – Compression, 8 ft at 400 °F

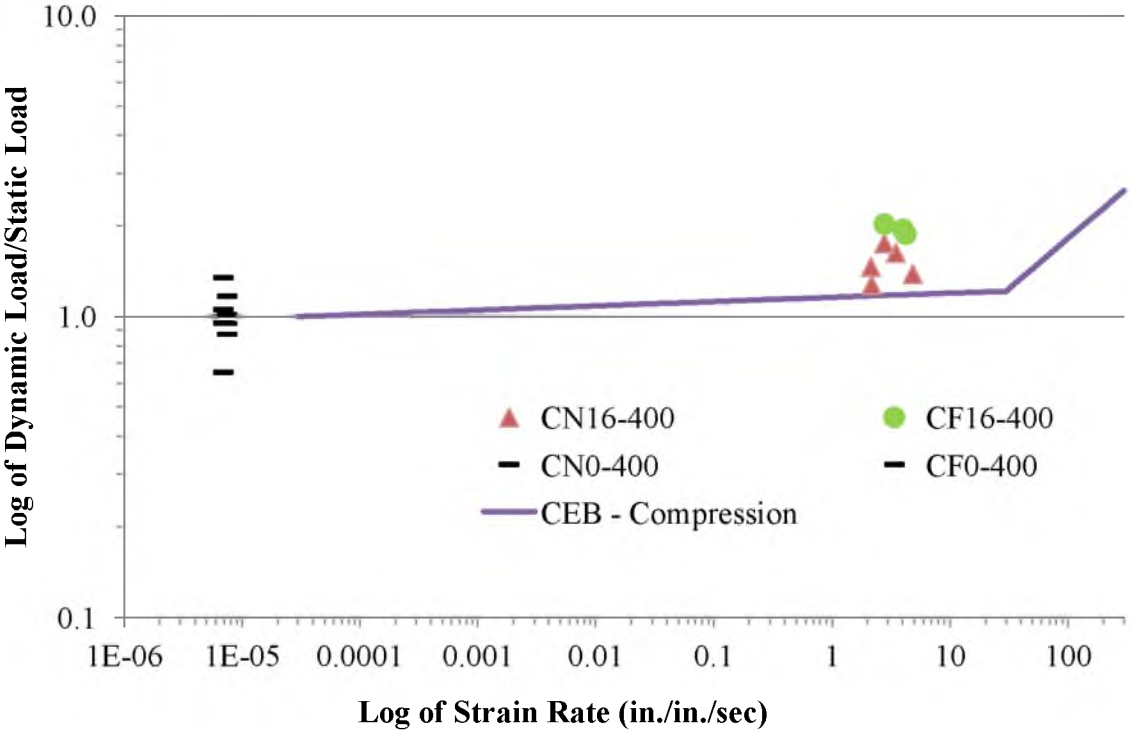

Figure F.6 – Compression, 16 ft at 400 °F

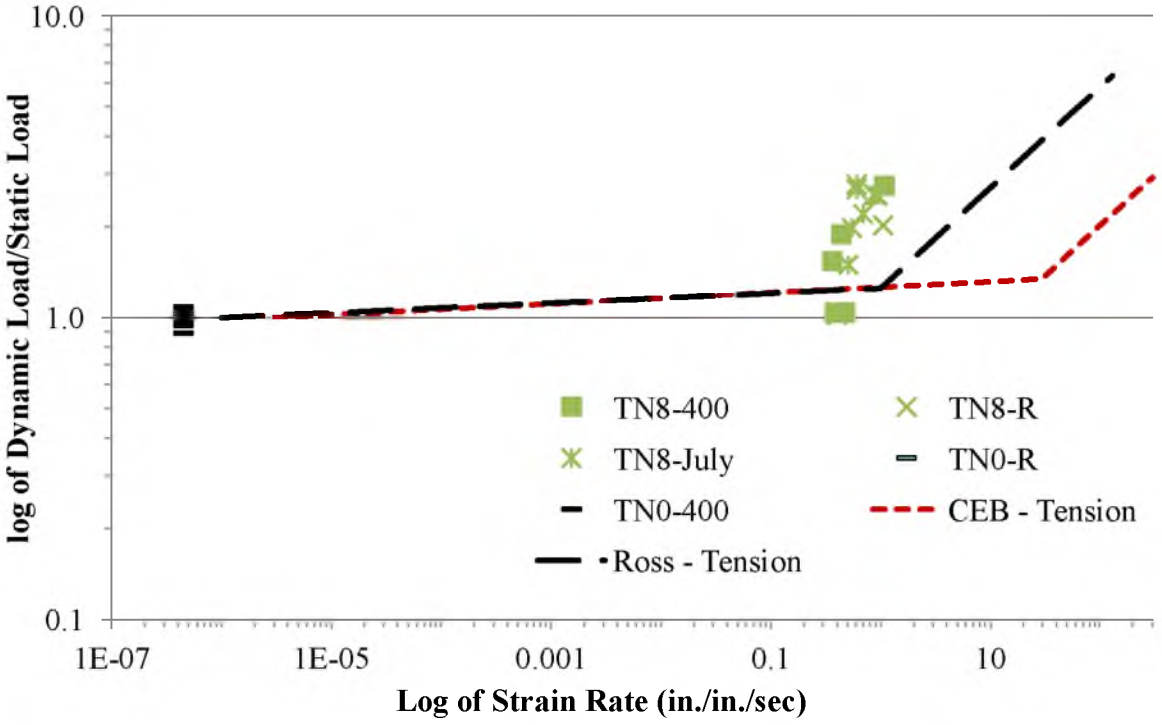

Figure F.7 – Tension, 8 ft – NWC at 400 °F and Room Temperature

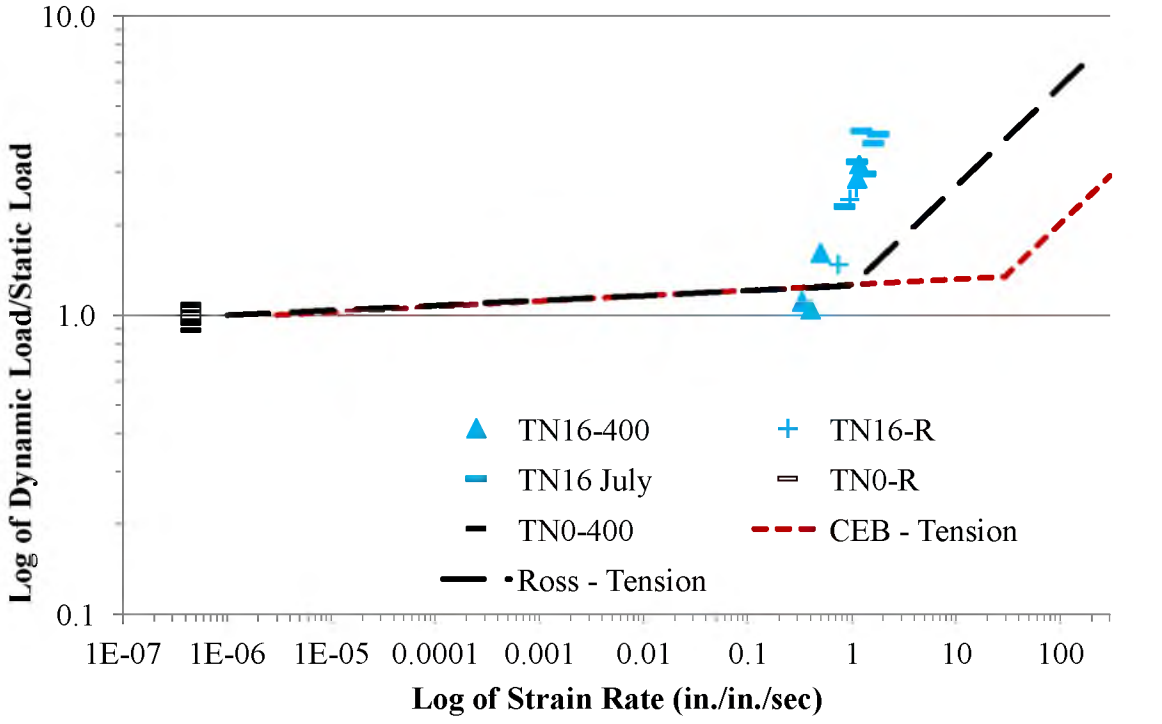

Figure F.8 – Tension, 16 ft – NWC at 400 °F and Room Temperature

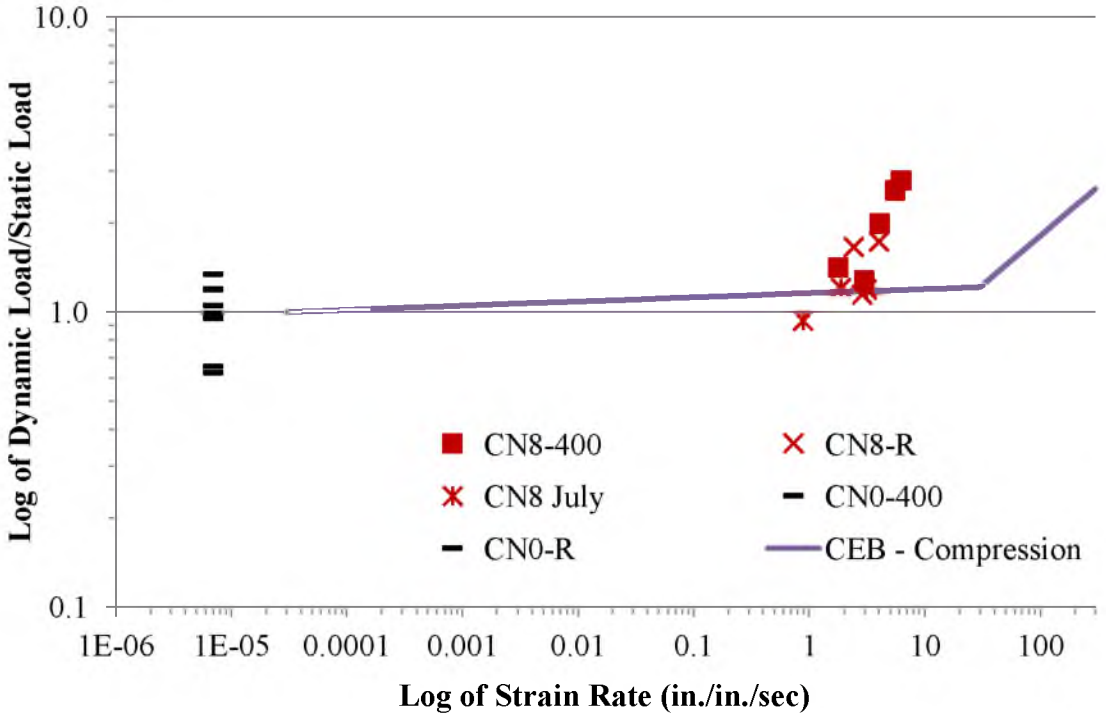

Figure F. 9 – Compression, 8 ft – NWC at 400 °F and Room Temperature

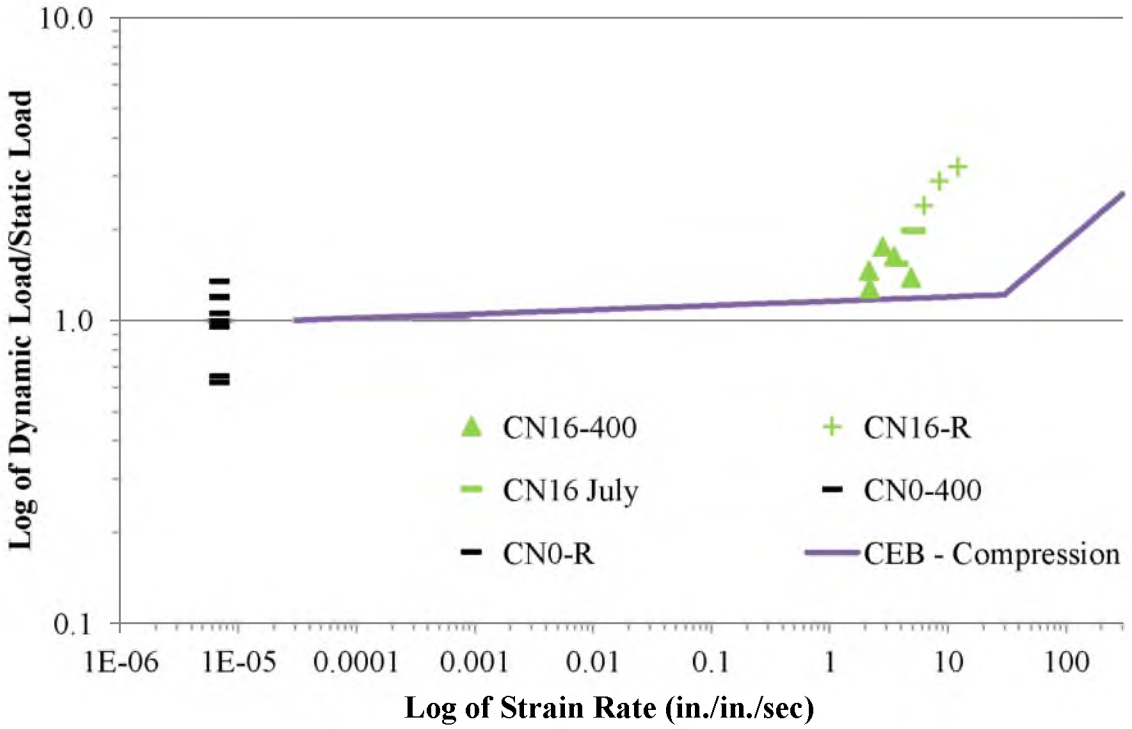

Figure F.10 – Compression, 16 ft – NWC at 400 °F and Room Temperature

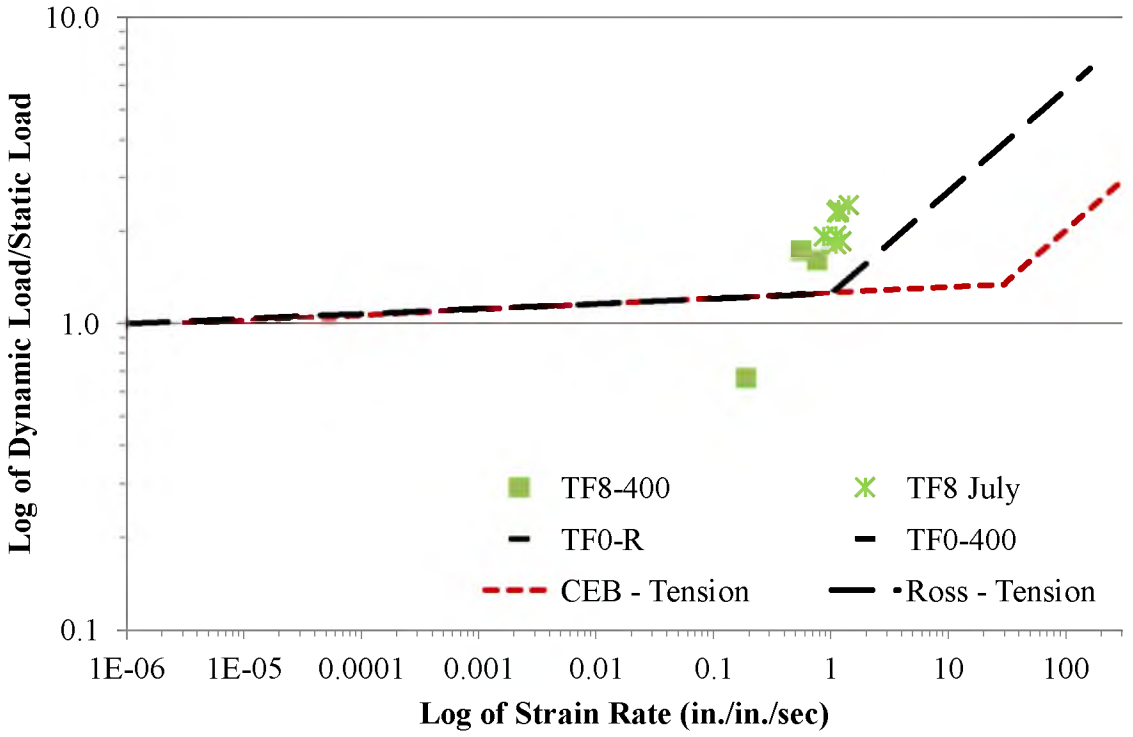

Figure F.11 – Tension, 8 ft – FRC at 400 °F and Room Temperature

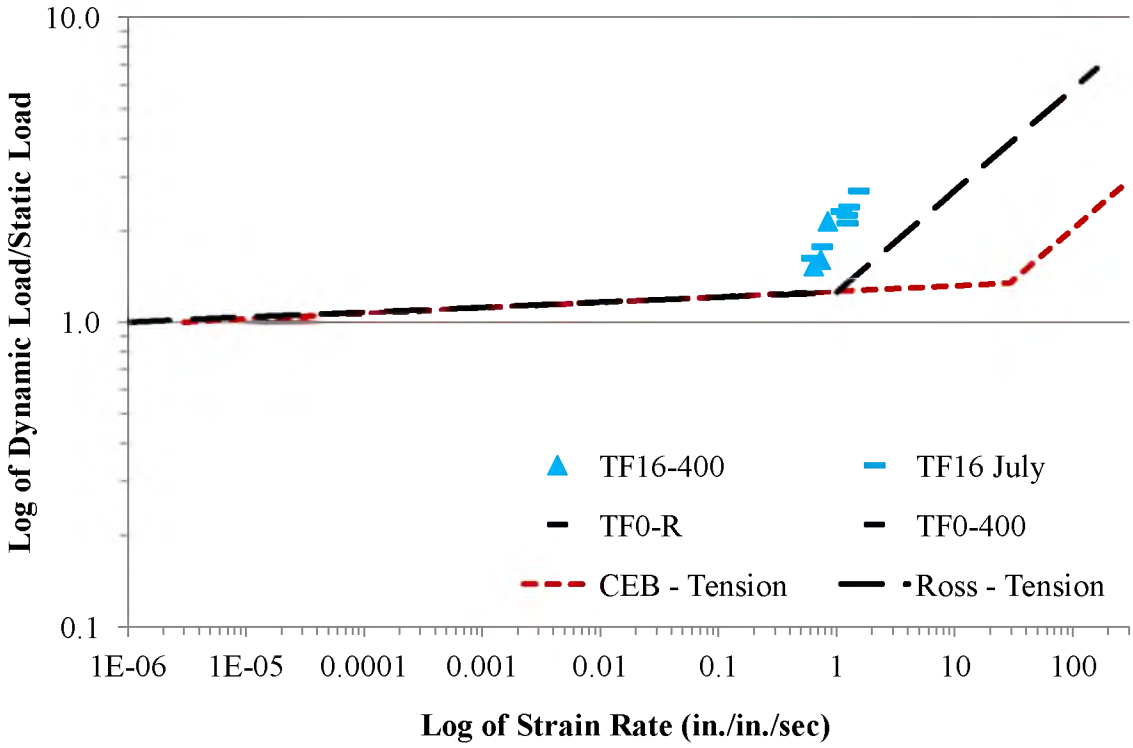

Figure F.12 – Tension, 16 ft – FRC at 400 °F and Room Temperature

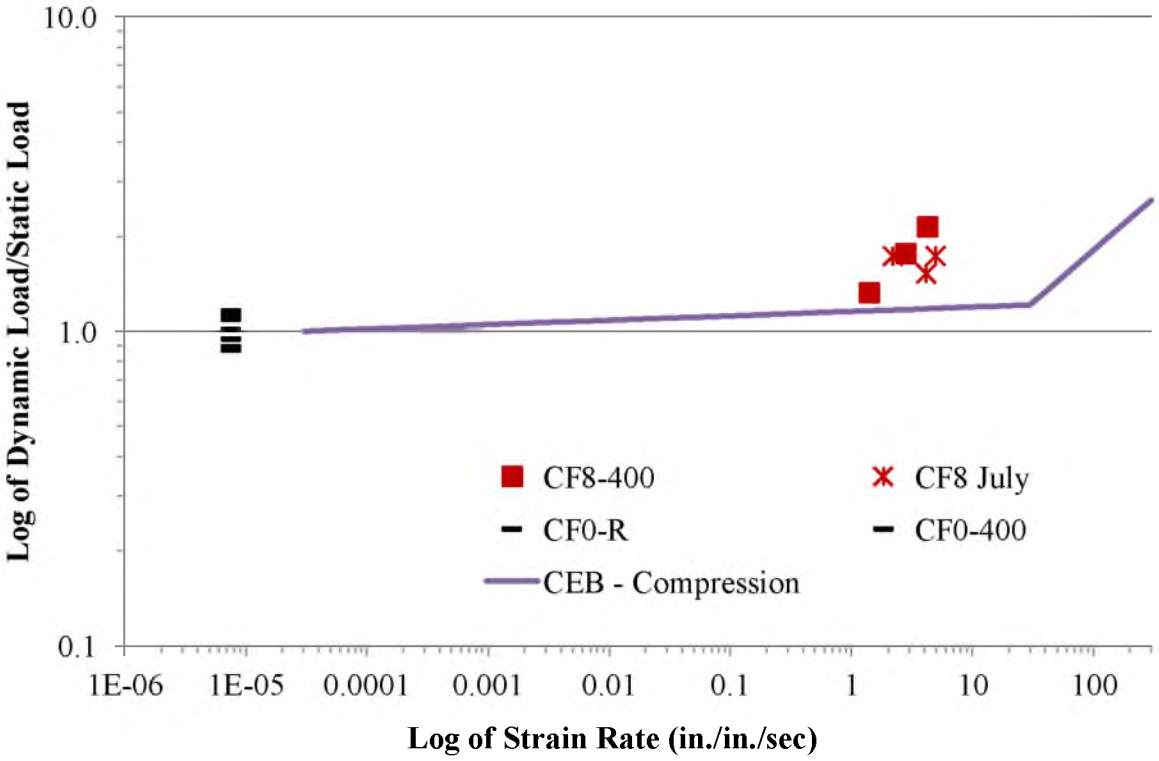

Figure F.13 – Compression, 8 ft – FRC at 400 °F and Room Temperature

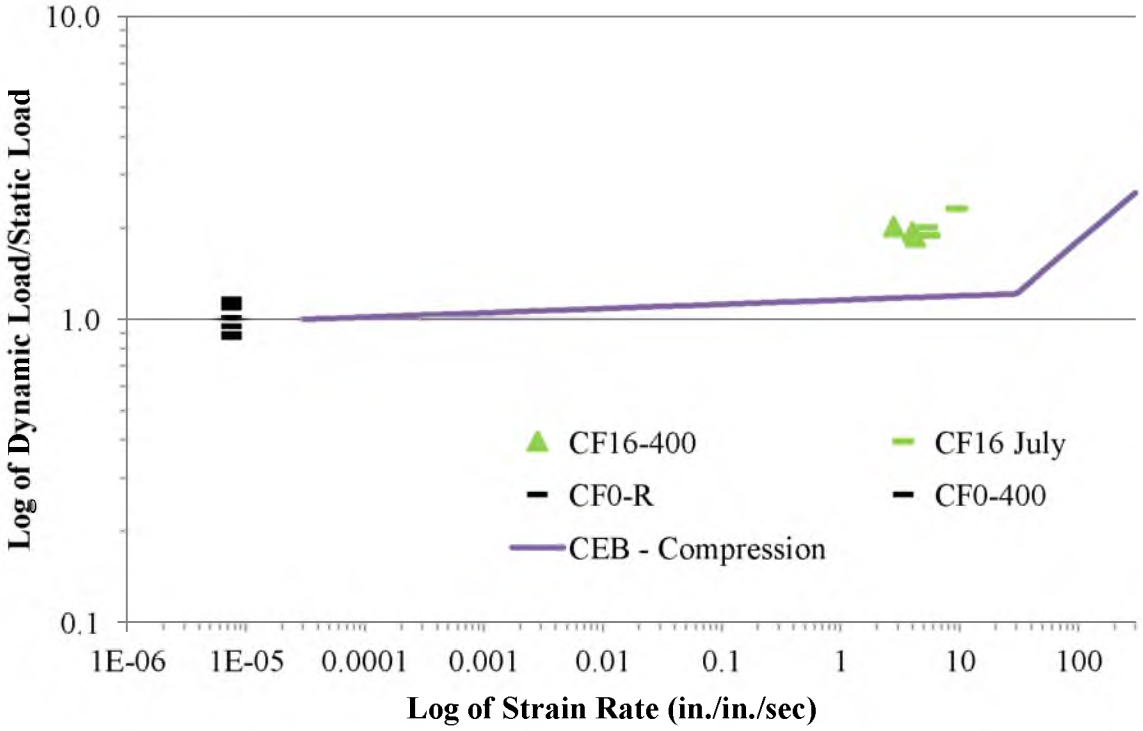

Figure F.14 – Compression, 16 ft – FRC at 400 °F and Room Temperature

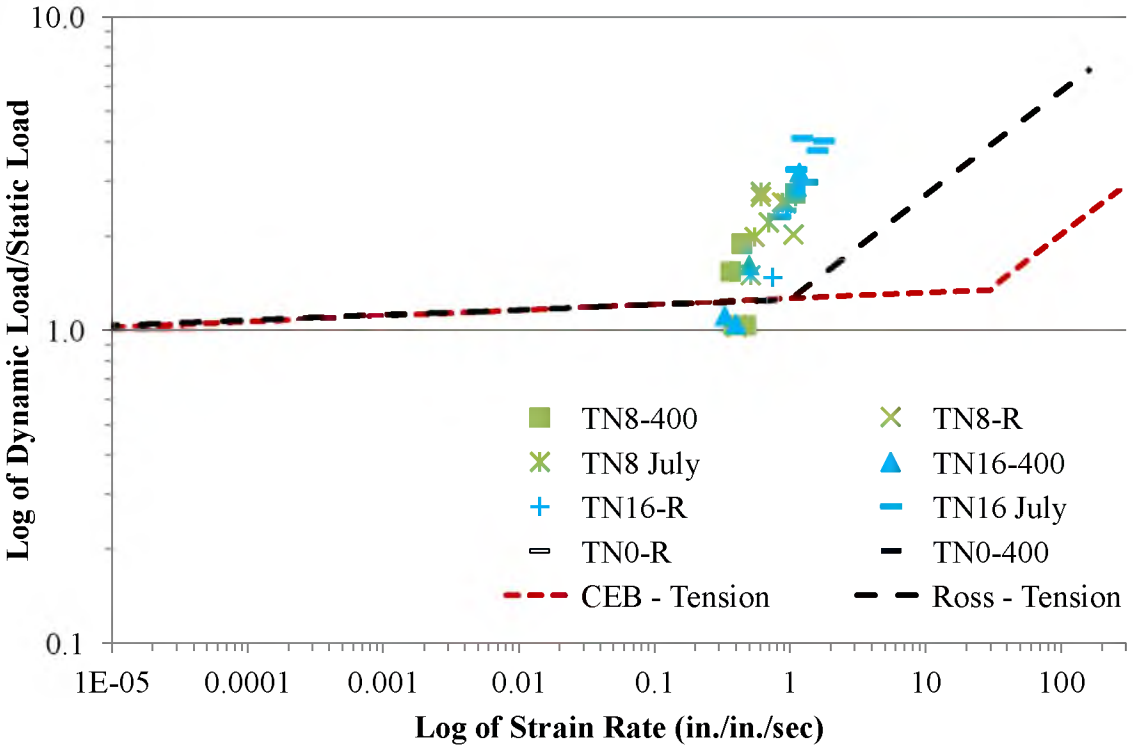

Figure F.15 – Tension – NWC at 400 °F and Room Temperature

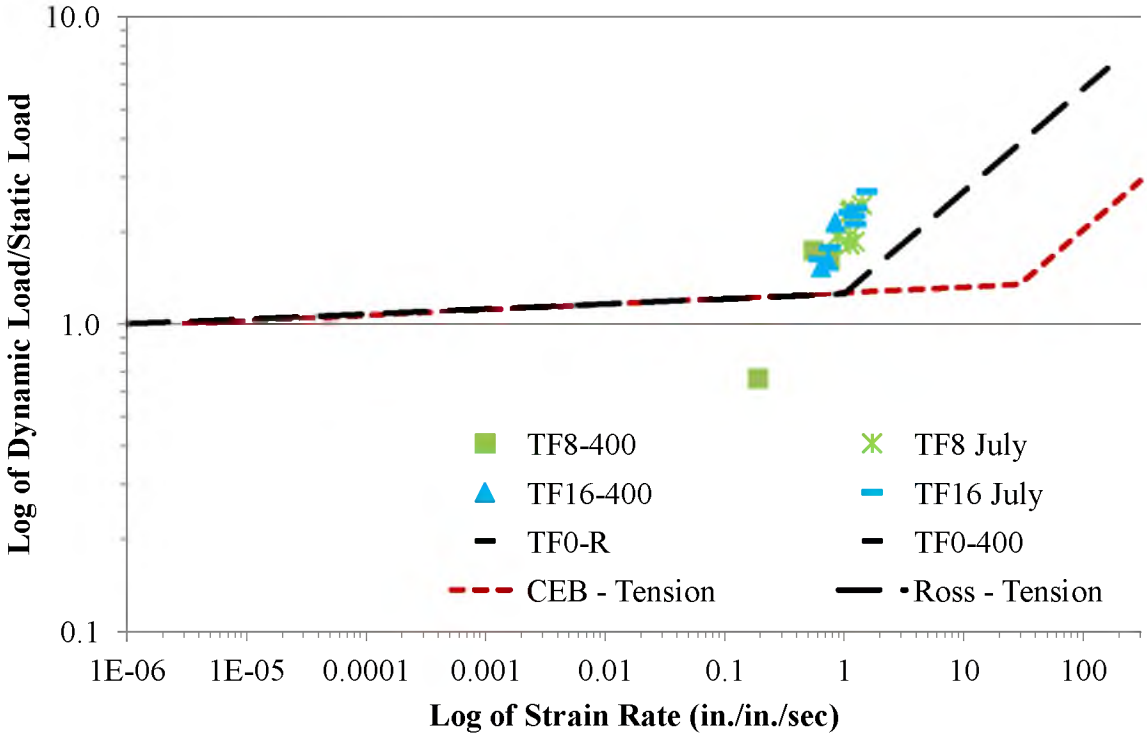

Figure F.16 – Tension – FRC at 400 °F and Room Temperature

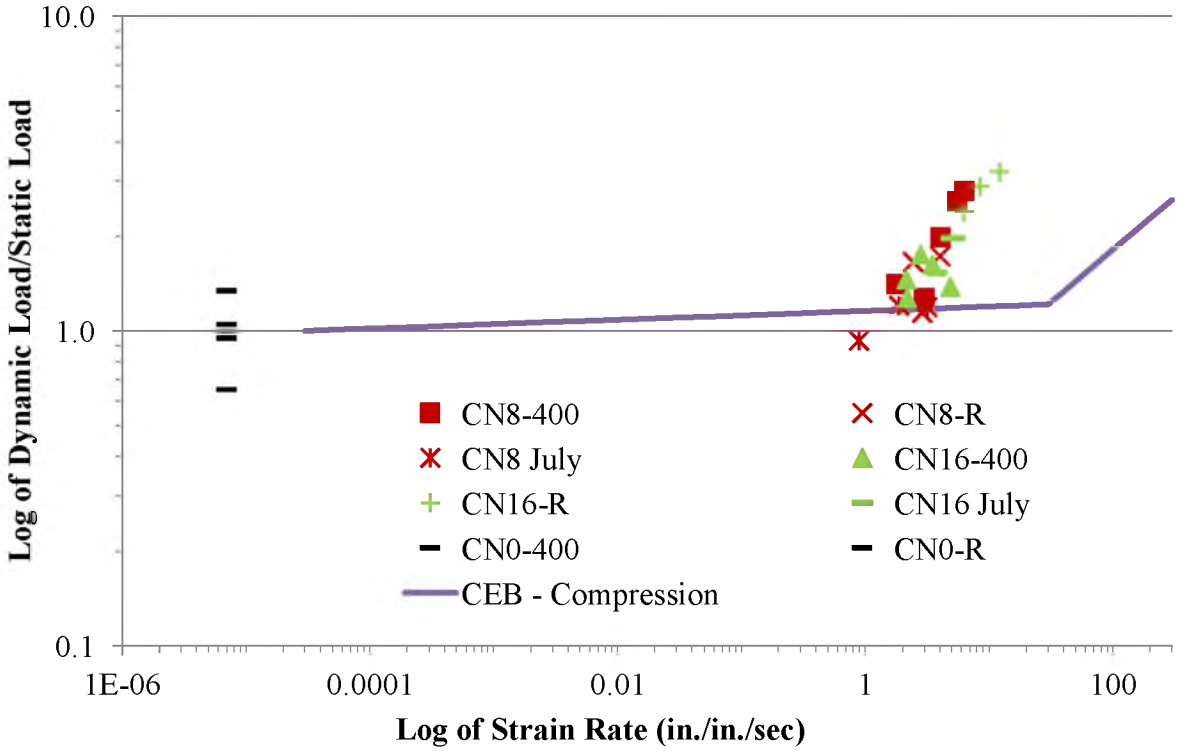

Figure F.17 – Compression – NWC at 400 °F and Room Temperature

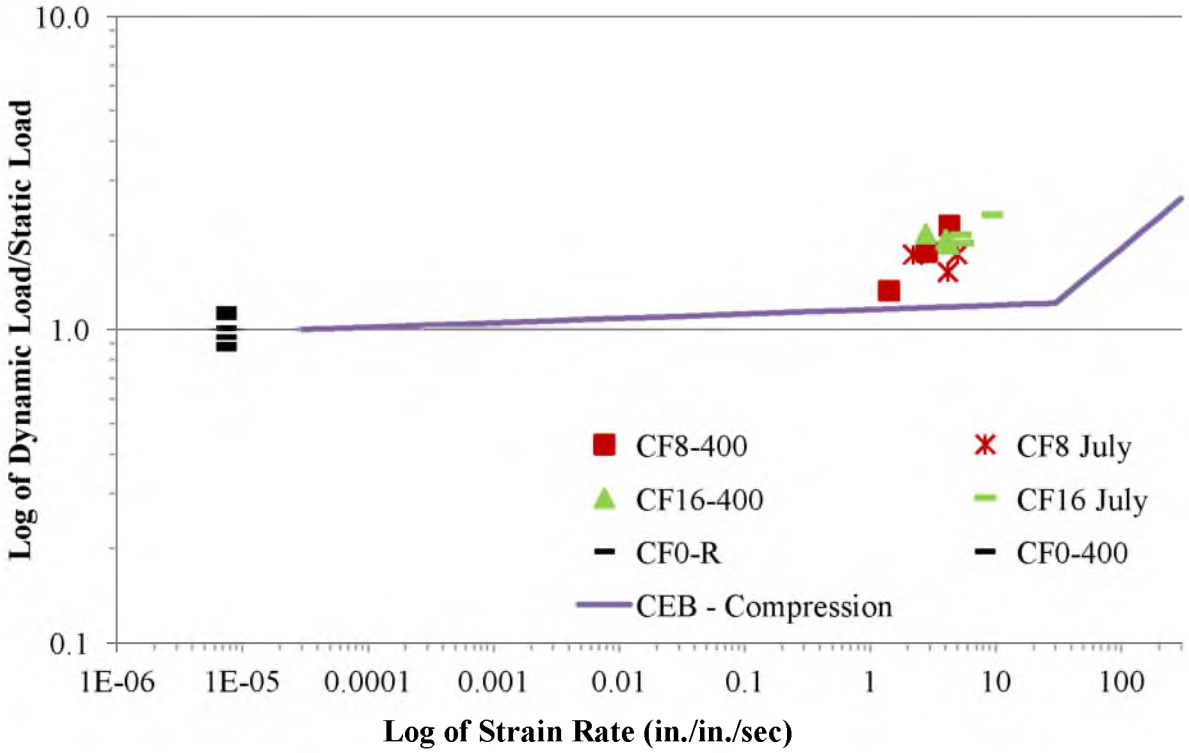

Figure F.18 – Compression – FRC at 400 °F and Room Temperature

APPENDIX G

PHOTOGRAPHS OF ADDITIONAL STATIC TEST SPECIMENS

Figure G.1 – CF0-R-6-1 After Static Test

Figure G.2 – CN0-R-6-4 After Static Test

Figure G.3 – CF0-400-6-2 After Static Test

Figure G.3 – CN0-400-6-2 After Static Test

REFERENCES

ACI 318. (1995). Building Code Requirements for Structural Concrete (ACI 318-95) and Commentary, Detroit, MI.

ASTM. (2004). Standard Test Method for Splitting Tensile Strength of Cylindrical Concrete Specimens, ASTM C496 / C496M - 04e1, West Conshohocken, PA.

ASTM. (2007). Standard Practice for Making and Curing Concrete Test Specimens in the Field, ASTM C31 / C31M – 10, West Conshohocken, PA.

ASTM. (2010). Standard Test Method for Compressive Strength of Cylindrical Concrete Specimes, ASTM C39 / C39M – 10, West Conshohocken, PA.

Banthia, N.P., Mindess, S., and Bentur, A. (1986). "High stress rate testing of concrete: an overview." *Indian Concrete J.*, 60(10), 265-270.

Behnood, A. and Ghandehari, M. (2009). "Comparison of compressive and splitting tensile strength of high-strength concrete with and without polypropylene fibers heated to high temperatures." *Fire Saf. J.*, 44(8), 1015-1022.

Birkimer, D.L. (1968). "Critical Normal Fracture Strain of Portland Cement Concrete." Ph.D. thesis, Univ. of Cincinnati, Cincinnati, OH.

Comite Euro-International du Beton. (1993). CEB-FIP Model Code 1990. Trowbridge, Wiltshire, UK.

Cowell, W.L. (1966). "Dynamic Properties of Plain Portland Cement Concrete." *Technical Report R447,* Naval Civil Engineering Laboratory, Port Hueneme, CA.

Garfield, T.T. (2011). "Performance of Reinforced Concrete Panels During Blast Loading." M.S. Thesis, Univ. of Utah, Salt Lake City, Utah.

John, R., Antoun, T., and Rajendran, A.M. (1992). "Effect of Strain Rate and Size on Tensile Strength of Concrete." *Proc., Shock Compression of Condensed Matter*, American Physical Society (APS), Williamsburg, VA, 501-504.

Lam, E. S., Wu, B., Liu, Q., and Ho, I. (2012). "Monotonic and Cyclic Behavior of High-Strength Concrete with Polypropylene Fibers at High Temperature." *ACI Mater. J.*, 109(3), 323-330.

Malvar, L.J. and Ross, C.A. (1998). "Review of Strain Rate Effects for Concrete in Tension." *ACI Mater. J.*, 95(6), 735-739.

Malvar, L.J. and Crawford, J.E. (1998). "Dynamic Increase Factors for Concrete." *Proc., Twenty-Eighth Seminar*, Department of Defense Explosives Safety Board (DDESB), Orlando, FL.

McVay, M.K. (1988). "Spall Damage of Concrete Structures." *Technical Report SL-88-22,* U.S. Army Corps of Engineers, Waterways Experiment Station, Vicksburg, MS.

Mellinger, F.M. and Birkimer, D.L. (1966). "Measurement of Stress and Strain on Cylindrical Test Specimens of Rock and Concrete under Impact Loading." *Technical Report 4-46,* U.S. Army Corps of Engineers, Ohio River Division Laboratories, Cincinnati, OH.

Millard, S.G., Molyneaux, T.C.K., Barnett, and S.J., Gao, X. (2010). "Dynamic Enhancement of Blast-resistant Ultra High Performance Fibre-reinforced Concrete Under Flexural and Shear Loading." *Int. J. Impact Eng.*, 37(4), 405-413.

Ross, A., Tedesco, J.W., and Kuennen, S.T. (1995). "Effects of Strain Rate on Concrete Strength." *ACI Mater. J.*, 92(1), 37-44.

Takeda, J.J. (1971). "Deformation and Fracture of Concrete Subjected to Dynamic Load." *Mechanical Behavior of Materials, Proceedings of the International Conference,* 64, 15-20.

Watstein, D. (1953). "Effect of Straining Rate on the Compressive Strength and Elastic Properties of Concrete." *Journal of the American Concrete Institute*, 24(8), 729-744.